BRNO UNIVERSITY OF TECHNOLOGY

VYSOKÉ UČENÍ TECHNICKÉ V BRNĚ

FACULTY OF ELECTRICAL ENGINEERING AND COMMUNICATION

FAKULTA ELEKTROTECHNIKY
A KOMUNIKAČNÍCH TECHNOLOGIÍ

DEPARTMENT OF ELECTRICAL AND ELECTRONIC TECHNOLOGY

ÚSTAV ELEKTROTECHNOLOGIE

THE EFFECT OF ELECTRODE BINDERS TO ELECTROCHEMICAL PROPERTIES OF NEGATIVE ELECTRODE MATERIALS

BACHELOR'S THESIS

VLIV POJIV NA ELEKTROCHEMICKÉ VLASTNOSTI ZÁPORNÝCH ELEKTRODOVÝCH HMOT

BAKALÁŘSKÁ PRÁCE

AUTHOR — **András Zsigmond**

AUTOR PRÁCE

SUPERVISOR — **Ing. Jiří Libich, Ph.D.**

VEDOUCÍ PRÁCE

BRNO 2016

BRNO UNIVERSITY OF TECHNOLOGY

Faculty of Electrical Engineering and Communication

Department of Electrical and Electronic Technology

Bachelor thesis

Bachelor's study field
Microelectronics and Technology

Student: András Zsigmond
ID: 154915
Year of study: 3
Academic year: 2015/16

TITLE OF THESIS:

The Effect of Electrode Binders to Electrochemical Properties of Negative Electrode Materials

INSTRUCTION:

Get acquaint with Lithium-Ion batteries and their characterictic electrochemicla properties. Study operation principle of Litihum-Ion battery along with intercalaction process. Lead experiments which involve different kinds of binders and their using in electrodes.

REFERENCE:

Podle pokynů vedoucího práce.

Assigment deadline: 8. 2. 2016 ***Submission deadline:*** 2. 6. 2016

Head of thesis: Ing. Jiří Libich, Ph.D.
Consultant:

doc. Ing. Jiří Háze, Ph.D.
Subject Council chairman

VYSOKÉ UČENÍ TECHNICKÉ V BRNĚ
FAKULTA ELEKTROTECHNIKY A KOMUNIKAČNÍCH TECHNOLOGIÍ

Bakalářská práce

bakalářský studijní obor **Mikroelektronika a technologie**
Ústav elektrotechnologie

Student: András Zsigmond ***ID:*** 154915
Ročník: 3 ***Akademický rok:*** 2015/16

NÁZEV TÉMATU:

Vliv pojiv na elektrochemické vlastnosti záporných elektrodových hmot

POKYNY PRO VYPRACOVÁNÍ:

Seznamte se s litihum-iontovými akumulátory, jejich charakteristickými vlastnostmi a s operačním principem. Prostudujte vlastnosti záporných elektrodových hmot v lithium-iontových akumulátorech. Proveďte experimenty s různými typy pojiv používanými v elektrodách. Získané výsledky vyhodnoťte.

DOPORUČENÁ LITERATURA:

Podle pokynů vedoucího práce.

Termín zadání: 8.2.2016 ***Termín odevzdání:*** 2.6.2016

Vedoucí práce: Ing. Jiří Libich, Ph.D.
Konzultant bakalářské práce:

doc. Ing. Jiří Háze, Ph.D., *předseda oborové rady*

ABSTRACT

This bachelor's thesis deals with various types of binders used in the negative electrode material of lithium-ion batteries. The materials used as binders were Polyvinylidene fluoride (PVDF), Styrene-butadiene rubber (SBR) and Polyimide P84. Each binder was used in three different weight percentages, PVDF and P84 at 3, 6 and 10 wt.%, while SBR was used at 2, 4 and 6 wt.%. The thesis contains the process of making the negative electrodes as well as the results of each measurement.

KEYWORDS

lithium, battery, binders, negative electrode, electrolyte, capacity, anode

ABSTRAKT

Táto bakalárska práca sa zaoberá rôznymi typmi spojív, používaných v lítium-iontových akumlátorov, a ich vpliv na vlastnosti záporných elektrodových hmôt. Použité pojivá boli: Polyvinylidenfluorid (PVDF), Styren-butadienového guma (SBR) a Polyimid P84. Každé spojivo bolo testované v troch rôznych hmotnostných percentách z PVDF a P84 3, 6 a 10 hm.%, zatiaľ čo SBR 2, 4 a 6 hm.%. Práca zahŕňa prípravu procesu elektródy a výsledky vykonaních meraní.

KĽÚČOVÉ SLOVÁ

lítium, batérie, spojivá, záporná elektróda, elektrolytu, kapacita, anóda

ZSIGMOND, A. *The Effect of Electrode Binders to Electrochemical Properties of Negative Electrode Materials*. Brno: Vysoké učení technické v Brně, Fakulta elektrotechniky a komunikačních technologií, Ústav mikroelektroniky (elektrotechnologie), 2016. 81 s., Bakalářská práce. Vedoucí práce: Ing. Jiří Libich, Ph.D.

OBLIGATORY STATUTORA DECLARATION

I declare that I have written my doctoral thesis **" The Effect of Electrode Binders to Electrochemical Properties of Negative Electrode Materials"** independently, under the guidance of the doctoral thesis supervisor and using the technical literature and other sources of information which are all quoted in the thesis and detailed in the list of literature at the end of the thesis.

As the author of the bachelor's thesis, I furthermore declare that, as regards the creation of this doctoral thesis, I have not infringed any copyright. In particular, I have not unlawfully encroached on anyone's personal and/or ownership rights and I am fully aware of the consequences in the case of breaking Regulation §11 and the following of the Copyright Act No. 121/2000 Coll., and of the rights related to intellectual property right and changes in some Acts (Intellectual Property Act) and formulated in later regulations, inclusive of the possible consequences resulting from the provisions of Criminal Act No. 40/2009 Coll., Section 2, Head VI, Part 4.

Brno ....

(signature)

ACKNOWLEDGEMENTS

I would like to thank my supervisor, Ing. Jiří Libich, Ph.D. for his help, valuable advice and time during the work on this thesis. I would also like to thank my family and friends for their support.

Brno ....

(signature)

CONTENTS

LIST OF IMAGES

LIST OF TABLES

INTRODUCTION

Batteries exist since the end of the 19th century. They provided the main source of electricity before the development of electric generators. Successful improvements in battery technology lead us to the use of portable computers, mobile phones, electric cars, and many other electrical devices.

The term "battery" was first used by Benjamin Franklin in the 18th century. He described a set of linked capacitors as a "battery". These capacitors were panels of glass coated with metal on each surface and were charged with an electrostatic generator and discharged by touching metal to their electrodes. The term originally meant "a group of two or more similar objects functioning together". Later on this term was used for voltaic piles and similar devices similar to Franklin's connected capacitors. Today even a single electrochemical cell is called a battery. [1]

Experimentation with lithium batteries began in 1912 by G.N. Lewis, and in the 1970s the first lithium batteries were sold. Important developments were made in the 1980s. An American chemist John B. Good experimented with $LiCoO_2$ as the positive electrode (cathode). Another research scientist Rachid Yazami at the same time discovered the graphite anode (negative electrode). The results of these experiments were put together by Akira Yoshino of Asahi Chemical in Japan. The first lithium-ion battery prototype was built in 1985. The commercialization of the lithium-ion battery was done by Sony in 1991. [1]

The goal of this bachelor's thesis is to examine the effect of the electrode binders on the electrochemical properties of the negative electrode. These electrodes were prepared on copper foil with different weight percentages for each binder. Polyvinylidene fluoride (PVDF) and Polyimide P84 were used at 3 %, 6 % and 10 %, while the Styrene-butadiene rubber (SBR) was used at 2 %, 4 % and 6 %.

1 BATTERIES

Battery is a device used to store electric energy. It changes chemical energy to electricity by putting certain chemicals in contact with each other in a specific way. During this process electrons travel from one kind of chemical to another under the right circumstances. When electrons flow, this makes an electrical current that can power a lot of different devices, mobile phones, e-cigarettes, remote controls, etc. [2]

Batteries come in several styles; the most common is the so called single-use alkaline batteries. NASA spacecraft usually use rechargeable nickel-cadmium or nickel-hydride batteries like those found in laptop computers or cellular phones. [2]

Batteries have three parts, a negative electrode (*anode* -), a positive electrode (*cathode* +), and the *electrolyte*. The positive electrode and negative electrode is used to connect the battery to an electrical circuit. The chemical reactions in the battery causes a buildup of electrons at the negative electrode. This results in an electrical difference between the two electrodes. The electrons want to rearrange themselves to get rid of this difference. They do this in a certain way, electrons repel each other and try to go to a place with fewer electrons. In a battery, the only place to go is to the positive electrode. But, the electrolyte keeps the electrons from going straight from the negative to the positive electrode within the battery. When the circuit is closed the electrons will be able to get to the positive electrode through the electrical circuit. [2]

The electrochemical processes in a battery change the chemicals in the negative and positive electrode resulting in a limited amount of power available in a battery. When the battery is recharged, the direction of the flow of electrons is changed using another power source. The electrochemical processes happens in reverse, and the negative and positive electrodes are restored to their original state and can again provide power. [2]

The subject of this thesis will be introduced in the next chapter, while a comparison between the performance of different types of batteries in the third chapter.

1.1 Lithium-ion batteries

Work with the lithium battery began in 1912 but it was not until the early 1970s when the first non-rechargeable lithium batteries became commercially available. The use of lithium metal was not possible due to the instability of the material, especially during charging. Research shifted to a non-metallic lithium battery using lithium ions. In comparison lithium-ion is more stable than pure lithium, however it is lower in energy density. [3]

The energy density of lithium-ion is twice as big as the standard nickel-cadmium. The load characteristics are good and when discharged it behaves similarly to nickel-cadmium. The high cell voltage of 3,6 volts allows battery pack designs with only one cell. Most of today's mobile phones run on a single cell. A nickel-based pack would require three 1,2-volt cells connected in series. [4]

Figure 1.1 Lithium-ion batteries. [7]

Figure 1.1 shows certain types of Li-ion batteries. The primary components of a lithium-ion battery are the positive and negative electrodes, the separator and the electrolyte. The negative electrode is generally made from carbon, while the positive electrode is metal oxide. Lithium salt in an organic solvent is used as the electrolyte. Depending on the direction of current flow the electrochemical roles of the electrodes reverse between anode and cathode. The most popular material used as the negative electrode is graphite. The positive electrode is either layered oxide (lithium cobalt oxide), a polyanion (lithium-iron phosphate) or spinel (lithium - manganese oxide). [5]

As mentioned before the electrolyte is a mixture of organic carbonates (ethylene carbonate or diethyl carbonate) containing lithium ions. These non-aqueous electrolytes use anion salts such as lithium hexafluorophosphate ($LiPF_6$), lithium hexafluoroarsenate monohydrate ($LiAsF_6$), lithium perchlorate ($LiClO_4$), lithium tetrafluoroborate ($LiBF_4$) and lithium triflate ($LiCF_3SO_3$). The reason why non-aqueous electrolytes are used lays in the highly reactive properties of lithium. The reaction with water produces lithium hydroxide and hydrogen gas, therefore the sealed container strictly excludes moisture from the battery pack. Material choices heavily affect the voltage, energy density, life and safety of a lithium-ion battery. Performance improvements have been employed by new architectures using nanotechnology. [5]

Figure 1.1 also shows the various shapes of the Li-ion batteries. These can be divided into four groups. Small cylindrical, which has a solid body without terminals and can be used in laptop batteries. Large cylindrical with solid body and large threaded terminals. Batteries with soft, flat body called pouch. These are mainly used in cell phones. The fourth type is a semi-hard plastic case with large threaded terminals, called prismatic and they are used as vehicle traction packs. [5]

When the battery is charging up, the lithium-cobalt oxide, positive electrode gives up some of its lithium ions. These ions move through the electrolyte to the negative, graphite electrode. The battery takes in and stores energy during this process. When the battery is discharging, the lithium ions move back to the positive electrode, producing the energy. In both cases, electrons flow in the opposite direction to the ions around the

outer circuit. Electrons do not flow through the electrolyte, it is an insulating barrier. The movement of ions and electrons are connected, if either one of them stops so does the other. Ions can stop moving through the electrolyte if the battery completely discharges, if that happens then the electrons can't move through the circuit, the battery loses power. Similarly, if the device powered by the battery is switched off, the flow of electrons stops and so does the flow of ions. [5]

Unlike simpler batteries, lithium-ion batteries have built in electronic controllers that regulate how they charge and discharge. They prevent the overcharging and overheating that can cause lithium-ion batteries to explode. [5]

Lithium-ion batteries became popular because they have a number of important advantages. They are lighter than other types of rechargeable batteries of the same size. Lithium is a highly reactive element, a lot of energy can be stored in its atomic bonds. The above mentioned energy density translated in to numeral information means, that a typical lithium-ion battery can store 150 watt-hours of electricity in 1 kilogram of battery. A Ni-MH (nickel-metal hydride) battery pack can store typically 60 to 70 watt-hours in 1 kilogram of battery, while a lead-acid battery can store only 25 watt-hours per kilogram. Using lead-acid technology means that, it would take 6 kilograms to store the same amount of energy that a 1 kilogram lithium-ion battery can handle. Other important advantages are related to charge. A lithium-ion battery pack loses only about 5 % of its charge per month, compared to a 20 % loss per month for Ni-MH batteries. They have no memory effect, which means that it does not have to be completely discharged before recharging. They can handle hundreds of charge/discharge cycles. [5]

Of course lithium-ion batteries have some flaws. They start degrading as soon as they leave the factory. They will only last a few years whether it is used or not. They are extremely sensitive to high temperatures. Heat causes lithium-ion battery packs to degrade much faster than they normally would. If it's completely discharged they are ruined. A lithium-ion battery pack must have an on-board computer to manage the battery. This makes them more expensive. There is a small chance that, if a lithium-ion battery pack fails, it will burst into flame. [5]

1.2 Cathode material

In the beginning of development $LiCoO_2$ (LCO) was the dominant cathode material, with the spinel $LiMn_2O_4$ (LMO) occupying only a small part of the market. Over time the LCO remained the most common cathode material, however the market has been flooded by other materials. By 2010, the use of $LiNi_{1/3}Mn_{1/3}Co_{1/3}O_2$ (NMC), a ternary system with nickel, manganese, and cobalt, had increased. For certain applications the use of $LiNi_{0,8}Co_{0,15}Al_{0,05}O_2$ (NCA) and LMO are preferred. With only a limited use, phosphates with an olivine structure is a promising new class of cathode materials, $LiFePO_4$ (LFP) being the most prominent. [6]

The next few sub-chapters show the recent technological trends of cathode materials. Most importantly the structures and the description of materials.

1.2.1 Three morphologies of cathode materials

The cathode materials are transition metal oxides containing lithium, and they can

be described as a type of functional ceramics. This means that the lithium ions must be able to diffuse freely through the crystal structure. The morphology of the crystal structure determines the number of dimensions in which lithium ions are able to move (one-, two-, or three- dimensional). Cathode materials currently in use or under development are described below. [6]

1.2.2 Layered rock salt structure materials

This first group of compounds have a two-dimensional crystal morphology. The most commonly used is the LCO. The $LiNiO_2$ and $LiMnO_2$ are also well known compounds, however they have proven to be unsuitable for use as LIB cathodes. This uselessness only appears in their simple form, combined with other elements performance improvements have been achieved. With this combination they form complex oxides such as NMC, $LiNi_{0,8}Co_{0,2}O_2$, and $LiNi_{0,5}Mn_{0,5}O_2$. Recently solid solution materials, described by the general formula Li_2MnO_3-$LiMO_2$ (where M stands for transition metal, Ni or Fe) are being researched. [6]

1.2.3 Spinel structure materials

In this category the most significant compound is LMO, which enables lithuim-ions to diffuse in all three dimensions. Spinels provide lower discharge capacity than layered rock salt materials, however they show advantages in other categories, like lower cost, high stability. Because of this they are gaining attention in medium- and large- scale lithium-ion battery applications. [6]

1.2.4 Olivine structure materials

The most well known of the olivines is LFP. This material restrict lithium-ion diffusion to a single linear dimension. The one-dimension movement of the ions means a performance disadvantage, which has been minimized through the development of nano-particles and other techniques. Discharge voltage for olivines is relatively low, around 3,5 V. Olivine cathode materials have been commercialized due to the outstanding stability they offer. [6]

1.2.5 Layered LCO series (two dimensional)

New improvements are constantly introduced to the LCO by employing new synthesis techniques. One example is the synthesis of nano-particles of overlithiated LCO, which provide significantly improved electrochemical properties. In this process the lithium acetate and cobalt acetate are mixed in solution, then dried, and as the last step calcined at 600 °C for 6 hours. The mentioned procedure differs from the general method of obtaining bulk LCO particles. During the general process a combination of Co_3O_4 and Li_2CO_3 is calcined at around 900 °C, which produces a material with a primary particle diameter of several micrometers, while the new method produces spherical nano-particles of LCO with a primary particle diameter of 5-25 nm. In the new material the lithium content is 9-21 times more than conventional bulk LCO particles. Spherical nano-particles with a primary particle diameter of 25 nm were obtained when the lithium content was increased by 8-12 times, while rod-shaped particles of 5 nm

diameter and 60 nm length were obtained when the lithium content was increased 21 times. Cathodes made of these rod-shaped particles maintain discharge capacity under high rate conditions and is suitable for hybrid electric vehicle applications. [6]

1.2.6 Layered $LiNiO_2$ series (two dimensional)

The $LiNiO_2$ with low cost and high discharge capacity, 200 mAh/g, 40 % higher than that of LCO, has been a candidate cathode material for some time. However, it has a few shortcomings, namely outgassing when stored at high temperatures and decreased thermal stability while charged. As a solution to these problems developments were made and a $LiNiO_2$-based material was created, which became practical for use as cathode materials. Presumably, the material was stabilized by the addition of cobalt or aluminum. Furthermore the cathode surface is coated with a heat-resistance layer to improve thermal stability. The improved $LiNiO_2$-based cathode material, achieves 3,1 Ah capacity, with an energy density of 660 Wh/l and 248 Wh/kg. These properties make such a material suitable for electric vehicle battery applications. [6]

1.2.7 Layered Mn compound series (two dimensional)

Layered $LiMnO_2$ in itself is not practical as cathode material, however by adding other elements to form more complex compounds, such as $LiNi_{0,5}Mn_{0,5}O_2$ performance can be improved. This material still has poor discharge performance due to low conductivity, so research has turned to the ternary NMC system. Research revealed that NMC provides a high enough discharge capacity of 150 mAh/g together with well-balanced battery characteristics. The characteristics of this material are dependent on the method of synthesis. Conventional cathode materials with a single transition metal element are prepared by solid-phase method, where cobalt acetate and lithium carbonate are calcined at around 900 °C. For materials with multiple transition metal elements the stoichiometrical precision is crucial to obtain the intended crystal structure. Even slight variations can result in unwanted characteristics. During research both the solid-phase method and the solution method were explored. Stable characteristics were shown by using the solution method, where Ni, Mn, Co, and Li salts are mixed and dried, and then the mixture is calcined. The solid-phase method was affected by cooling conditions after calcination. In other areas of research within the Mn group are solid-solution materials described by the general formula Li_2MnO_3-$LiMO_2$. Several materials have been reported and researched, such as Li $(Li_{x/3}Mn_{2x/3}Co_{1-x})$ O_2 $(0 < x < 1)$ and Li $[Cr_xLi_{(1/3-x/3)}Mn_{(2/3-2x/3)}]$ O_2 $(0 < x < 1)$. These materials are still under research, where the first-charge electrochemical behavior, mechanisms of deterioration, mechanisms of high durability, mechanisms of high capacity, mechanisms of ion transport and the relationships between performance and the crystal structure is observed. [6]

1.2.8 Spinel structure cathode materials (three dimensional)

The spinel structure is generalized as AB_2O_4, with $MgAl_2O_4$ being a typical example. There are lithium ion tunnels in all three-dimensions through manganese oxide skeleton. LMO is not without shortcomings, low discharge capacity and the elution of manganese during charging and discharging as well as during storage at high temperature is an issue. However, the manganese elution can be suppressed by doping

at the Mn site with elements such as Al, Cr, Ti, and Ni, or by increasing the ratio of Li to Mn. Despite these shortcomings reasonable price and high safety characteristics make LMO an attractive cathode material for medium- and large- scale applications. [6]

1.2.9 Olivine structure cathode materials (one dimensional)

LFP is the most well-known olivine cathode material. Because of the one-dimensional crystal morphology, mobility of lithium ions is limited, resulting in low ion diffusion rate and low ionic conductivity. These problems were successfully overcome by producing the material in nano-particle form, also coating the cathode surface with a carbon layer and doping the material with a different element such as niobium. Whit this improved version of the material, the application in lithium-ion batteries for power tools and electric vehicles became possible. The LFP has a low cell voltage, which prevents improvement in energy density, therefore limiting its appeal in medium- and large- scale applications. Recently olivines such as $LiMnPO_4$ and $LiCoPO_4$ have been gaining attention with a cell voltage of 4,1 V and 4,8 V. [6]

1.3 Anode material

In 1995, the most common anode materials were graphite and hard carbon. The reason graphite gained such overwhelming dominance is the superior discharge rate compared to hard carbon. The discharge profile for lithium-ion battery anode made of graphite, has a curve characterized by a very broad, flat range (shown on Figure 1.2). For hard carbon the discharge profile is characterized by a steadily declining curve across the charge range, shown on Figure 1.3. For the rapidly spread mobile phones a flat discharge profile is preferable, meaning graphite became the dominant anode material. Among the various types of graphite, modified natural graphite has become the most common. Mostly because natural graphite is inexpensive, available, however its high reactivity to electrolyte prevents its use without modification. The most widely used technology is to coat the graphite surface with thin carbon layer. A more recent development in the anode market is the resurgence of hard carbon. It is making a comeback, due to its suitable use for HEV applications. [6]

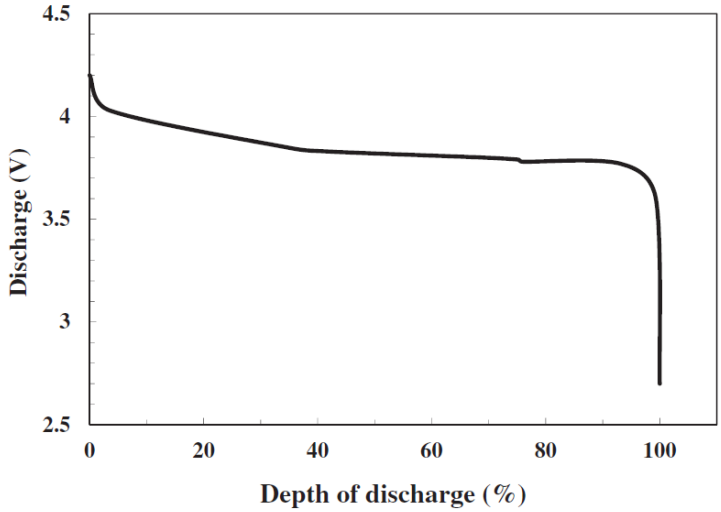

Figure 1.2 Discharge curve with a graphite anode. [6]

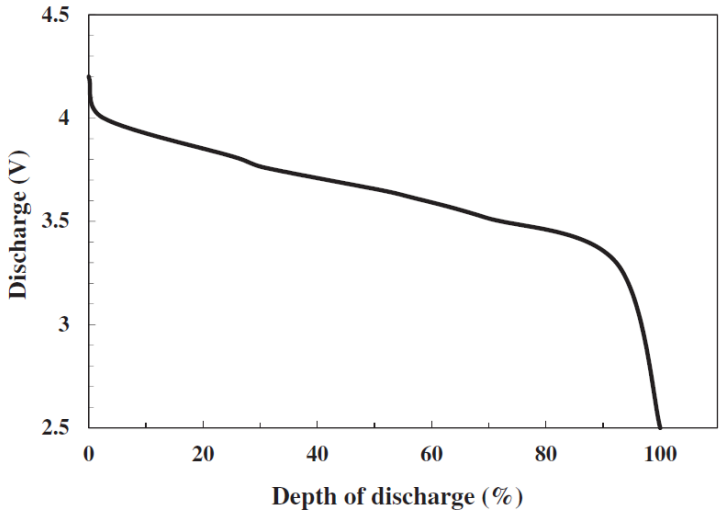

Figure 1.3 Discharge curve with a hard carbon anode. [6]

1.3.1 Recent research on anode materials

The further increase of capacity in graphite anodes have become nearly impossible. Further developments were made by using other new materials including metal oxides such as Co_3O_4, CoO, CuO, and FeO, and lithium metal alloys such as Cu-Sn-Li, Cu-Sb-Li, In-Sn-Li, Si-Li, and Si-C-Li. Figure 1.4 shows the discharge capacity of different lithium-metal alloys. These alloys provide much higher capacity than graphite, but a serious drawback is the large expansion and contraction of volume which occurs during the charge-discharge cycles. The volume expansion and contraction is shown on Figure 1.5. The formation of the material in nano-particles diminishes this problem. Another solution to this is using the material as a composite with carbon, such materials have begun to be adopted in practice. [6]

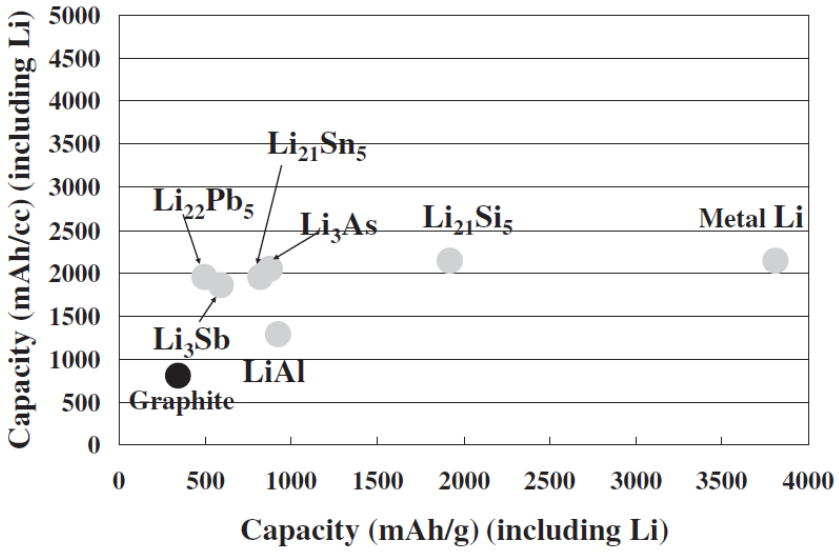

Figure 1.4 Theoretical discharge capacity of metal alloy anodes. [6]

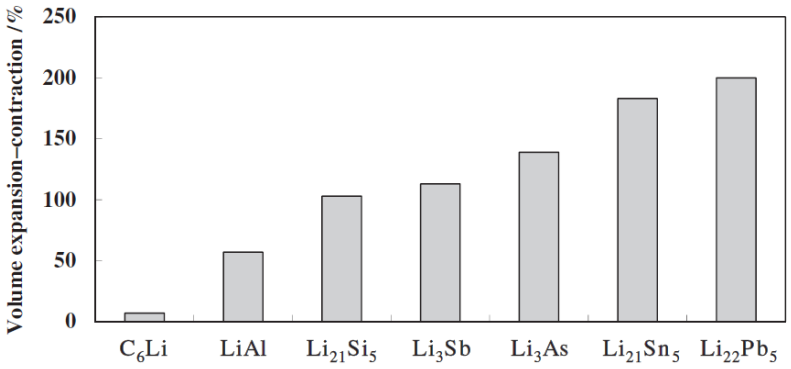

Figure 1.5 Volume expansion - contraction of metal alloy anodes at charge and discharge. [6]

1.4 Electrolyte solutions

The electrolyte for LIBs is a mixture of organic solvents and an electrolyte salt compound, most commonly mixtures of cyclic carbonate esters (ethylene carbonate, propylene carbonate), and linear carbonate esters (dimethyl carbonate, diethyl carbonate). The added salt compound is commonly $LiPF_6$ or $LiBF_4$. The free transport of lithium ions requires high dielectric constant and low viscosity. The required dielectric constant and viscosity can be achieved by mixing cyclic carbonate esters and linear carbonate esters. [6]

1.4.1 Recent research on electrolyte solutions

The most important areas during research are: functional electrolyte additives, flame-resistant or nonflammable electrolyte solutions, and new electrolyte salts.

The first group, functional electrolyte additives, are responsible for battery

performance improvements. The basic technology for the improvements is well established. Early example is the addition of propane sultone to the nonaqueous electrolyte solution of a rechargeable battery using a metallic lithium anode. Since then many different compounds have been used as additives, most notably vinylene carbonate, phenylcyclohexane, and fluoroethylene carbonate. The key aspect in search for new materials is the selection of additives and determination of their appropriate formulations. [6]

In order to create flame-resistant or nonflammable electrolyte solutions phosphate compounds are employed. This is done by using cyclic phosphoric acid ester as solvent or by adding a phosphazene compound as flame retardant. The other commonly used approach is to use halogen compounds, fluorine compounds (fluorocarbon ester, fluorinated ether) as solvent. The latest safety mechanism uses a flame retardant encased in microcapsules. The content of the capsules is released in case of battery malfunction. [6]

The latest improvements in the third area of research is the replacement of $LiPF_6$, however this introduces challenges in terms of performance and cost. Newly developed salts as candidates for use are shown on Figure 1.6. These compounds are currently under evaluation for commercialization. A very promising candidate is the lithium bis (oxalate) borate, due to its low costs and containment of no fluorine, alongside with availability and easy production from boric acid and oxalic acid. [6]

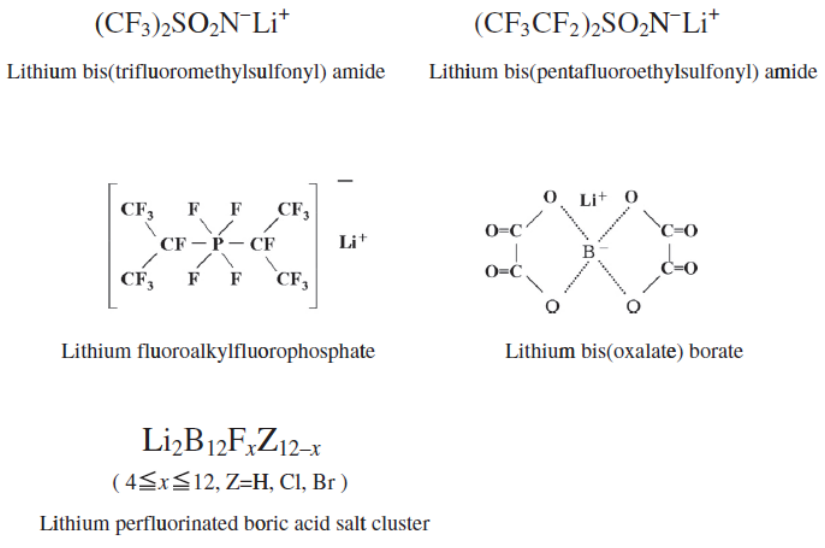

Figure 1.6 New electrolyte salt materials under development. [6]

1.5 Separators

The separator in lithium-ion batteries is a thin microporous membrane made of polyolefin. It is used to prevent contact between the anode and cathode, while enabling lithium ions to pass through. The three basic categories of separator are classified based on their production methods, with different morphologies and characteristics, each for different battery applications. The typical separators produced by each of the three methods are shown on Figure 1.7. [6]

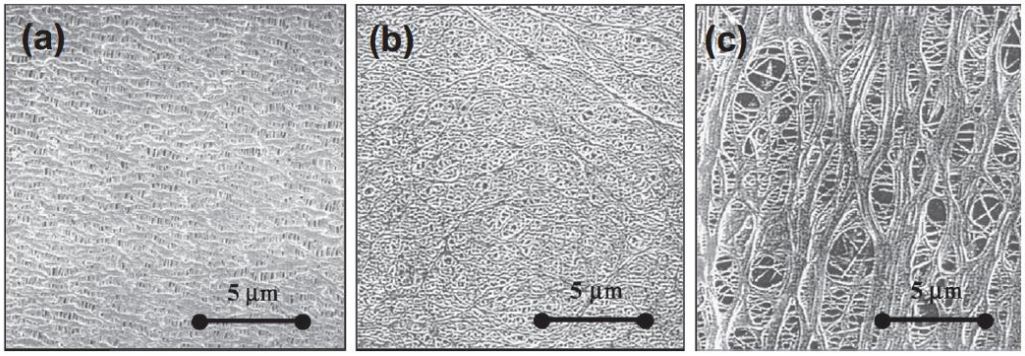

Figure 1.7 Pore characteristics (a) Dry-process one-component system (b) wet-process two-component system and (c) wet-process three-component system. [6]

1.5.1 Dry-process one-component system

The expression “dry process” means that no solvent is used, and it is a “one-component” system because only the polymer material of the membrane itself is used. The separator is produced extruding molten polymer as a thin film and its followed by the forming of pores around spherulites by stretching the film during its cooling process. This is a low cost procedure, requiring no additional processing. With this process the control of pore size and pore structure is limited, therefore control of physical characteristics is limited. Another important drawback is the difficult endowment of the safety shutdown function. [6]

1.5.2 Wet-process two-component system

The term “wet” indicates the use of a solvent to remove the plasticizer, and the term “two-component” describes the polymer and plasticizer present in the extruded mass. First the plasticizer is mixed into the polymer before extrusion. This process comes about in the microscopic regions within the molten bulk during cooling after extrusion, and it creates phase separation between the plasticizer and the polymer. The pores are formed by removing the plasticizer. The pore size and pore structure is controlled by selecting different polymer and plasticizer materials, which enables the production of separators with a wide range of physical characteristics. [6]

1.5.3 Wet-process three-component system

This is similar to the system with two-components, however particles of inorganic filler are also mixed into the polymer before extrusion. The removal of the plasticizer is also similar with the added particles of filler. The biggest difference in the end product and a significant advantage compared to the other systems is the size of the created pores. Larger pores provide greater ion mobility. [6]

1.5.4 Shutdown function

Most of the separators are designed to have a shutdown function. This function is achieved through different physical characteristics, which enable the polymer to melt, closing the micropores and thus preventing ion transport between the electrodes. This

function also prevents battery overheating, improving battery safety. The temperature at which the shutdown function engages is determined by the melting point of the polymer. Figure 1.8 shows the degree of impedance to ion transport at different temperatures for polyethylene and polypropylene separators. [6]

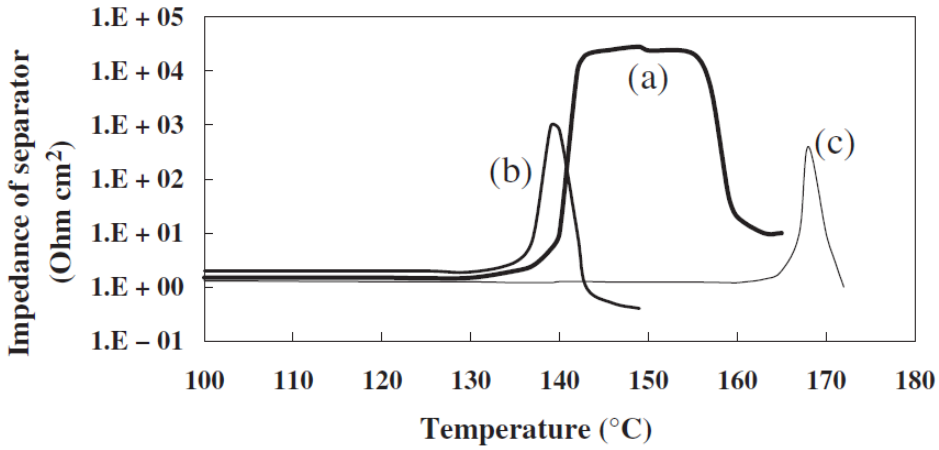

Figure 1.8 Shutdown temperature for polyethylene separators. Impedance (1 kHz AC) change of electrolyte-penetrated separators at elevated temperature (a, b) Polyethylene and (c) polypropylene. [6]

The rise in impedance at high temperature illustrates the closing of the pores. For polyethylene separators, the impedance rises (the pores close up) between 130 °C and 140 °C, while the melting point is 170 °C. The shutdown function does not engage until the battery reaches the above mentioned temperatures. The characteristics shown on Figure 1.8 are dependent on a complex combination of factors such as pore size, pore structure, and molecular weight of the polymer. [6]

1.5.5 New materials

Because of the limited heat resistance of polyolefins research shifted to separators made of different materials, such as heat-resistant rubber (silicone rubber, fluororubber), aromatic polyamide resin, liquid crystalline polyester resin, heat-resistant resin containing polyoxyalkylene, and resin with crosslinked groups. The expected properties from these materials are high temperature stability and superior ion transportation. [6]

1.5.6 Inorganic coating

The problem presented by polyolefin separators is the possibility of membrane rupture when battery temperature continues to rise after the shutdown function is engaged. To prevent this the membrane surface is coated with a heat-resistant inorganic layer (alumina, silica, titania, magnesia). For further improvements vitreous materials, antioxidant ceramic particles, clay minerals, metal salt compounds and tabular fillers can be included. As a binder to hold the layer onto the surface of the separator a heat-resistant resin is used, more specifically aromatic polyamide resin, polyimide resin, liquid crystalline polyester, and aromatic polyether. The addition of an inorganic layer with antioxidant properties improves stability on the side that contacts the cathode, preventing rupture of the separator at high temperature and during overcharging. These

coated separators have been used in limited commercial use, mainly applied in high-power lithium-ion batteries. [6]

1.5.7 Separators containing inorganic material

Reaching greater heat resistance can be done by mixing inorganic materials into the bulk of the separator, additionally increasing ion permeability. The used inorganic materials need to have antioxidant characteristics and resistance to the electrolyte solution. Alumina, silica, and titania are materials that meet these requirements. Another candidates are inorganic materials that absorb heat through dehydration reaction. This technology is applicable not only for polyolefin separators but also for those made from heat-resistant resin as described above. [6]

1.5.8 Nonwoven separators

As an alternative type of separator nonwoven fabrics have been considered, thanks to their low cost, high ion permeability and heat-resistance characteristics. Materials, like liquid crystalline polyester, aromatic polyamide and cellulose are great candidates. The biggest disadvantages in these materials, such as the thickness and too large pore sizes, prevent them to be used on their own. In order to reduce pore size a porous inorganic layer is added, which closes the larger gaps in the fabric. Materials studied for this purpose include alumina, silica, and titania. The forming of the nonwoven material with ultrafine fibers and special spinning technologies (flash spinning, electro-spinning) also reduce the pore size and thickness. [6]

1.5.9 Laminated separators

Another possible way to obtain the desired shutdown function and toughness is by lamination. For this conventional polyethylene and polypropylene microporous membranes can be used. The latest materials used for research are microporous membrane of liquid crystalline polyester, polyphenylene ether, aromatic polyamide, polyimide, polyamide imide resin, acrylic resin, and cross-linked polymer. With these material, theoretically, even greater heat resistance can be achieved. [6]

2 ELECTROCHEMICAL REACTIONS

This chapter contains the description of chemical reactions occurring in one battery cell. A schematic diagram of the cell is shown providing visual information about the chemical reactions, which are also described by chemical equations. The forming of the solid electrolyte interphase (SEI) is also described in this chapter.

2.1 Reactions in a lithium-ion cell

Figure 2.1 shows a schematic diagram of a lithium-ion cell. The positive electrode is made of lithium metal oxide ($LiMO_2$), where M stands for a metal such as Co, while the negative electrode is lithiated carbon (LixC). The active materials are connected to current collectors at both ends of the cell. The electrolyte between the active materials are electrically isolating and they are usually made of a microporous polymer or gel-polymer. Liquid or gel-polymer electrolytes enable lithium ions (Li^+) to diffuse between the positive and negative electrodes. The lithium ions are inserted into or de-inserted from the active materials through an intercalation process. [8]

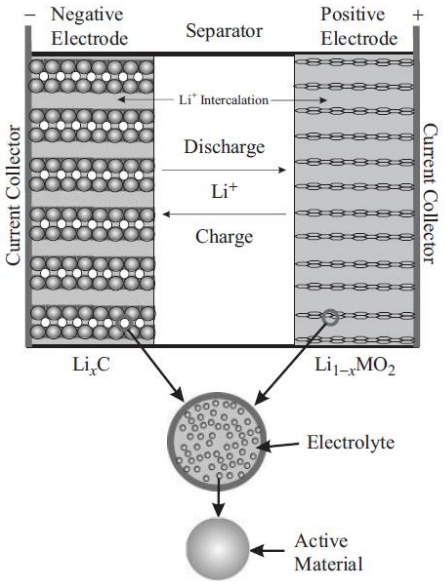

Figure 2.1 Schematic diagram of lithium-ion cell. [8]

During charge in the positive electrode the active material is oxidized and lithium ions are de-intercalated:

$$Li_{1-x}CoO_2 + xLi^+ + xe^- \xleftarrow{charge} \xrightarrow{discharge} LiCoO_2 \text{ . [8]} \qquad (2.1)$$

In the negative electrode during charge, the active material is reduced and the lithium ions that migrate from the positive electrode are intercalated in the reaction:

$$Li_xC \xleftarrow{charge} \xrightarrow{discharge} C + xLi^+ + xe^- \text{ . [8]} \qquad (2.2)$$

These reactions produce a theoretical cell voltage of 4,1 V, which is a higher value than the Ni-MH (Nickel-metal hydride) or lead-acid cells. The capacity of a lithium-ion

battery fades with cycling. This is due to the increase of internal resistance or impedance. Thanks to these ohmic losses, energy is wasted, heat is produced and the aging is accelerated. Losses in capacity can also be caused by the degradation of the positive and negative electrodes and the electrolyte. The degradation mechanisms are dependent on cell chemistry, design and manufacturing. In the negative electrode, the dominant aging mechanisms are: SEI growth, lithium corrosion, contact loss and lithium plating. [8]

The growth of the SEI leads to an impedance rise and the entraining of lithium atoms. The SEI layer forms at the beginning of cycling and grows during cycling and storage, especially at higher temperatures. Lithium corrosion causes capacity fade due to the irreversible loss of lithium. The corroding lithium is found in the active carbon material of the negative electrode. Contact loss means that the impedance of the cell increases by the disconnection of the SEI layer from the negative electrode. If the cell is at low temperatures with high charge rates, the lithium metal can plate on the negative electrode. This leads to irreversible loss of lithium. [8]

Recent studies show that impedance rise and capacity fade can be caused by the positive electrode. The rise in impedance and the capacity fade primarily happens during cycling. The discharge capacity may be limited by a decrease in active lithium intercalation sites in the oxide particles. A passivation layer also forms on the positive electrode which can change properties during cycling, resulting in cell impedance rise and power fade. [8]

2.2 Forming of the SEI layer

SEI is a ionically conductive, electronically not conductive polymer layer. A schematic representation is shown on Figure 2.2. This layer is created at the first formation by a strong reaction between the carbon anode and the electrolyte, which requires about 15-45 % of the total battery capacity. Maintaining stability, reduction of fluctuations during charging or temperature fluctuations is among the main characteristics of this layer, together with an effect on overall battery life. The thickness of the SEI layer varies over time. The increase in thickness contributes to a reduction in capacity. In materials that have a higher charge/discharge potential than lithium, the SEI layer thickness is much smaller. On the surface of materials like the LTO (where the charge/discharge potential is 1,55 times bigger than lithiums) the SEI layer is very thin, it can almost be completely ignored. [9]

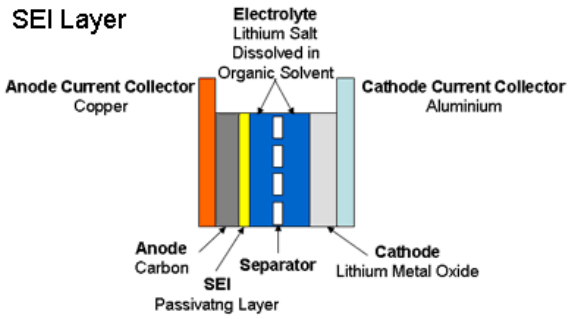

Figure 2.2 SEI layer. [2]

The major components of SEI layer are degraded products of electrolyte solvents and salts, which were identified by using spectroscopic analysis. The mentioned degraded products include Li_2CO_3, lithium alkyl carbonate, lithium alkyoxid and other groups of salts, such as LiF. Based on the layer composition two mechanisms were identified in the formation process while using an electrolyte with carbon solvents. An example of the SEI layer formation in an ethyl carbonate (EC) solvent is shown on Figure 2.3. [9]

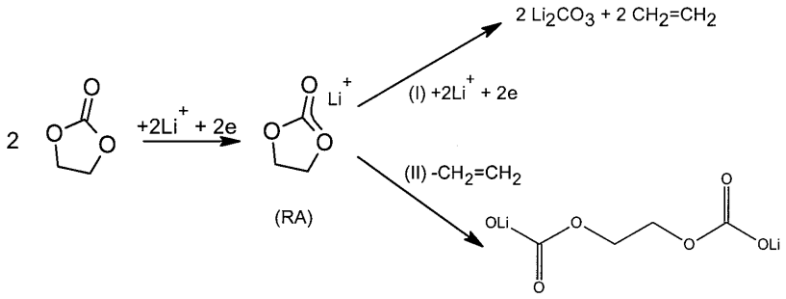

Figure 2.3 Formation of the SEI layer in EC solvent. [9]

Acronym RA on the figure means radical anion, it's the reactive compound in the solution. The formation of the SEI layer happens with both reactions present, as seen on the figure. With the domination of mechanism (I) the decomposition of the compound generates gaseous products, resulting in less stable Li_2CO_3 as the final layer. Mechanism (II), on the other hand, generates less gaseous products, forms a layer insoluble in the electrolyte. Another advantage of mechanism (II) is greater stability in the battery. These two mechanisms involved in the formation of SEI layer also depend on the graphite surface morphology. The layer formed on the edges of the surface is oriented towards pyrolytic graphite and is rich in inorganic compounds. In contrast, the middle layer is formed predominantly by organic compounds. [9]

The creation of the SEI layer can also be categorized into two stages. The first stage takes place before the intercalation of lithium ions into the graphite. This results in a structurally porous, highly resistive and dimensionally unstable layer. At the end of the second stage the layer is formed by the intercalation of lithium, producing a more compact and highly conductive layer. The capacity created in the second stage is connected not only to the reduction of the solvent molecules, but to the electrochemical reduction of functional surface groups on the side of the graphite as well. [9]

2.3 Additives for improving the SEI layer

The SEI layer formed before the intercalation of lithium is unstable and full of inorganic compounds. Furthermore, the formation is accompanied by the generation of gas. A possible method for suppressing this layer is done with a chemical coating on the graphites surface by a layer of organic film. These types of additives have a higher reduction potential than electrolytic solvents, and are selected because they are insoluble and protect the surface of the graphite against reaction within the electrolyte. Reduced generation of gas and an increased overall stability can be achieved with the use of these additives. Figure 2.4 shows possible additives, containing one or more double carbon-carbon bonds. [9]

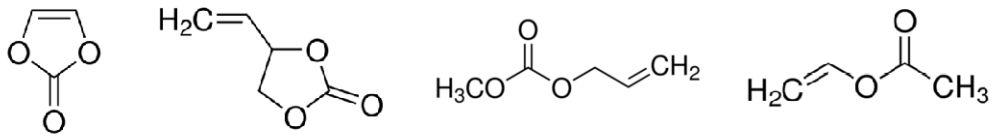

Figure 2.4 The chemical structures of the additives: a.) vinyl carbonate, b.) vinyl ethylene carbonate, c.) allyl ethyl carbonate, d.) vinyl acetate. [9]

During the creation of the SEI layer the products of reducing agents are absorbed into the graphite. The effectiveness of facilitating the formation of the layer depends on the molecular groups. These groups can help create the layer, they belong to the group of sulfuric compounds, including SO_2, CS_2 and others. Sulfuric compounds are not soluble in organic electrolytes and are unstable at higher potentials, resulting in self-discharge. This means that the amount of sulfuric additive has to be limited. Other usable types of reducing agents contain nitrogen, such as N_2O. [9]

The next type of additive is capable of devouring radical anions, which are undesirable solvents, or can combine products such as lithium alkyl dicarbonate, thereby creating a more stable SEI layer. The above mentioned improvements can be done with CO_2. Instead of CO_2 dialkyl pyrocarbonate is a possible additive, with a weaker solubility and higher pressure, capable of reaching higher conductivity within the SEI layer under lower temperatures. Other types of reagents, certain boron compounds increase the life of the battery, while LiBOB increases high-temperature parameters. [9]

Salts of alkali metals reduce the irreversible capacity, improving the holding of the capacity during cycling. SEI layer formed in the presence of Na_2CO_3 has a higher conductivity. The results of pretreated graphite in a solution containing Na_2CO_3 is shown on Figure 2.5. This figure shows reduced irreversible capacity and reduced possibility for Li^+ intercalation and de-intercalation in the graphite structure. [9]

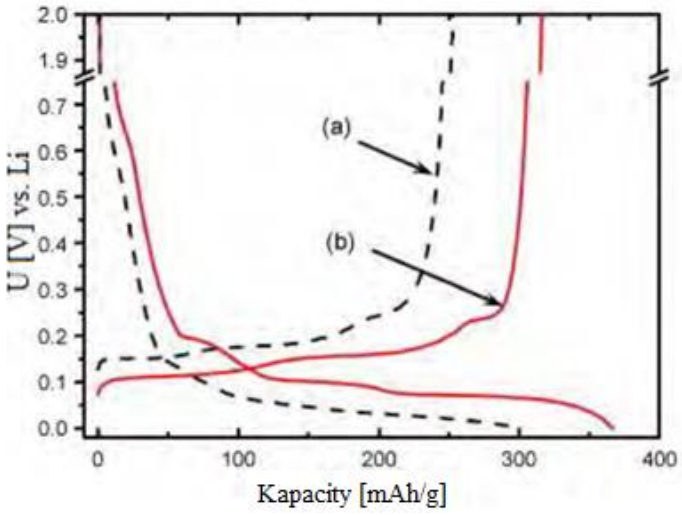

Figure 2.5 Characteristics of the graphite, (a) without pretreatment, (b) pretreatment with Na_2CO_3. [9]

3 PERFORMANCE COMPARISON

This chapter contains the comparison between the most popular types of batteries. For each type of battery (lead-acid, nickel-metal hydride and lithium-ion batteries) a description about the energy density, charge and discharge characteristics, cycle life and information about the temperature operating range is included.

3.1 Energy density and specific energy

The key categories of the comparison are shown in Table 3.1. The electrode materials determine the theoretical voltage, while the practical voltage is what can be achieved in a real battery. For lead-acid and lithium-ion batteries the practical values and the theoretical values are essentially the same, however the nickel-metal hydrnide (Ni-MH) batteries show a 10% difference. Following the previous values the specific energy is listed, which is the energy storage capacity in watt-hours (Wh) divided by the mass of the battery in kilograms (kg). Equivalent weight of the active materials participating in the electrochemical reaction determines the theoretical capacity in ampere-hours/gram (Ah/g). Multiplying the theoretical capacity and voltage gives the theoretical specific energy in Wh/kg. [8]

Table 3.1 lists a number of properties, and in most of them the lithium-ion battery excels over the lead-acid and nickel-metal hydride batteries.

Table 3.1 Comparison of lithium-ion, lead-acid and nickel-metal hydride performance. [8]

	lithium-ion	nickel-metal hydride	lead-acid
Theoretical			
Voltage [V]	4,1	1,35	1,93
Specific energy [Wh/kg]	410	240	166
Practical			
Specific energy [Wh/kg]	150	75	35
Energy density [Wh/L]	400	240	70
Coulometric efficiency	>0,85	0,65 - 0,70	0,80
Energy efficiency	~0,80	0,55 - 0,65	0,65 - 0,70
Specific power, 80% DOD [W/kg]	350	150	220
Power density [W/L]	>800	>300	450

An important metric for batteries, listed in Table 3.1, is the energy storage efficiency. This can be determined by two metrics: coulometric efficiency and energy efficiency. Coulometric efficiency:

$$f = \frac{\int_{discharge} Idt}{\int_{charge} Idt}, \tag{3.1}$$

where I (t) is the battery current and t is time. Energy efficiency:

$$\eta = \frac{\int_{discharge} IUdt}{\int_{charge} IUdt}, \tag{3.2}$$

where V(t) is the battery voltage. Lithium-ion has the most efficient chemistry followed by lead-acid and nickel-metal hydride. [8]

3.2 Charge and discharge

Charge and discharge operation regulates the speed of current put into and taken from storage, this is called dynamic performance. The terminal voltage rises and falls during steady charging and discharging. At the end of charging or discharging the transient voltage response settles out, for sufficient long charges, the battery voltage saturates at a maximum value. These are overcharged situations, where most of the input energy goes to heat losses or harmful side reactions. [8]

Similarly, undercharge occurs when the battery voltage falls below the end or cut-off voltage causing damage to the battery. The state of charge (SOC), defined as the percentage of maximum possible charge that is present inside a rechargeable battery, determines the working range of a battery. A fully charged battery is at 100 % SOC, however a more practical example would be 30 to 70 % SOC with a Ni-MH battery in hybrid electric vehicle (HEV) applications having a very high coulometric efficiency. The depth of discharge (DOD = 100 % - SOC) is another way to quantify stored charge. [8]

Measurements of voltage under constant charge and discharge current inputs characterizes the charge and discharge dynamics of batteries. The rate of charge or discharge is measured relative to the battery capacity C, meaning that a 0,1 C discharge rate for a 5 Ah battery is 0,5 A or a 2 C discharge rate for a 10 Ah battery is 20 A. Figure 3.1 shows discharge plots at low, medium, and high rates. [8]

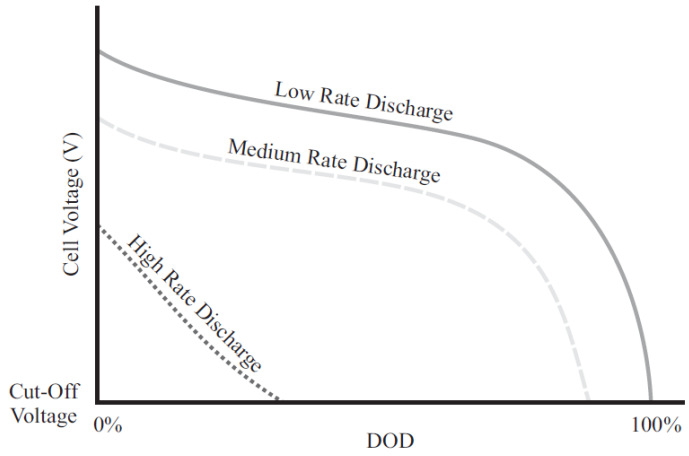

Figure 3.1 Example voltage curves for different discharge rates. [8]

The low rate curve approximates the equilibrium cell (or open-circuit) potential.

For the voltage to remain constant during discharge the optimal open-circuit potential curve is flat over a broad range of DOD. This simplifies the design and reduces the cost of the added voltage-regulation circuits. Due to ohmic losses over the entire DOD range the medium rate discharge curve shifts downward. Charge transfer kinetic losses and mass transport limitations at low and high DOD are also responsible for the discharge curve to shift downward. [8]

The high rate discharge case demonstrates that only a fraction of the capacity can be utilized at high discharge rates due to quick voltage drops. A good way to summarize the statistics for battery discharge performance is with specific power (W/kg) and power density (W/L). These values are shown in Table 3.1, where lithium-ion has the highest specific power and power density. [8]

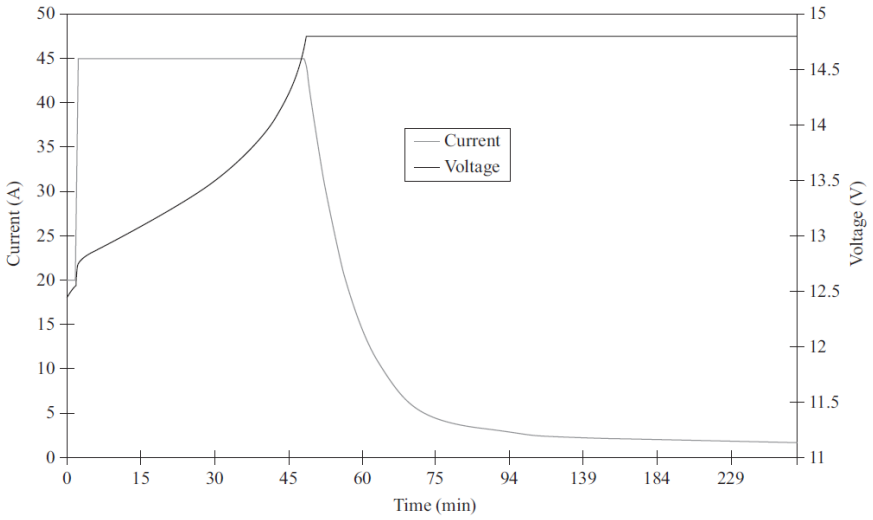

Figure 3.2 Constant-current and constant-voltage charge curves. [8]

Charging batteries replaces the energy expended during discharge, either by controlling current or voltage, not both. Typically charging is made up of periodicly changing constant current (CC) or constant voltage (CV). Figure 3.2 shows an example CC-CV charging profile for a lead-acid battery. A battery with low SOC is charged by applying a CC charge to bring the voltage up to the CV level. When the desired voltage level is achieved the charger switches to CV mode ending in a decreased current reaching 100 % SOC. In order to minimize potential damage to the battery and maximize life, safety, and efficiency, chargers use multiple CC and CV steps of different current and voltage levels. Lead-acid, nickel-metal hydride, and lithium-ion batteries can all be CC charged. The slight overcharge of lead-acid and nickel-metal hydride batteries can be tolerated, however lithium-ion batteries are irreversibly degraded and may vent during overcharge. The CC-CV method shown in Figure 4.3 is recommended for lead-acid and lithium-ion batteries, however the nickel-metal hydride batteries require CC approach with stepped or tapered current. [8]

The charge acceptance dictates how fast the battery can be charged. The three types of batteries mentioned are recommended to be charged at C/3. [8]

3.3 Cycle life

The most reliable way to determine cycle life is to test several batteries from the same batch. Test results depend on battery chemistry, discharge-charge cycle, temperature, prior history of storage and manufacturer, and are conducted on a cycling machine that repeats a prescribed current trajectory representing a typical cycle. During the testing process one of the batteries is randomly selected from cycling to be tested for capacity. This way, a plot of capacity versus number of cycles can be obtained. Generally all batteries have longer life for lower depths of discharge (DOD) cycles. At 100 % DOD Li-ion batteries typically last 3000 cycles at low charge/discharge rates and room temperature. A 20-40 % DOD, however can last 20 000 cycles. Other types of batteries, like the nickel-metal hydride and lead-acid batteries only last a few hundred cycles at 80-100 % DODs. The end of life is characterized by a drop in capacity by 50-80% from the initial capacity, depending on the chemistry and application. [8]

3.4 Temperature operating range

The use of batteries at extremely low or high temperatures is not optimal. Problems occurring at low temperature are tied to ionic diffusion and migration with possible lithium plating. The battery used in higher temperatures is exposed to corrosion and gas generation. For lithium-ion and lead-acid batteries, charge and discharge temperatures should be between -40 and 60 °C. The operating range for nickel-metal hydride batteries is a bit narrow, it's between -20 and 45 °C. [8]

4 MATERIALS USED FOR ELECTRODES

The most commonly used material for the negative electrode is graphite, usually on a copper collector. Other forms of carbon have not been used due to their worse properties, such as capacity, irreversible capacity and number of cycles. Graphite allows an intercalation of one ion for six carbon atoms, which gives a theoretical capacity of 372 mAh/g. The diffusion rate of lithium into the graphite is between 10^{-9} and 10^{-7} cm^2s^{-1}, which means that the graphite has a low energy density. [11]

Due to the extremely small expansion and contraction during charge and discharge cycles of the battery the attention shifted towards LTO (lithium titane oxid).

4.1 Lithium titanate oxid (LTO)

LTO has a relatively high density, good adhesion to the electrode and has better overall properties than the graphite electrode. It operates at a potential of 1,55 V vs. Li/Li^+. This material can be used in combination with high-voltage positive electrodes and super capacitors up to a couple hundred Farads. In use with low voltage applications LTOs potential (1,55 V vs. Li/Li^+) poses a major disadvantage. For these applications electrodes made of graphite are more suitable. [11], [12], [13]

The electrochemical properties of LTO are highly dependent on the purity, composition, morphology, crystallization and surface area of the material. With the appropriate synthesis these properties can be highly influenced. LTO can be synthesized by a variety of methods, including solid, gel, hydrothermal and microwave methods.

The solid synthesis takes place at temperatures between 800-1000 °C for 10 to 24 hours. The optimal calcination atmosphere is made of hydrogen and nitrogen. Hydrogen atmosphere is used to increase the diffusion of oxygen ions during heat treating, while under nitrogen the initial burning is carried out. During the initial burning as a reducing agent TiO_2 alongside with carbon is used. There are two important disadvantages with this method: it does not provide a sufficiently small particle size and the homogeneity of the material is inadequate.

With gel synthesis high homogeneity and submicron particle sizes can be achieved. The heat treating process takes place in a temperature range from 700-800 °C. With the use of acetic acid and citric acid cyclability and the current load capacity of the LTO is changed.

Hydrothermal synthesis is more economical method for providing a nano-structured material. This process is easier to control and provides various structures. The most appropriate for lithium-ion batteries is the "nanoflower-like" structure, with a basic material of TiO_2 (with a thickness of 400 nm) and LiOH. By using various additives different thicknesses and electrochemical properties can be achieved.

Compared to the already mentioned methods, microwave synthesis can be conducted at low temperatures, it has a rapid volumetric heating process and a shorter reaction time. For the radiation 2,45 GHz is used. [12]

4.1.1 Properties of LTO

When the lithium intercalates and deintercalates into the structure of LTO only a minimal change occurs in the dimensions of the structure, up to 0,2 %. Lithium ions only occupy as much space as is their size, so LTO does not change its structure when ions enter or leave. This feature helps to maintain the structural stability with minimal difference during cycling, resulting in a long life cycle. With electrolyte $LiPF_6$, LTO forms a relatively clean interface. However the SEI layer is not formed, because the potential 1,55 V vs. Li/Li^+ is much higher than the reduction potential of the solvent. The high potential of LTO has a positive effect on the safety of batteries. [12], [15], [16]

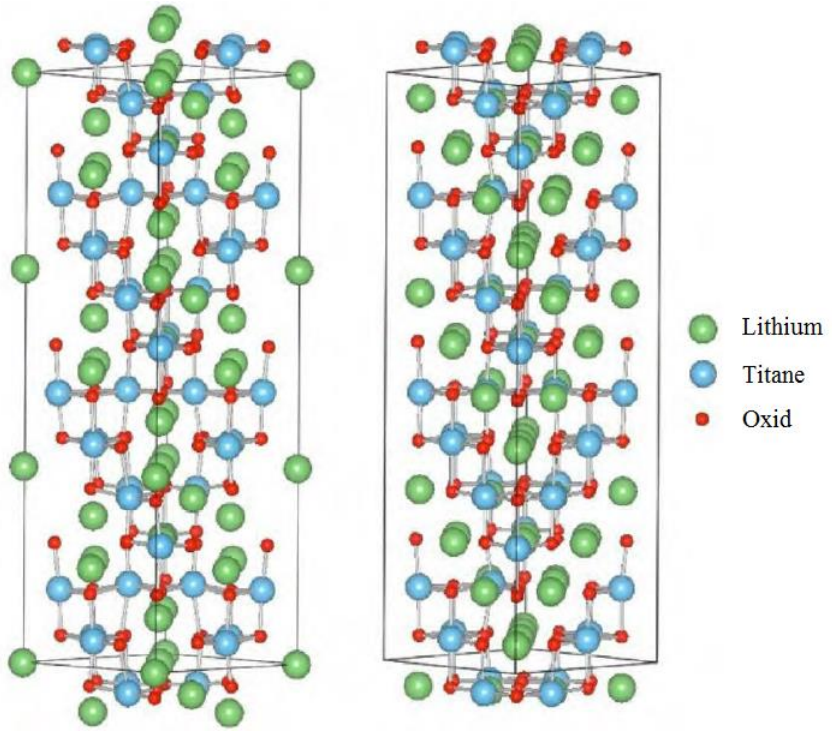

Figure 4.1 The structure of $Li_4Ti_5O_{12}$ (on the left) and $Li_7Ti_5O_{12}$ (on the right). [17]

LTO has a cubic spinel structure, more specifically $Li_4Ti_5O_{12}$. After lithium intercalation, it structurally changes into $Li_7Ti_5O_{12}$, which is a structured rock salt. By the insertion of lithium ions into the structure below 1 V vs. Li/Li^+ there is a large volume expansion. The band gap is 2-3 eV, which means that the LTO has an insulating character. One mol of LTO can accept 3 mols of Li^+ ions. The theoretical capacity is 175 mAh/g. The chemical reaction for this is:

$$Li_4Ti_5O_{12} + 3Li^+ + 3e^- \Leftrightarrow Li_7Ti_5O_{12}\,.\,[12] \qquad (4.1)$$

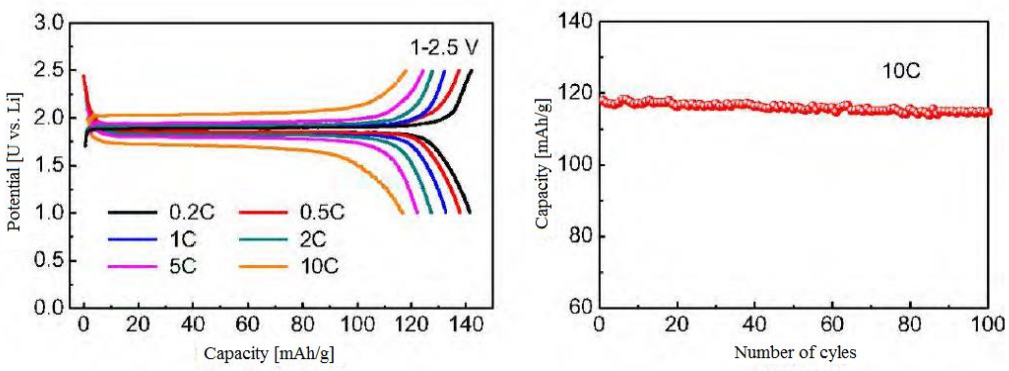

Figure 4.2 Typical charge/discharge characteristics. [18]

Figure 4.2 shows, that with an increasing speed (higher charging current), the capacity of the negative electrode decreases. With the increasing number of charge/discharge cycles the capacity of the negative electrode decreases from about 118 mAh/g to 115 mAh/g after 100 cycles.

4.2 Natural graphite

Naturally occurring graphite is formed in a hexagonal shape. These shapes contain six atoms of carbon, each at the point of the hexagon closing a 120° with each other. The crystal structure of the graphite is made of stacked up graphene layers, which are held together by van der Waals forces with an energy of 0,2 eV/atom. The distance between each atom is 142 pm, while the distance between layers is 335 pm. Graphite can be easily identified with a physical appearance of a soft, dark grey material. Other important properties are the excellent conductivity of heat and electricity, furthermore it is resistant to a lot of chemicals. Graphite retains these properties up to 3500 °C. Figure 4.3 shows the above mentioned crystal structure. [19]

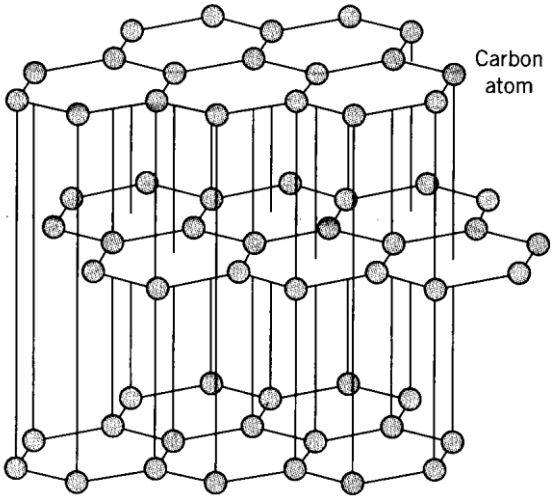

Figure 4.3 Hexagonal structure of graphite. [21]

The two types of naturally occurring graphite can a have macro, or micro crystalline structure. The two forms of graphite, having a macro crystalline structure, are called flake form and vain form. [25]

Graphite in the form of vain is the rarest and most valuable type. This type can be found in high-altitudes, because of its purity it's very desired. Despite the purity of the vein form, the most known and used is the flake type. It occupies almost 40 % of total market and it's mined in China, Brazil, Canada and Africa. The pure graphite in the flake type is between 5 % and 40 %. As the name suggests the material is made of flakes, which are approximately 2,5 mm wide. After mechanical, thermal or chemical treatment the flakes can achieve a few micrometers in width. The most important properties are good thermal and electrical conductivity, chemical inertness, small thermal expansion, compressibility and it's also non-toxic. By using mechanical separation and flotation a 99,5 % of purity can be achieved. To achieve greater purity chemical or high temperature treatments are necessary. [25]

Figure 4.4 Natural graphite in the form of vein (on the left) and flake (on the right). [22], [23]

Microcrystalline graphite is the most frequent form and it occupies approximately 60% of the market. The carbon content in some cases reaches 75%. This type of graphite is created by converting anthracite coal seams and is often called amorphous graphite, because the typical graphite morphology, like the vein and flake forms, are not visible. During the purifying process it's very difficult to separate it from coal, resulting in a lower grades and prices. Other components are separated by flotation and chemical methods. The level of purity can reach 75 to 85 %, with good conductive properties and chemical stability. It is mostly used in lubricants and greases. [25]

Expanded graphite is a special form of flake graphite created by the intercalation of strong acid anions. This process separates the graphene plates in the atomic structures. Afterwards, with immediate heating, the anions are evaporated and the crystalline structure is cut into 100 nm thick plates. [25]

With this process the graphite expands up to 300 % of its original volume. For use in batteries the expanded graphite is grinded into fine powder. Thanks to its characteristics such as compressibility, chemical resistance, excellent thermal conductivity it can be used in many different branches of industry. Expanded graphite is characterized by large capacities and high electrical conductivity. [25]

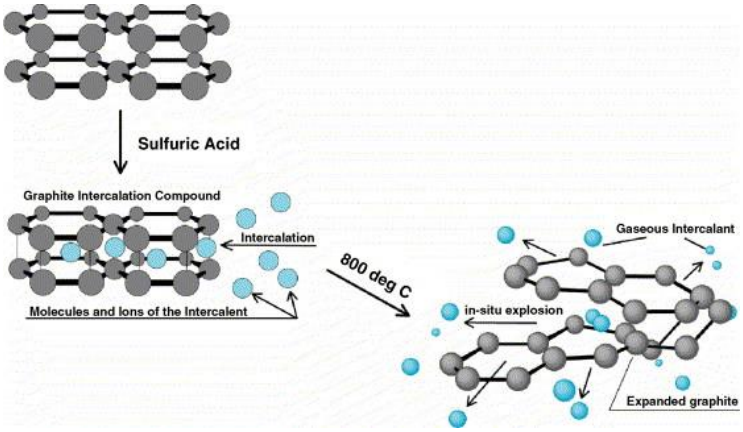

Figure 4.5 Expanded graphite. [20]

The methods used for creating expanded graphite differ mainly in the synthesis part, where the acid intercalates into the graphite. These methods can be divided into chemical, gas, liquid and electrochemical intercalation, where the presence of an oxidizing agent with low redox-potential is essential. The following oxidants may be used: CrO_3,$K_2Cr_2O_7$, HNO_3, $KMnO_4$. At the beginning of the process the oxidants (Ox) modify the composition of the acid on the surface carbon layers of the graphite. During the process Cp^+ cation is produced between the carbon layers, and the created conditions allow for the solicitation of acid anions. At the end of the process specific locations are filled with sulfuric acid and nitric acid, described by the chemical equation:

$$24nC + Ox^z + mH_2SO_4 \rightarrow C_{24n}{}^+.HSO_4{}^-.(m-1)H_2SO_4 + HOx^{(z-1)}. \text{ [26]} \qquad (4.2)$$

4.3 Synthetic graphite

Synthetic graphite can be produced from materials containing carbon or from pure carbon, however not all types of carbon can be used. The process of graphitization includes the restrictions on movements and new arrangements of carbon atoms, which undergoes the transformation during a thermal process. Formation of graphite from the amorphous carbon requires movements in three planes in the graphite matrix. The degree of movement is very important during the heat treatment, when the carbon changes into liquid. In this phase, the molecules are capable of moving and creating the graphite structure. During the above mentioned process a lot of the materials properties change. The resistivity, density, weight and elasticity decreases, while the thermal and electrical conductivity increases. [27]

Carbon materials that can temporarily change into a liquid form are referred to as soft carbon, while hard carbon cannot be graphitized. Suitable forms of carbon for the heat treatment are found in coal tar, oil and other substances. The mentioned materials are good to form graphite, because they contain relatively small amount of hetero-atoms (another type of the atom in the substance, such as oxygen, nitrogen), they have low molecular weight and they melt in an acceptable range of temperature. Industrially employed processes are Acheson graphitization, Castner process, Desulco® process and others. [27]

Typical expansions during graphitization:

• Room temperature, until the start of the heat treatment, no changes.

• 900 - 1200 °C: after passing the calcining temperature the filler components are slowly starting to form the graphite structure.

• 1500 - 2000 °C: at this point hydrogen and sulfur is released from the binder, this leads to irreversible volume expansion.

• Above 1800 ° C: The creation of graphite structure is accelerated.

• Above 2600 ° C: Volume expansion is slowly stops and the forming of the crystalline structure starts.

• 3000 ° C: Thermal and electrical conductivity achieves optimal values.

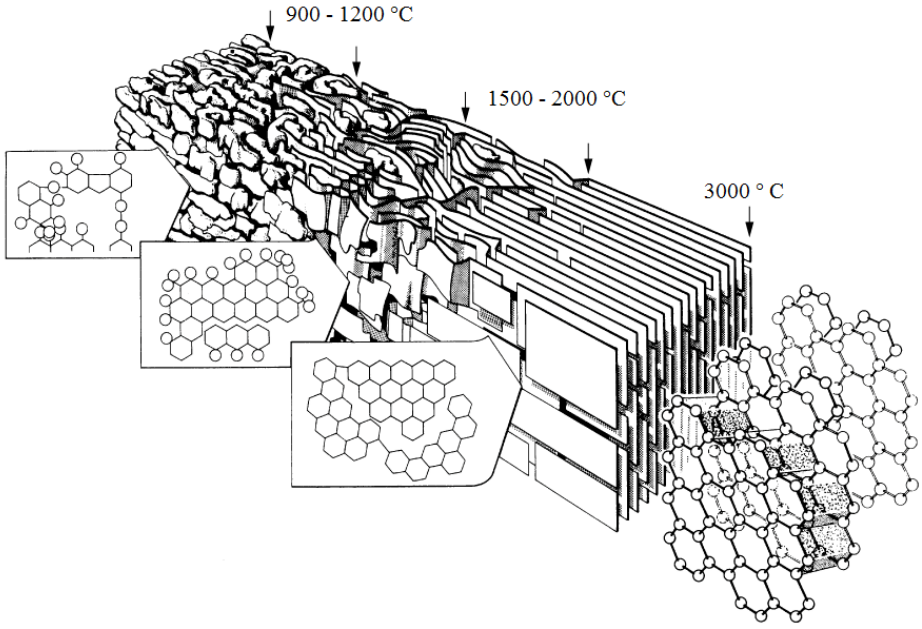

Figure 4.6 Changes in the structure. [28]

The Acheson graphitization process produces graphite powder of high purity. The storage is set into blocks placed horizontally to the bed of the furnace. The space between these segments is filled with resistive material, consisting of cox and graphite in a granulated mixture. Current is supplied through two water-cooled electrodes on the sides of the furnace which is also thermally insulated by cox and sand, while protecting the material against oxidation. With increasing graphitization, the electrical resistance of the furnace decreases, so the main electrode must be constantly monitored. The furnace temperature can reach 2800 °C in several days, and depending on the size of the furnace, one operating cycle lasts two to three weeks. The furnace is shown on Figure 4.7. [28]

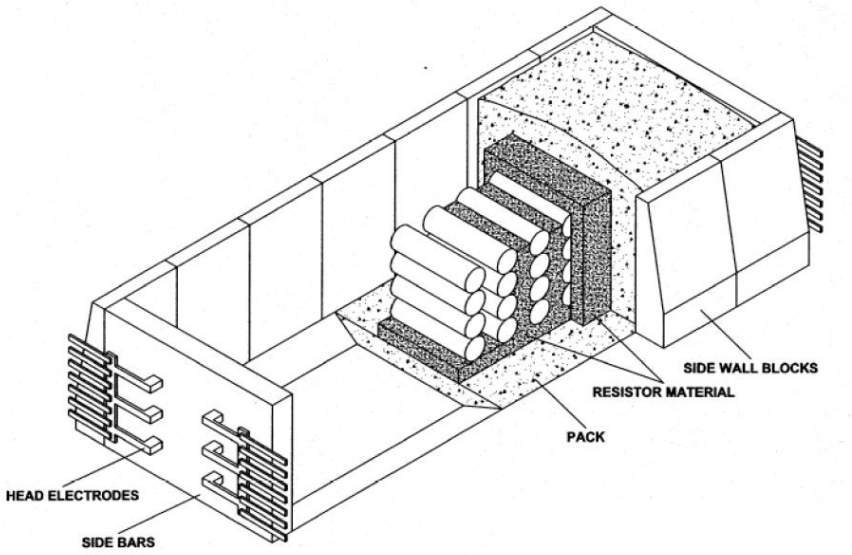

Figure 4.7 Acheson furnace. [28]

The Castner (lengthwise, longitudinal array graphitization) furnace is characterized by the direct connection of the stock in a row, without a resistor material in between. This type of furnace is shown on Figure 4.8. The current directly passes through the artifacts, which are clamped between the head electrodes of the furnace to heat it up. The graphitized materials contact area has to fit well, it requires plane-parallel machining and an adjustable clamping device. With this construction a secure and constant, tight electrical contact is made with a low-contact resistance. The insulation against oxidation and high heat losses is identical to the Acheson furnace. This graphitizing method has the advantage of shorter heating periods, less power consumption and smaller furnace dimensions. [28]

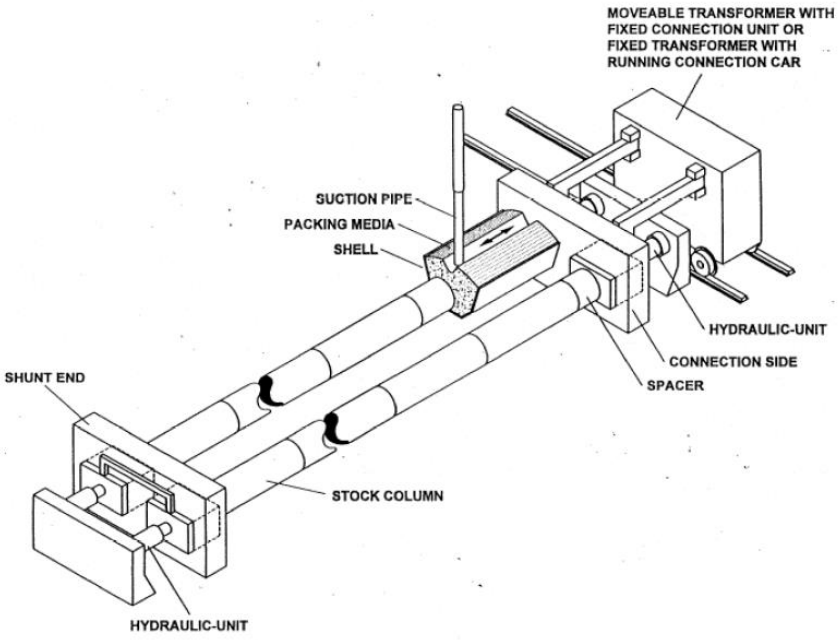

Figure 4.8 Castner furnace. [28]

5 BINDERS

In the production of lithium ion battery electrodes, the binder plays an important role. It not only binds the active materials and the conductive additive to the current collectors, but also strongly affects the electrode processing and the electrochemical performance of the laminate. Polyvinylidene fluoride (PVDF) is the generally used binder, which requires the use of the volatile, organic compound N-methyl pyrrolidone in its application. Recently, sodium salt of carboxymethyl cellulose (CMC) and styrene-butadiene rubber (SBR) have been introduced as a suitable replacement in the manufacture of lithium ion anodes. The use of the water soluble binder system leads to a cheaper and greener electrode processing. [29]

5.1 Polyvinylidene fluoride (PVDF)

Polyvinylidene fluoride (PVDF) is a highly non-reactive and pure thermoplastic fluoripolymer. It is produced by the polymerization of vinylidene difluoride and is used in applications requiring the highest purity, strength, and resistance to solvents, acids, bases and heat. Compared to other fluoropolymers, it has a lower melting point, around 177 °C, also a lower density (1,78 g/cm^3). It is available as piping products, sheet, tubing, films, plate and an insulator for premium wire. It can be injected, molded or welded and is commonly used in the chemical, semiconductor, medical and defense industries, as well as in lithium ion batteries. The Structural schematic is shown on Figure 5.1. [30]

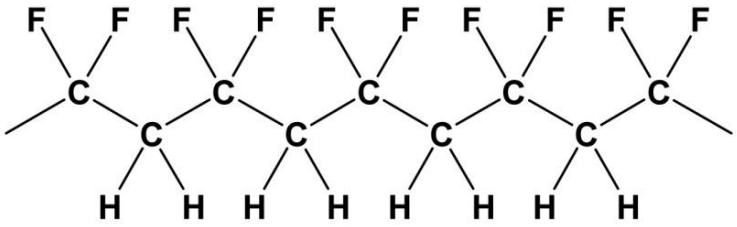

Figure 5.1 Polyvinylidene fluoride (PVDF). [31]

Strong piezoelectricity was observed in PVDF, ten times larger than in any other polymer. During the observation PVDF was placed under a strong electric field to induce a net dipole moment. The poled thin films had a piezoelectric coefficient of 6-7 pC/N. [30]

PVDF has a 50-60 % crystalline structure with a glass transition temperature (Tg) of - 35 °C. The material is mechanically stretched to orient the molecular chains and then poled under tension to achieve piezoelectric properties. When poled, PVDF also has ferroelectric polymer and pyroelectric properties, making it useful in sensor and battery applications. [30]

PVDF can be used as binder material in the production of composite electrodes for lithium ion batteries. A weight solution of 1-2 % PVDF dissolved in N-methyl-2-pyrrolidone (NMP) is mixed with an active lithium storage material (graphite, silicon, tin, $LiCoO_2$, $LiMn_2O_4$, $LiFePO_4$) and a conductive additive (carbon black, carbon

nanofibers). This slurry is cast onto a metallic current collector and the NMP is evaporated to form a composite or paste electrode. The advantage of using PVDF is that it is chemically inert over the potential range used and does not react with the electrolyte or lithium. [30]

PVDF can be used in a variety of situations, such as insulation on electrical wires, tactile sensor arrays, inexpensive strain gauges, lightweight audio transducers. In the biomedical sciences PVDF is used in immunoblotting as an artificial membrane. [30]

5.2 Styrene-butadiene rubber (SBR)

Styrene-butadiene or styrene-butadiene rubber (SBR) is derived from styrene and butadiene, a type of synthetic rubber. These materials have good abrasion resistance and good aging stability when protected by additives. SBR is not to be confused with athermoplastic elastomer made from the same monomers, styrene-butadiene block copolymer. [32]

Latex (emulsion) SBR is extensively used in coated papers, being one of the cheapest resins to bind pigmented coatings. It is also used in building applications, as a sealing and binding agent behind renders, an alternative to PVA. SBR can be used to 'tank' damp rooms or surfaces, a process in which the rubber is painted onto the entire surface (sometimes both the walls, floor and ceiling) forming a continuous, seamless damp-proof liner; a typical example would be a basement. It is also used by speaker driver manufacturers as the material for Low Damping Rubber Surrounds. Additionally, it is used in some rubber cutting boards. [32]

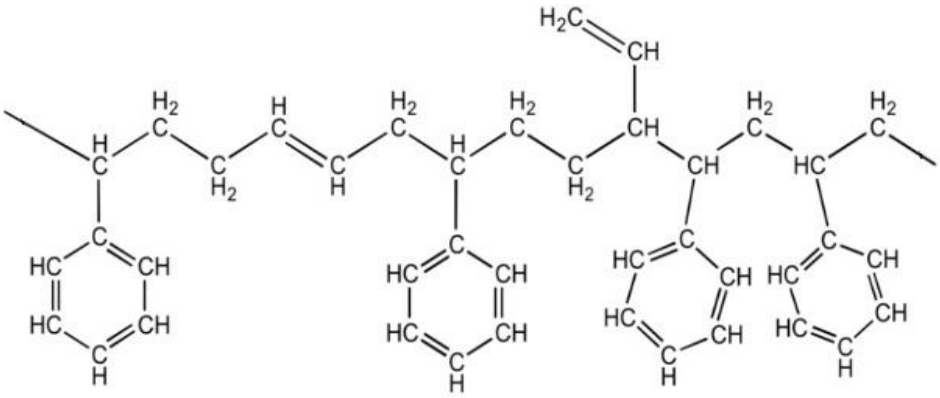

Figure 5.2 Structure of Styrene-butadiene. [33]

The structure is shown on Figure 5.2. A possible way of using SBR as a binder is to use it together with carboxymethyl cellulose (CMC). The active material would be mixed with approximately 2 % CMC aqueous solution, additionally with a 4 % of SBR. [34]

5.3 Polyimide P84

The P84 polyimide can be produced in different forms. The base material for P84 fibres is composed of aromatic backbone units. Despite the non melting aromatic, halogen free structure it is classified as non flammable. P84 fibers are used as filter media for high temperature filtration, protective clothing, sealing materials for space craft and high temperature applications such as thermal insulation. [35]

Another form is a solution of P84, a fully imidized polyimide. It is used for coatings in the electric and electronics industry, due to its low dielectric constant or high dielectric strength. Available solvents are dimethylformamide (DMF) or N-methyl pyrrolidon (NMP) or N-ethyl pyrrolidon (NEP). [35]

The third form of P84 is polyimide powder. This powder shows typical properties of polyimide, high temperature stability up to 350 °C, chemical resistance, high mechanical strength, a low friction coefficient and minimal abrasion. It can be used in industrial applications, such as automotive industry, aerospace applications and office machines. [35]

6 METHODS FOR MEASUREMENT

One of the basic electronic hardware required for the measurements is called a potentiostat. The system maintains the potential of the working electrode at a constant level. This equipment is used in electrochemical studies, measuring redox chemistry and other chemical properties. Early versions functioned on their own, providing data output through a physical data trace, while the modernized versions are used together with a personal computer operating with the help of a software. The potentiostat varies the current supplied to the system, with higher resistance the current decreases, with a lower resistance the current increases, in order to keep the voltage constant. [36]

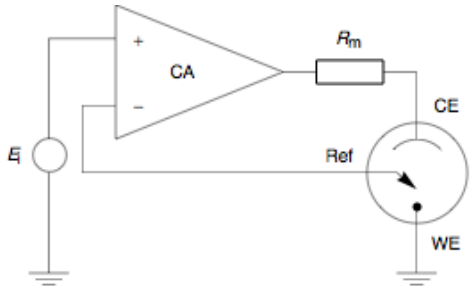

Figure 6.1 Schematic of a potentiostat. [36]

Another device used for these measurements is a galvanostat. This device is capable of keeping the current even through an electrolytic cell, disregarding changes in the load itself. It has an extremely high internal resistance and can supply and measure pico-amperes to amperes of both polarity. [36]

6.1 Cyclic Voltammetry

Cyclic voltammetry is characterized by continuously growing potential from one limit to the other and back. This means that the parameters in the experiment are the adjustable limits and the speed of the potential growth. The result of this method is the polarization curve (the dependence of current flowing through the electrode on its potential). This method gives us information about each current producing reaction in the analyzed material. [37]

6.2 Galvanostatic Cycling with Potential Limitation

This method simulates the cyclic charging and discharging of a battery. Through the measured sample a defined current passes, which is potentially limited. This happens both for charging and discharging cycles. During cycling (alternating each charge and discharge cycle) a potential (open circuit voltage) is recorded, or after some time a constant potential can be applied, until it reaches the limit potential. The output data represents the stability (cyclability) and the battery capacity. [37]

7 PREPARING THE NEGATIVE ELECTRODE

The process of preparing the electrode can be divided into several phases. The first phase is the preparation of the electrode mixture, the second is the deposition of the mixture on a copper foil, the third is the pressing of the electrodes and the last phase is the drying. Following the production of the electrode comes the assembly of a battery cell.

7.1 Preparation of the electrode mixture

Based on the information gathered from the literature and previous experiments the ratio of the individual components was determined, see Table 2. The weight of the electrode material was 0,4 g. The instruments used to prepare the material had to be properly washed in demineralized water and isopropyl alcohol to prevent the contamination of the prepared mass.

Table 7.1 The ratio of ingredients in the electrode materials

	Active material [wt.%]	Binder [wt.%]	Conductive additive [wt.%]	Total [wt.%]
Polyvinylidene fluoride (PVDF), with Super C65 as conductive additive				
	80	10	10	100
	84	6	10	100
	87	3	10	100
Polyimide P84, with Super C65 as conductive additive				
	80	10	10	100
	84	6	10	100
	87	3	10	100
Styrene-butadiene rubber (SBR), with carboxymethyl cellulose (CMC) as conductive additive				
	92	6	2	100
	94	4	2	100
	96	2	2	100

The main component is the active electrode material, in this case natural graphite CR5995. The second component of the electrode material is the binder. In this thesis three different types were tested, polyvinylidene fluoride (PVDF), Polyimide P84 and Styrene-butadiene rubber (SBR). For the binders PVDF and P84 the use of a solvent, which allows homogenization is necessary. This solvent was the N-methyl 2-pyrrolidone (NMP), which is a nitrogenous heterocyclic compound. The solvent for SBR was demineralized water.

The third component of the electrode material is the conductive additive. For the binders PVDF and P84 amorphous carbon (also called "Carbon black") was used. The small crystals in this material are able to accept a certain amount of lithium ions in the

first charging cycle, after that they start to decay in the subsequent cycles. In our case, the material from TIMCAL labeled Super C65 was used. The conductive additive with SBR is carboxymethyl cellulose (CMC).

The following description is for the binders PVDF and P84. In the mixing process the first step was to add the solvent and the binder. This was mixed for approximately 24 hours, at this point 1000 µl of solvent was enough. The second step was to add the conductive additive, in the case of P84 further addition of the solvent was not necessary, however the PVDF required another 1000 µl of solvent. This was further mixed for another 24 hours. The last step was to add the active material and solvent if necessary. The P84 only required 200 µl of solvent, while the PVDF another 1000 µl. This was followed by another 24 hours of mixing.

With the SBR binder the mixing process was similar. In this case the solvent was demineralized water, and as the first component the conductive additive (CMC) was used. Other than that, the process was the same. After each component a 24 hour mixing ensued.

The Figure 7.1 shows the first phase in the preparation of the electrode. The numbers on the figure are: 1. the active material (natural graphite CR5995), 2. the solvent (NMP), 3. a phial, which contains the mixture (on the figure the mixing was already in progress, the binder and the conductive additive were mixed in the solvent), 4. micropipette (which was used to add the NMP to the mixture) and 5. a scale to measure the components.

Figure 7.1 Preparation of the electrode mixture

7.2 Deposition of the mixture on copper foil

Deposition of the material was done by a conventional technology, consisting of the application of a viscous mixture on the copper foil. A polished copper foil with a

thickness of 50 µm was used. For the deposition itself a special rod was used (see Figure 7.2 below), which guaranteed that the layer will be homogeneous with a precise thickness of 100 µm. The figure below shows: 1. The rod used to apply the mixture, 2. A phial containing the mixture and 3. The copper foil.

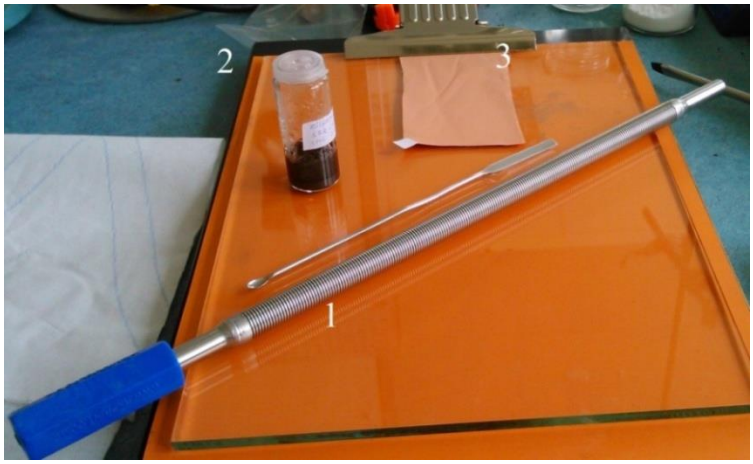

Figure 7.2 Deposition of the mixture on a copper foil

7.3 Pressing of the electrodes

After the deposition of the material on a copper collector, a drying process follows in the presence of air and atmospheric pressure at an elevated temperature of 50 °C. During this process the NMP solvent evaporates. After drying, individual electrodes are cut out in the shape of a disc ready for measurement. Figure 7.3 shows the tools for cutting these discs out. Each electrode has the shape of a disc with a diameter of ⌀ 18 mm and a surface area of 2,55 cm^2. A pure copper disc with a diameter ⌀18 mm weights 27,7 mg. The prepared electrodes were then pressure pressed with 2 tons per cm^2.

Figure 7.3 Tools for cutting out the electrodes

Figure 7.3 shows: 1. the dried copper foil with the electrode material on it, 2. a hole puncher, a pair of tweezers and a hammer and 3. a plexi plate. The copper foil was placed on the plexi plate, then with the hole puncher and the hammer the discs were cut out, approximately six to eight samples were made.

Figure 7.4 Pressure press

7.4 Drying

The last phase in the preparation of the electrodes is their dehydration. Drying was carried out at reduced pressure, approximately around 100 Pa. In these conditions, the electrodes were at least for 24 hours, after this, the electrodes were moved into the glove box. The assembly of measuring cells were carried out in a protective argon (Ar) atmosphere glove box.

Figure 7.5 Reduced pressure compartment and the glove box

7.5 Measuring cells and their assembly

Before the assembly, the cell was thoroughly washed and dried. Together with the electrode material the cell was placed in the glove box. A disc of lithium (with a

diameter of ⌀ 16 mm) cleaned with a scalpel was placed at the bottom of the cell. After this, a separator was placed on top of it, which was drenched in 130 ml of $LiPF_6$ electrolyte by a micropipette. As the last step the separator was covered by the negative electrode. Before completing the last step, the electrodes weight was measured. At the beginning of the assembly the box had to be properly closed to prevent any oxygen to enter. The two types of measuring cells and the glove box are shown on Figure 7.6 and 7.7.

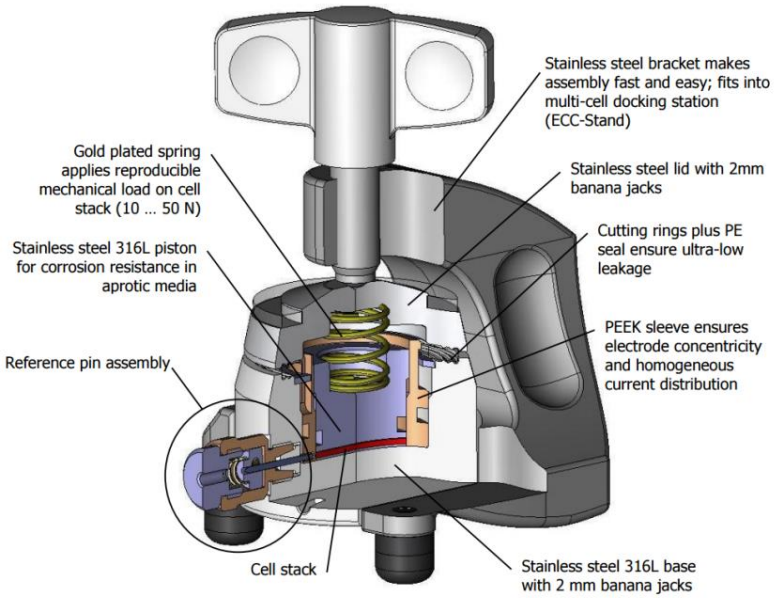

Figure 7.6 Ell-cell 0

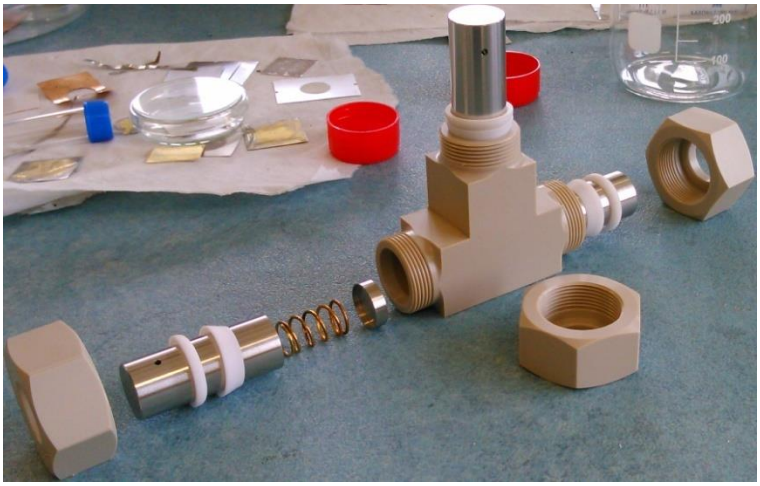

Figure 7.7 T-cell

8 RESULTS OF THE MEASUREMENTS

The measurements were conducted with the VMP-300 device, galvanostatic measurement (GPLC) and cyclic voltammetry (CV) as the methods. With the help of the EC-lab software every detail of the measurement was set up and with Microsoft Excel the data was processed and graphs were generated.

After the initial measurements (with ±100 µA) the weight of the negative electrode mass, the charge and discharge current and the irreversible capacity (in percents) were calculated alongside with the Coulomb efficiency, which is the relation between the discharging and charging capacity. The weight of the electrode material mass is simply calculated by the subtraction of the copper foil discs weight (27,7 mg):

$$m_{mass} = m_{electrode} - m_{copperdisc}. \tag{8.1}$$

The current was calculated with the equation:

$$I = Q.m_{mass}.C, \tag{8.2}$$

where Q is the measured capacity in the last cycle of the initial measurement, it's in mAh/g, m_{mass} is the weight of the electrode material mass calculated with (8.1), and last C, the charging constant, in our case 0,2.

Next up is the irreversible capacity in percents (C_{irr}). This is calculated by the subtraction of the discharge capacity (C_{dis}) from the charge capacity (C_{char}) in a given cycle. The received number is then divided by the charge capacity and to get it in percents it's multiplied by hundred. The equation is:

$$C_{irr} = \frac{C_{char} - C_{dis}}{C_{char}}.100. \tag{8.3}$$

The last equation is to determine the Coulomb efficiency:

$$CE = \frac{C_{dis}}{C_{char}}.100. \tag{8.3}$$

With the methods mentioned in chapter seven, the electrodes were prepared. At the beginning of the measurements the m_{mass} and the current was calculated with the help of (8.1) and (8.2). For each type of binder and for each wt.% the figures in the next chapters show the voltage spikes in every cycle, the first two charging and discharging cycles, the charge and discharge capacity spikes across cycles, the Coulomb efficiency and the irreversible capacity in percentage for each cycle. Also tables presenting the results of the GCPL method are included. The content of these tables was received from the EC-lab software. With the help of the cursor option every charge and discharge capacity was read, the rest was calculated with the equations (8.3) and (8.4).

8.1 Results with the PVDF binder

Individual samples of the electrode (with 10, 6 and 3 wt.% of binder) were examined from the perspective of reversible and irreversible capacity during cycling. The characteristics for the 10 wt.% of PVDF are on figures 8.1, 8.2, 8.3, 8.4 and 8.5. Capacity values are also included in the Table 8.1. The characteristics for the 6 and 3 wt.% of PVDF are shown similarly, figures 8.6 to 8.10 and 8.11 to 8.15 respectively. Tables are also included (Table 8.2 and 8.3).

For the 10 wt.% of PVDF the mass of the electrode material was 4,1 mg and the current was ± 230 µA. Figure 8.1 shows the voltage in every cycle, reaching around 2,5 Volts. Measuring the ten cycles took around 80 hours.

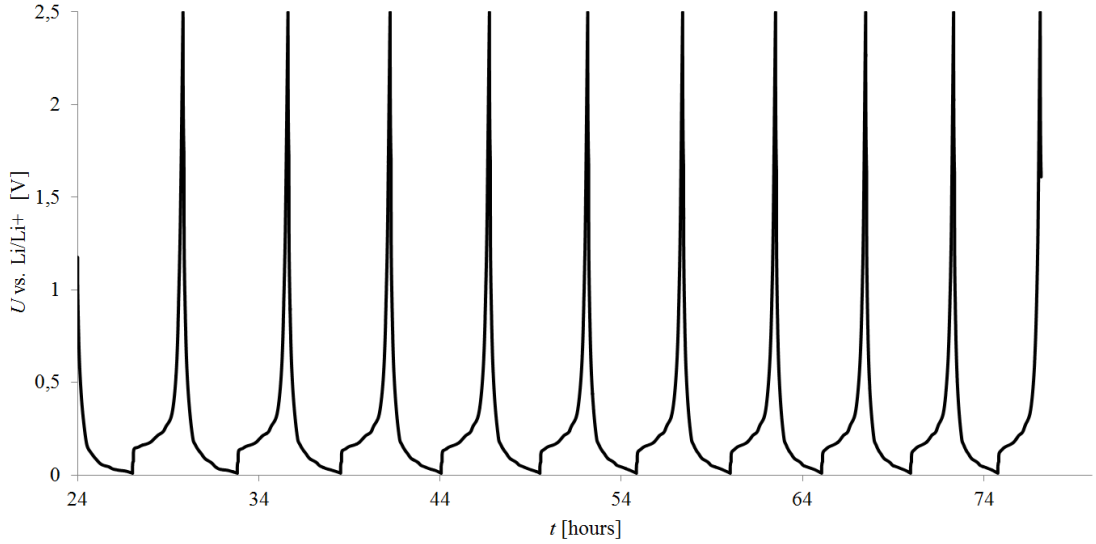

Figure 8.1 Voltage spikes in every cycle (10 wt.% of PVDF)

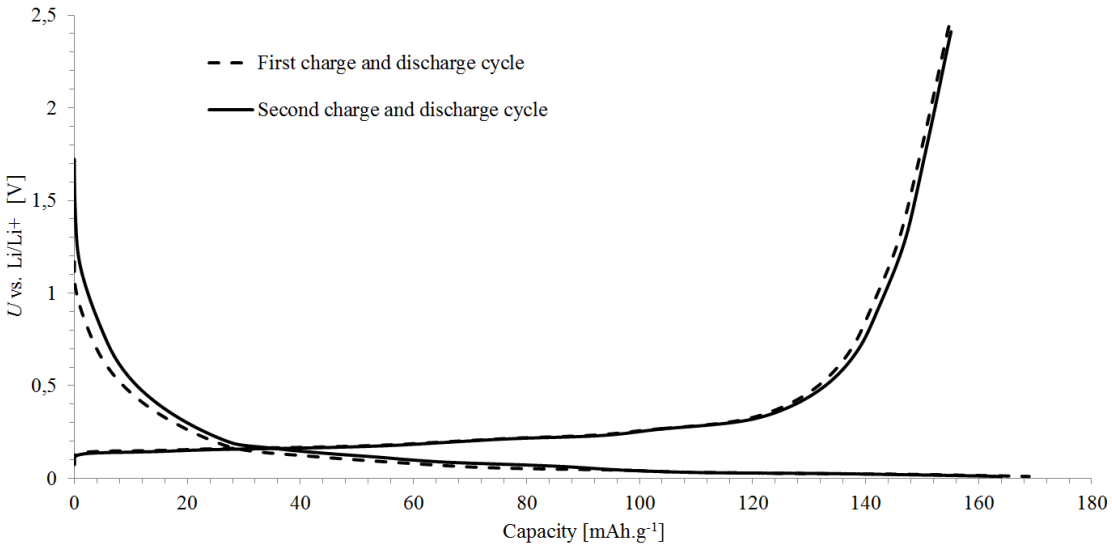

Figure 8.2 The first two charging and discharging cycles (10 wt.% of PVDF)

The next three characteristics show the charge and discharge capacity spikes across the cycles (Figure 8.3), the Coulomb efficiency (Figure 8.4) and the irreversible capacity (Figure 8.5).

Table 8.1 Charge and discharge values, Coulomb efficiency and irreversible capacity (10 wt.% of PVDF)

Cycle	Charge [mAh/g]	Discharge [mAh/g]	C. Efficiency [%]	Irr. Capacity [%]
1	169	155	91,7	8,3
2	164	156	95,1	4,9
3	159	152	95,6	4,4
4	154	148	96,1	3,9
5	152	147	96,7	3,3
6	147	142	96,6	3,4
7	143	139	97,2	2,8
8	139	135	97,1	2,9
9	135	132	97,8	2,2
10	133	130	97,7	2,3

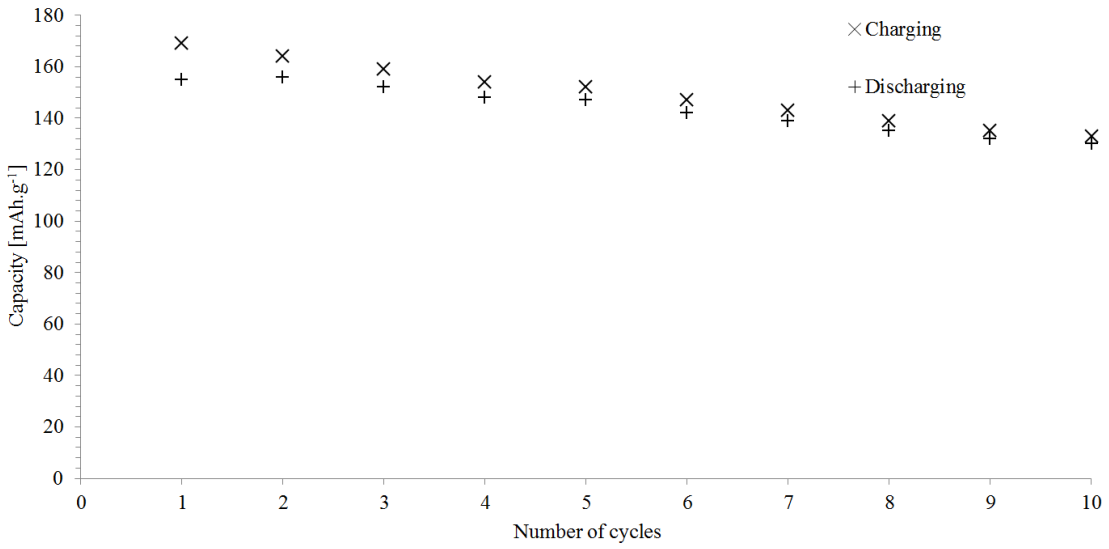

Figure 8.3 The charge and discharge capacity spikes across the cycles (10 wt.% of PVDF)

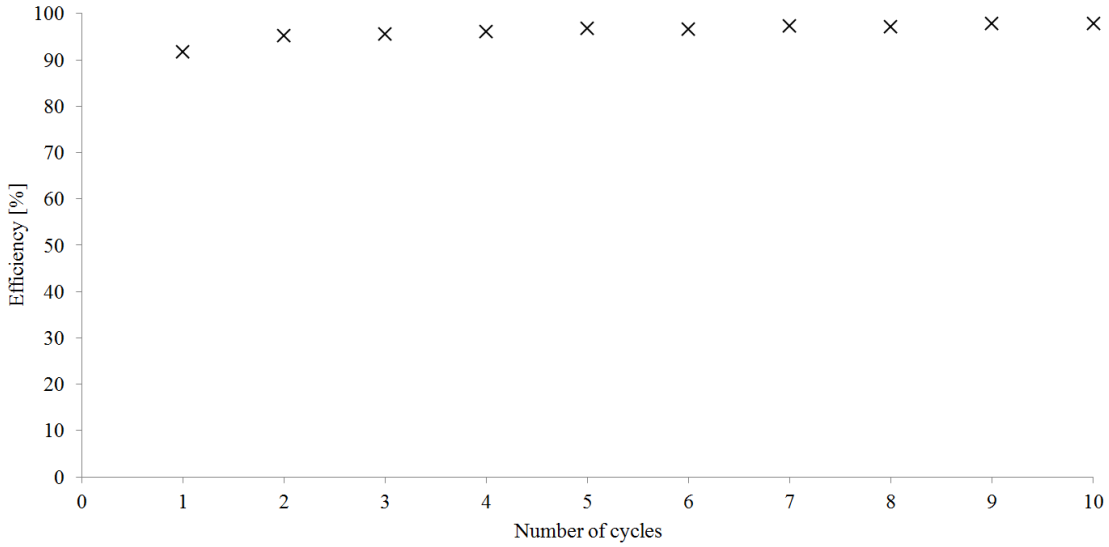

Figure 8.4 The Coulomb efficiency (10 wt.% of PVDF)

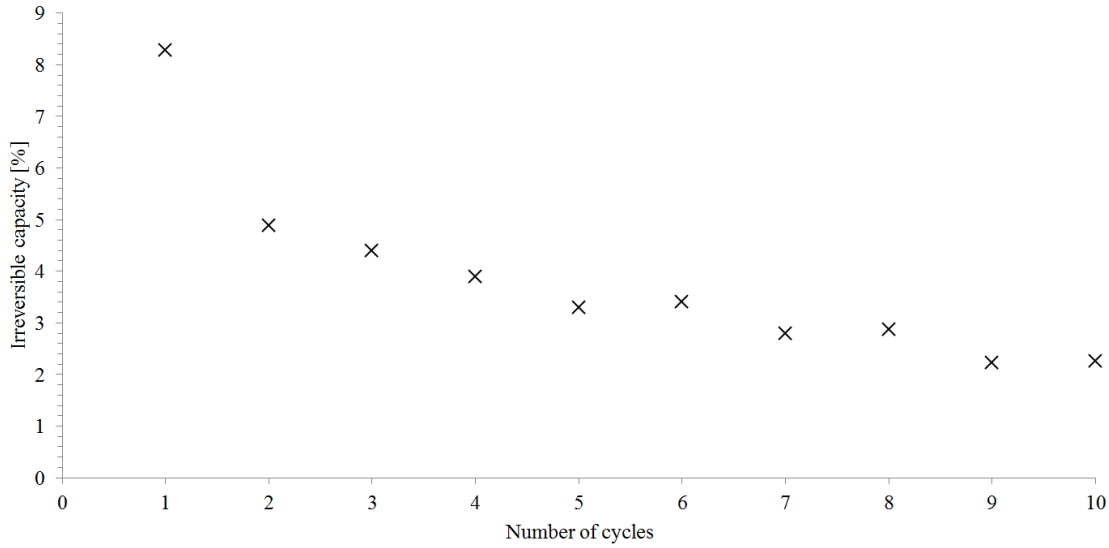

Figure 8.5 The irreversible capacity in percentage (10 wt.% of PVDF)

With 6 wt.% of PVDF the mass was 3,8 mg and the current was ± 239 µA. During the galvanostatic charging around 2,5 Volts were measured in every cycle. Measuring the ten cycles took around 95 hours.

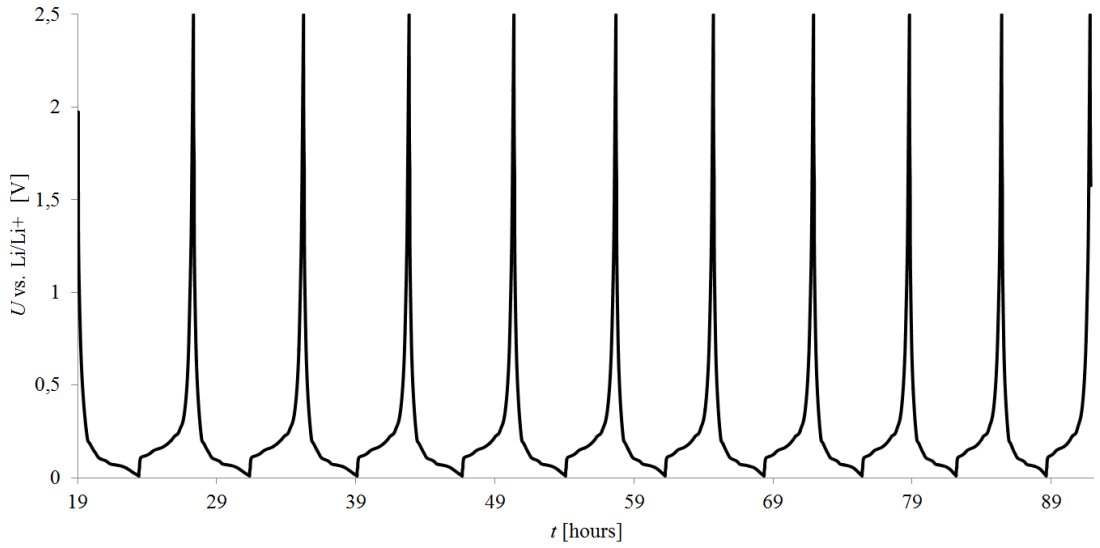

Figure 8.6 Voltage spikes in every cycle (6 wt.% of PVDF)

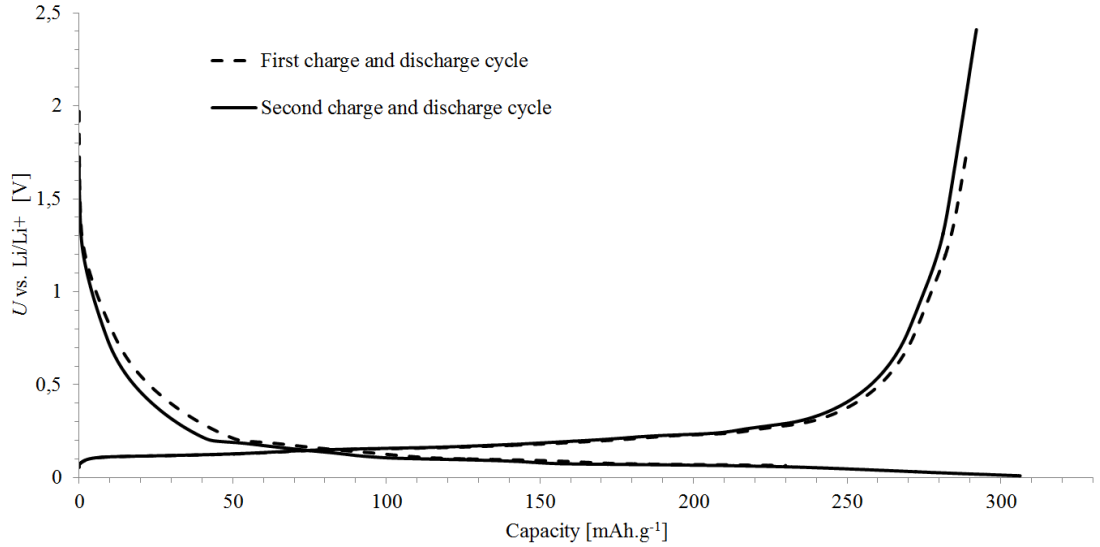

Figure 8.7 The first two charging and discharging cycles (6 wt.% of PVDF)

Like before the next three characteristics show the charge and discharge capacity spikes across the cycles, the Coulomb efficiency and the irreversible capacity. However with 6 wt.% of PVDF the measurements provided better results, in the first cycle charging capacity reached 334 mAh/g. The Coulomb efficiency reached over 95 % in cycles 2 through 10.

Table 8.2 Charge and discharge values, Coulomb efficiency and irreversible capacity (6 wt.% of PVDF)

Cycle	Charge [mAh/g]	Discharge [mAh/g]	C. Efficiency [%]	Irr. Capacity [%]
1	334	296	88,6	11,4
2	306	293	95,8	4,2
3	292	283	96,9	3,1
4	289	281	97,2	2,8
5	281	273	97,2	2,8
6	268	262	97,8	2,2
7	276	268	97,1	2,9
8	264	257	97,3	2,7
9	254	247	97,2	2,8
10	242	238	98,3	1,7

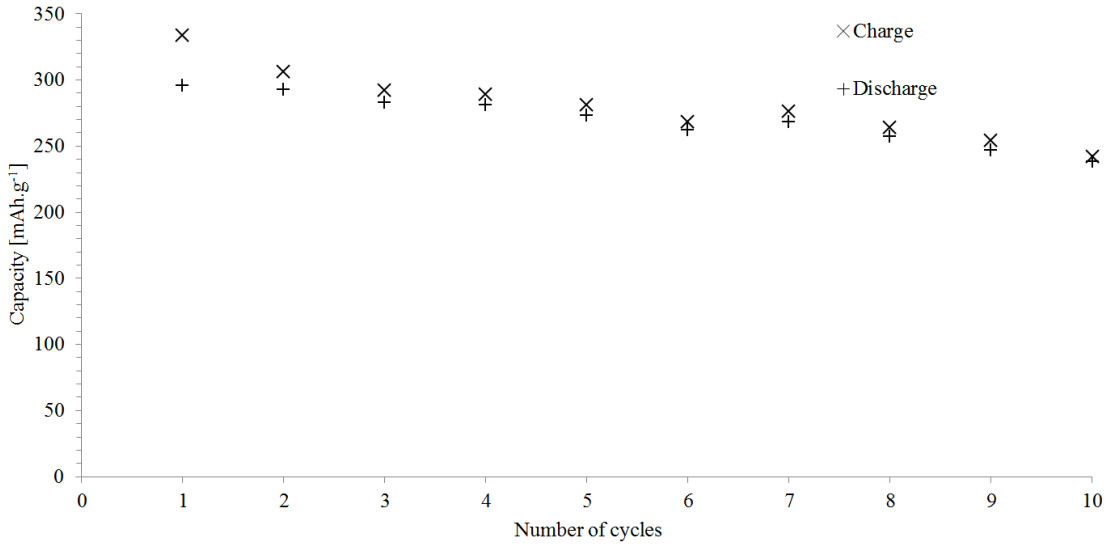

Figure 8.8 The charge and discharge capacity spikes across the cycles (6 wt.% of PVDF)

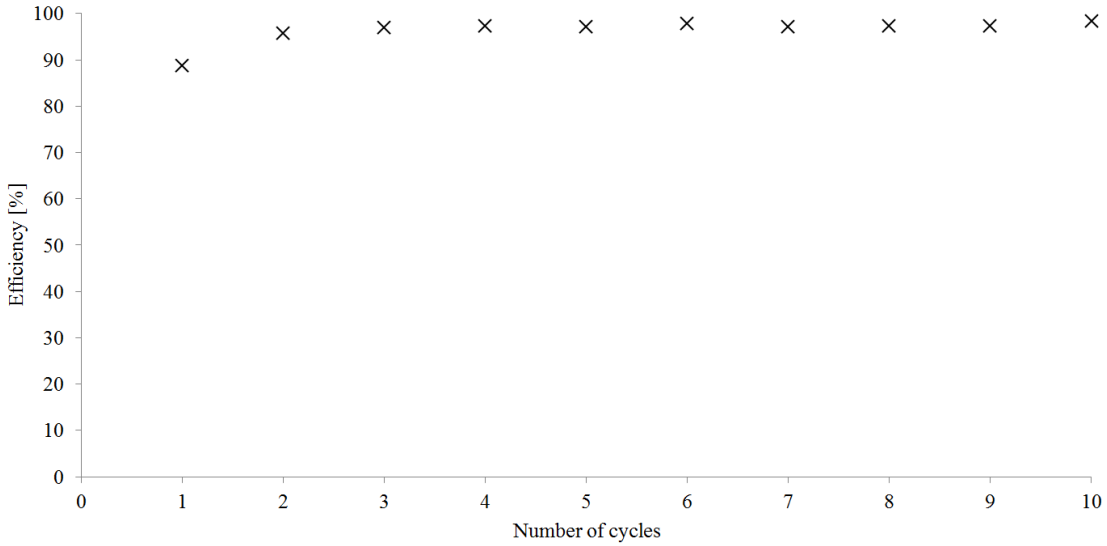

Figure 8.9 The Coulomb efficiency (6 wt.% of PVDF)

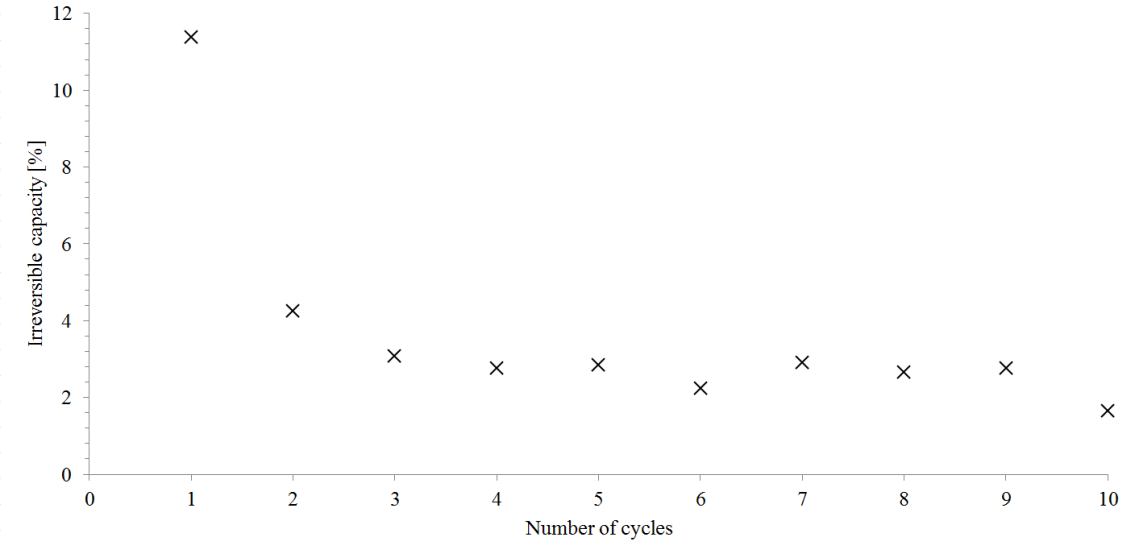

Figure 8.10 The irreversible capacity in percentage (6 wt.% of PVDF)

The negative electrode mass with 3 wt.% of PVDF was 4,3 mg. A current of ± 266 µA was calculated. As before, around 2,5 Volts were measured in every cycle during the galvanostatic charging. Measuring the ten cycles took a little less than 104 hours.

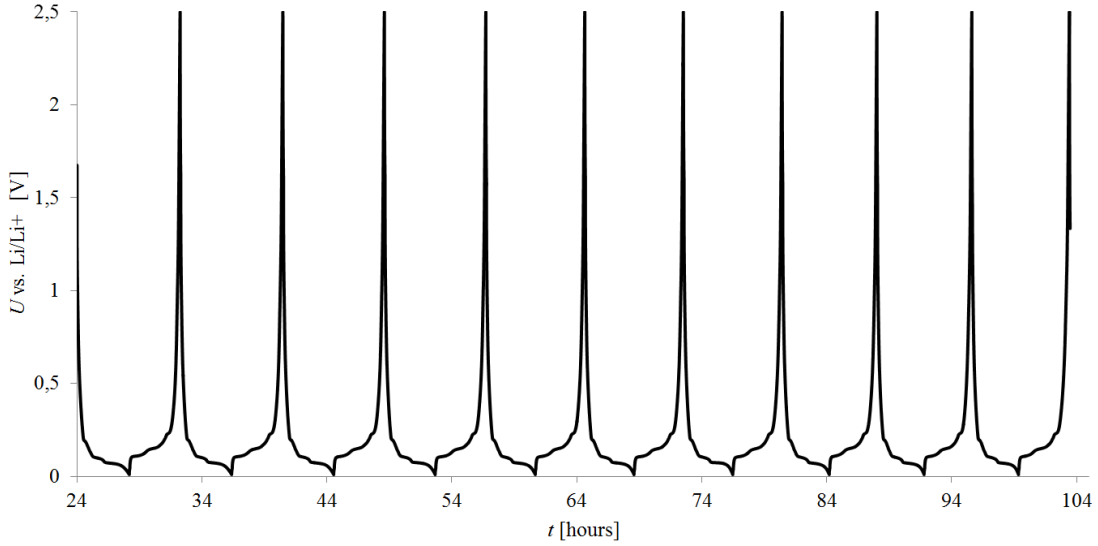

Figure 8.11 Voltage spikes in every cycle (3 wt.% of PVDF)

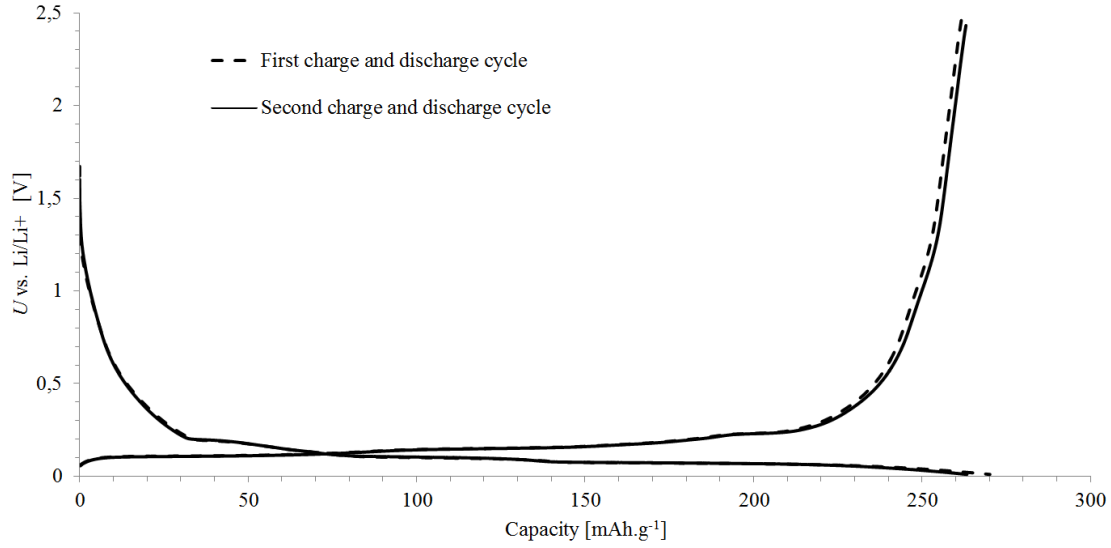

Figure 8.12 The first two charging and discharging cycles (3 wt.% of PVDF)

In the case of irreversible capacity an interesting phenomenon occurred. In cycles 3, 6, 8, 9 and 10 a negative irreversible capacity was measured. The negative sign means, that in a given cycle a larger amount of charge was received than was delivered into it. This is probably caused by the lithium atoms, which during the previous cycle were unable deintercalate and remained trapped. This is probably due to the fast volume change of the electrode. These numbers affect the Coulomb efficiency numbers and characteristics. In these cycles the efficiency reaches over a 100 %.

Table 8.3 Charge and discharge values, Coulomb efficiency and irreversible capacity (3 wt.% of PVDF)

Cycle	Charge [mAh/g]	Discharge [mAh/g]	C. Efficiency [%]	Irr. Capacity [%]
1	270	262	97,1	2,9
2	263	261	99,2	0,8
3	260	283	108,8	-8,8
4	260	259	99,6	0,4
5	253	252	99,6	0,4
6	252	262	103,9	-3,9
7	253	249	98,4	1,6
8	241	253	104,9	-4,9
9	241	245	101,7	-1,7
10	238	262	110,1	-10,1

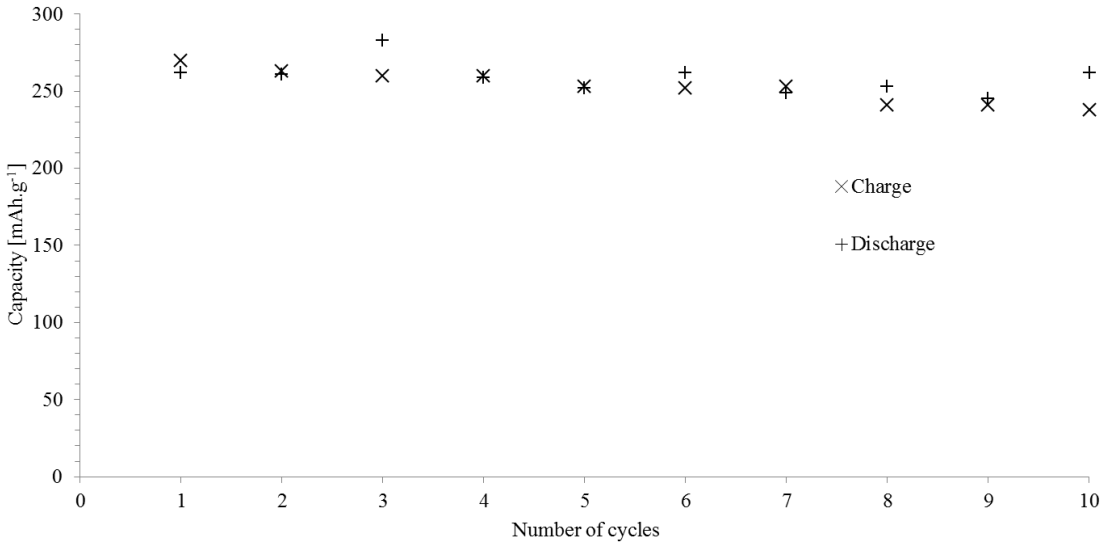

Figure 8.13 The charge and discharge capacity spikes across the cycles (3 wt.% of PVDF)

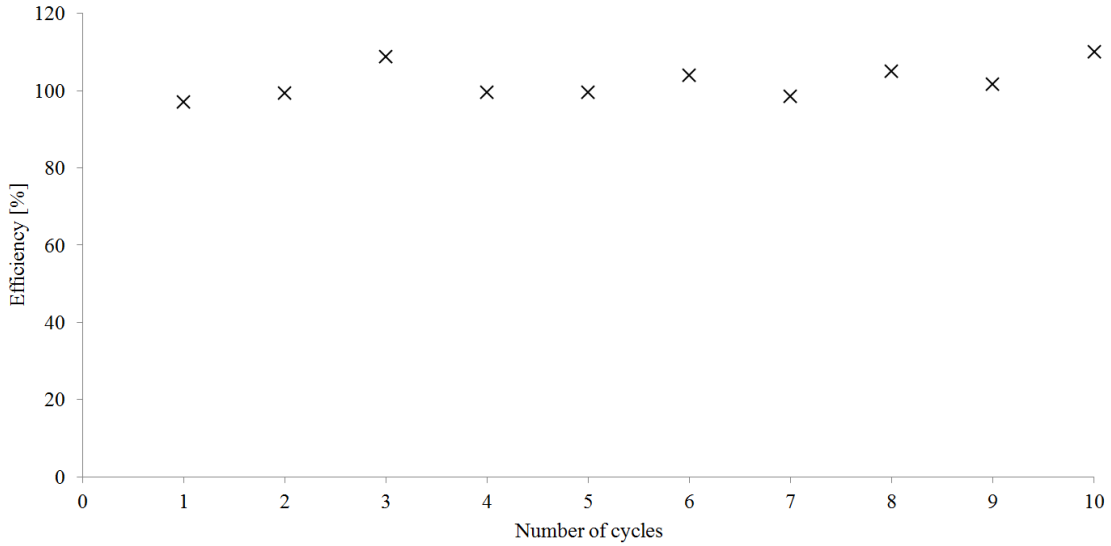

Figure 8.14 The Coulomb efficiency (3 wt.% of PVDF)

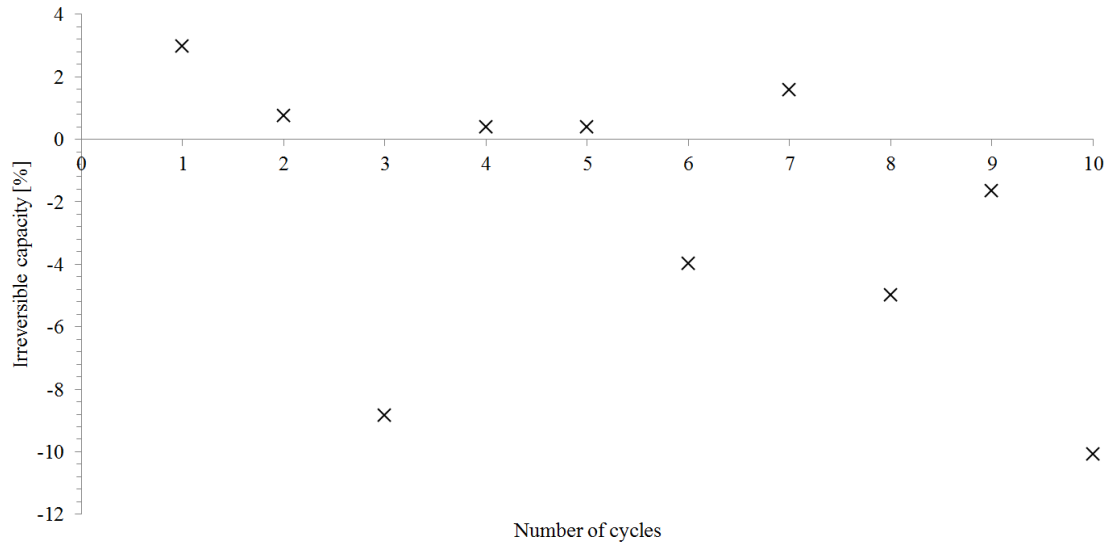

Figure 8.15 The irreversible capacity in percentage (3 wt.% of PVDF)

At the end of these measurements the conclusion is that the 10 and 6 wt.% of PVDF binder can be used in battery applications. The 3 wt.% of PVDF electrode material didn't show optimal characteristics, however the voltage produced by the cell and even the charge and discharge capacities were satisfactory. The previously described trapping of the lithium ions (resulting in negative irreversible capacity values) most likely happened because 3 wt.% of the binder was not enough (the mixture of the mass contained 87 wt.% of natural graphite). This binder is used in conventional lithium-ion batteries with a 8 to 12 wt.%.

8.2 Results with the P84 binder

As mentioned before the samples of the electrode (with 10, 6 and 3 wt.% of binder) were examined from the perspective of reversible and irreversible capacity during cycling. The results are shown on characteristics 8.16 to 8.20 (10 wt.% of P84), 8.21 to 8.25 (6 wt.% of P84) and 8.26 to 8.30 (3 wt.% of P84). Capacity values are also included in Tables 8.4, 8.5 and 8.6.

With 10 wt.% of P84 the mass of the electrode material was 5,7 mg and the current was ± 163 µA. The measurements took only 30 hours. The voltage spikes didn't show an optimal form, however it's still adequate.

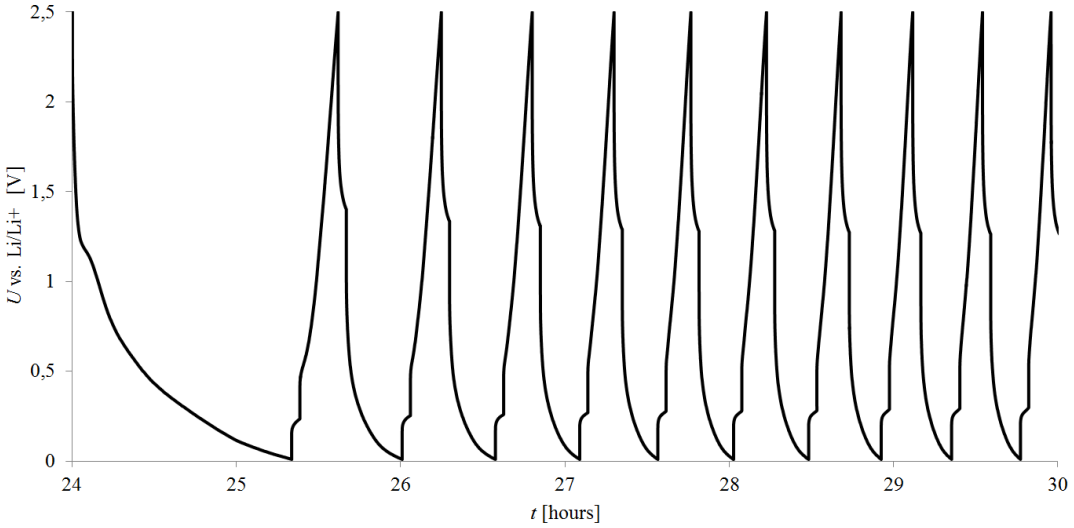

Figure 8.16 Voltage spikes in every cycle (10 wt.% of P84)

This experiment didn't produce the expected results. This can be seen on Figure 8.17, during the first two charge and discharge cycles the capacity was only 39 and 10 mAh/g, and 7 and 5 mAh/g (also shown on the next characteristics and Table 8.4).

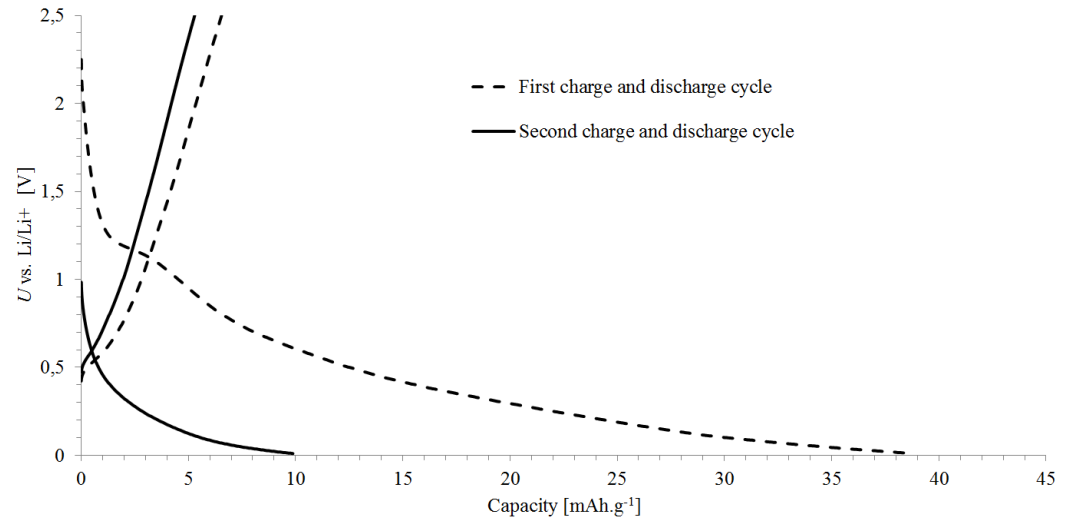

Figure 8.17 The first two charging and discharging cycles (10 wt.% of P84)

The next few characteristics show unwanted results. The charge and discharge capacity spikes across the cycles (Figure 8.18) were too low to be considered successful. The Coulomb efficiency (Figure 8.19) and the irreversible capacity (Figure 8.20) characteristics also show the results of this experiment.

Table 8.4 Charge and discharge values, Coulomb efficiency and irreversible capacity (10 wt.% of P84)

Cycle	Charge [mAh/g]	Discharge [mAh/g]	C. Efficiency [%]	Irr. Capacity [%]
1	39	7	17,9	82,1
2	10	5	50,0	50,0
3	8	5	62,5	37,5
4	7	5	71,5	28,5
5	6	4	66,7	33,3
6	6	4	66, 7	33,3
7	6	4	66, 7	33,3
8	6	4	66, 7	33,3
9	5	4	80,0	20,0
10	5	4	80,0	20,0

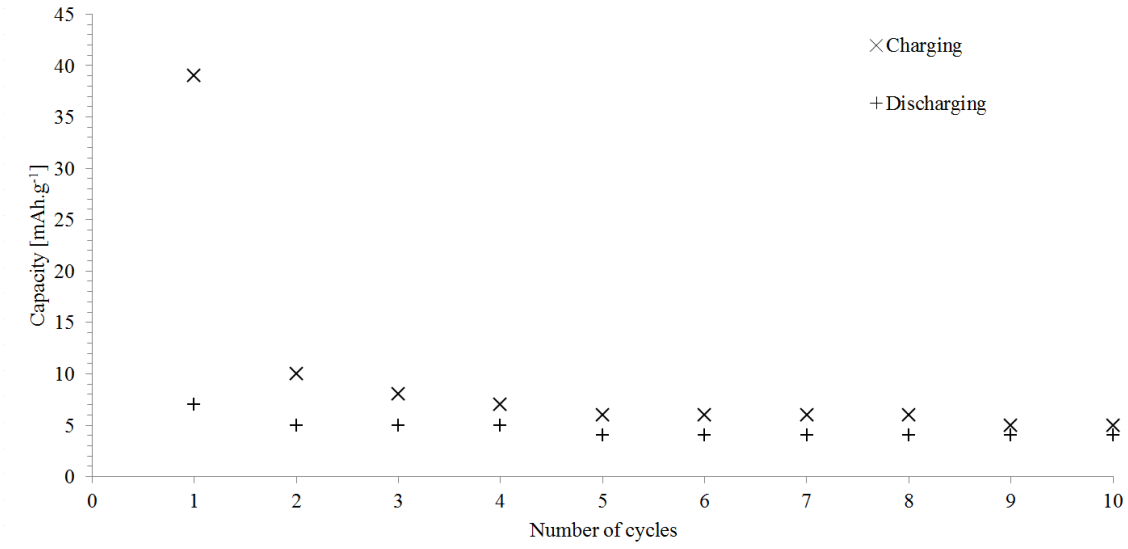

Figure 8.18 The charge and discharge capacity spikes across the cycles (10 wt.% of P84)

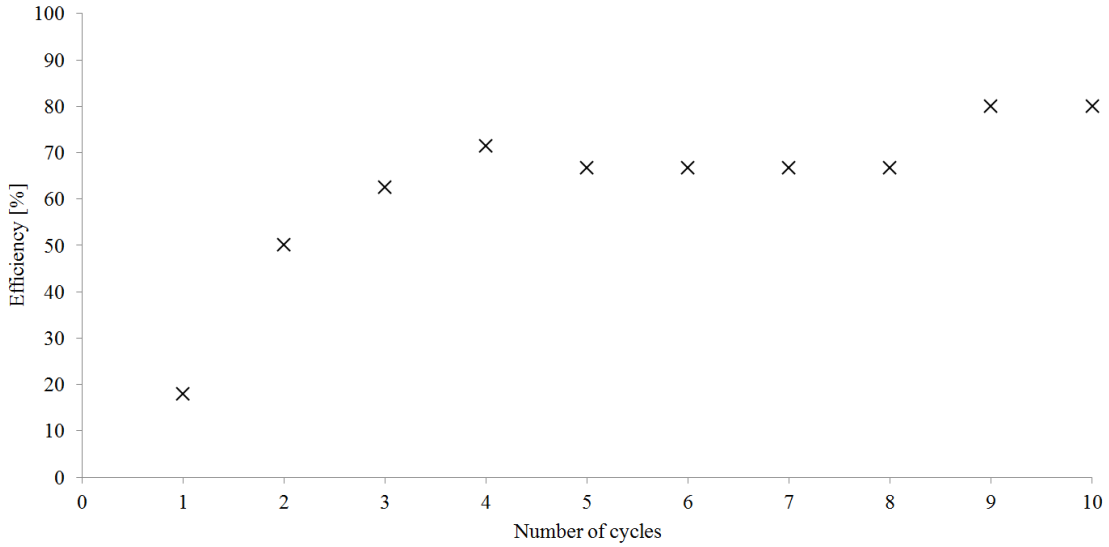

Figure 8.19 The Coulomb efficiency (10 wt.% of P84)

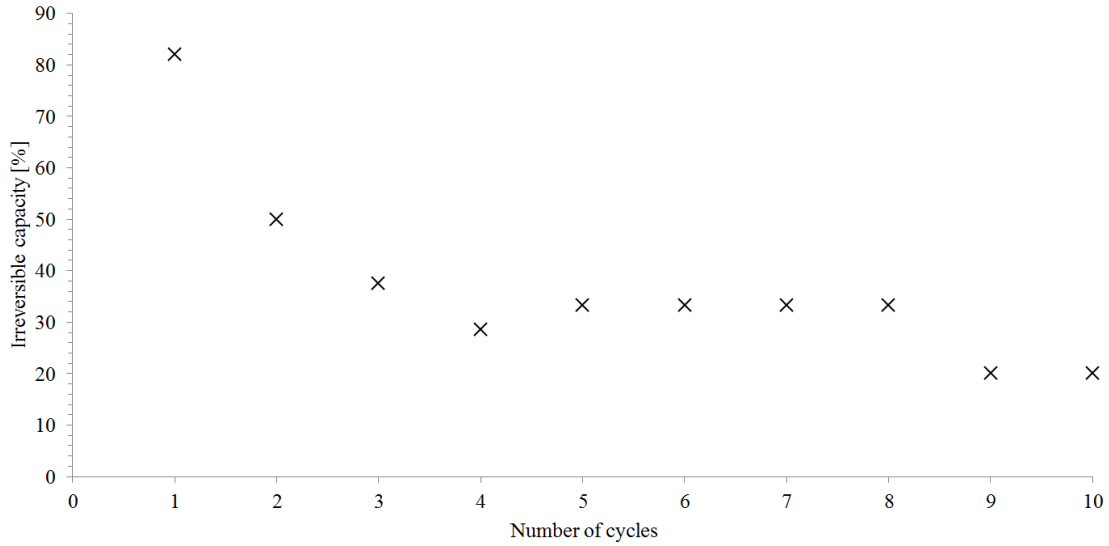

Figure 8.20 The irreversible capacity in percentage (10 wt.% of P84)

These results may be caused by the amount of binder in the electrode material. However a more viable answer might be the inadequate assembly of the cell or the contamination of the negative electrode. A third possible answer is that this binder is not suitable for battery applications. The answer depends on how the other samples perform with this binder.

The sample with 6 wt.% of P84 had a mass was of 2,4 mg. The current calculated was ± 124 µA. During the galvanostatic charging around 2,5 Volts were measured in every cycle. Measuring all ten cycles took around 59 hours. The measurements with this sample had to be repeated due to the unsatisfactory results.

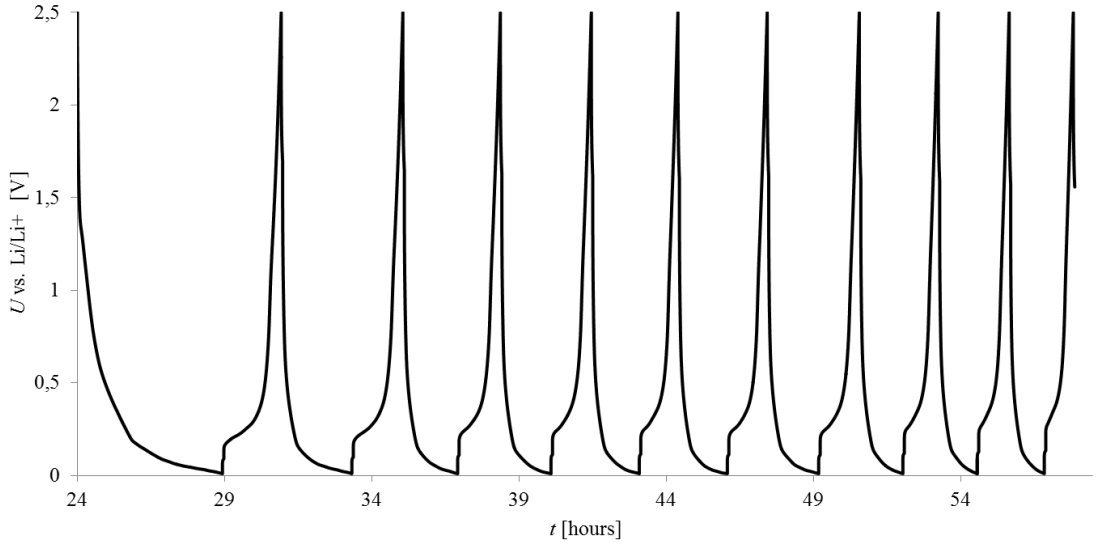

Figure 8.21 Voltage spikes in every cycle (6 wt.% of P84)

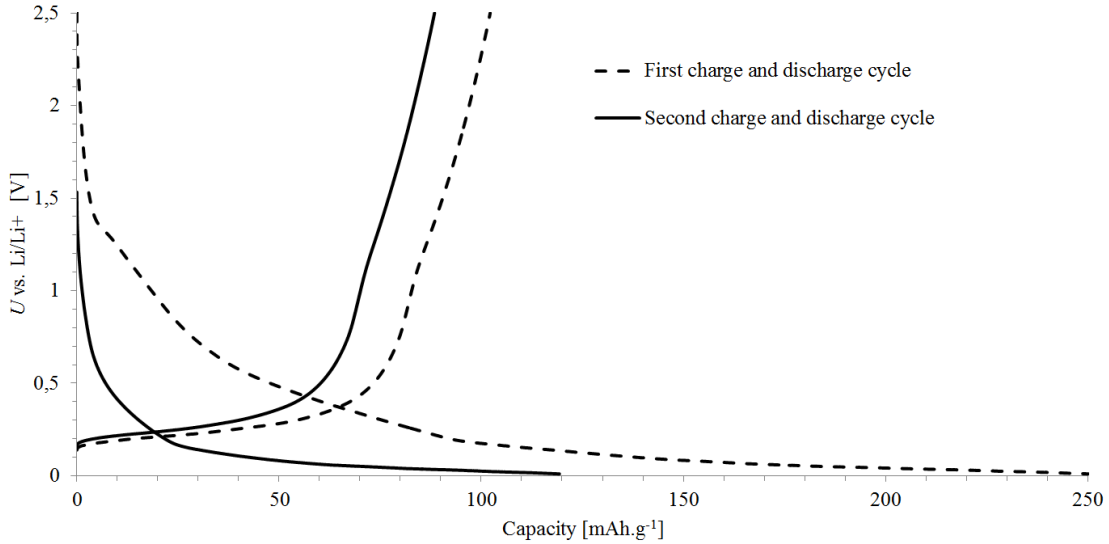

Figure 8.22 The first two charging and discharging cycles (6 wt.% of P84)

Like before the next three characteristics show the charge and discharge capacity spikes across the cycles, the Coulomb efficiency and the irreversible capacity. With this binder the 6 wt.% sample performed better than the previous 10 wt.%. In the first cycle charging capacity reached a very good 250 mAh/g, however in latter cycles this dropped significantly. The Coulomb efficiency reached over 80 % in cycles 3 through 10.

Table 8.5 Charge and discharge values, Coulomb efficiency and irreversible capacity (6 wt.% of P84)

Cycle	Charge [mAh/g]	Discharge [mAh/g]	C. Efficiency [%]	Irr. Capacity [%]
1	250	102	40,8	59,2
2	120	89	74,2	25,8
3	92	74	80,4	19,6
4	85	69	81,2	18,8
5	80	66	82,5	17,5
6	82	68	82,9	17,1
7	86	70	81,4	18,6
8	73	60	82,2	17,8
9	65	54	83,1	16,9
10	58	49	84,5	15,5

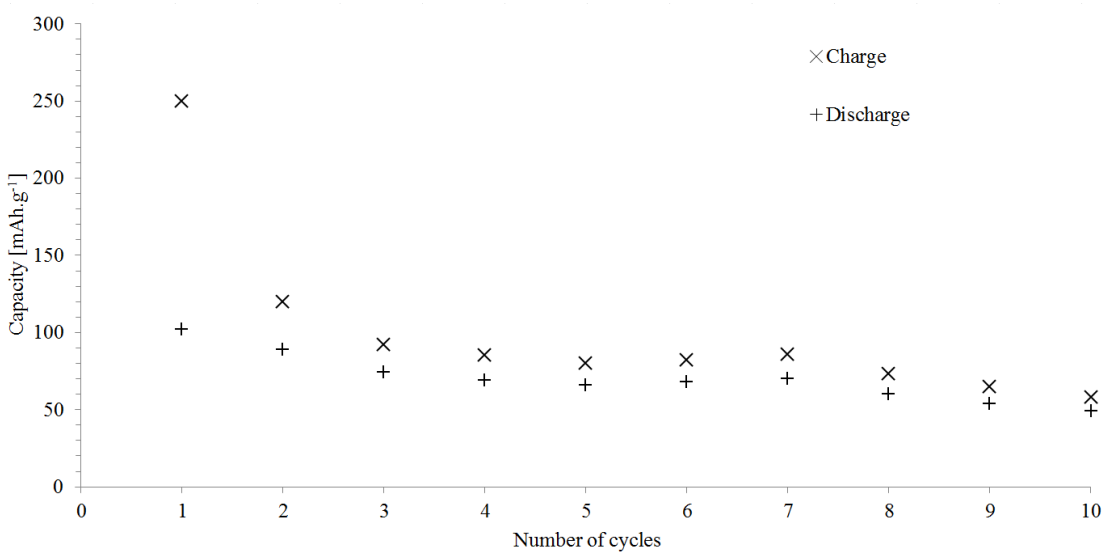

Figure 8.23 The charge and discharge capacity spikes across the cycles (6 wt.% of P84)

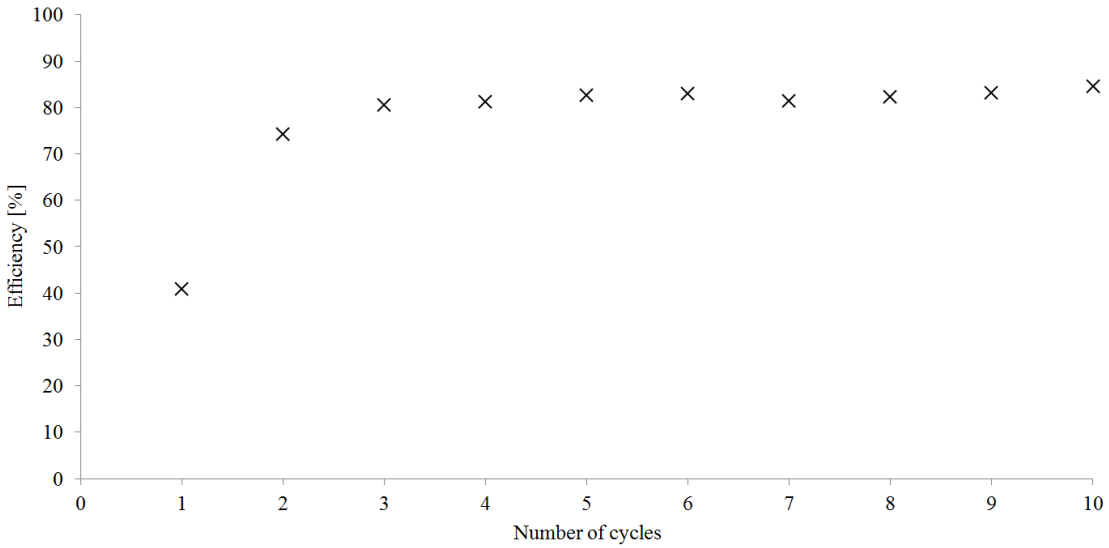

Figure 8.24 The Coulomb efficiency (6 wt.% of P84)

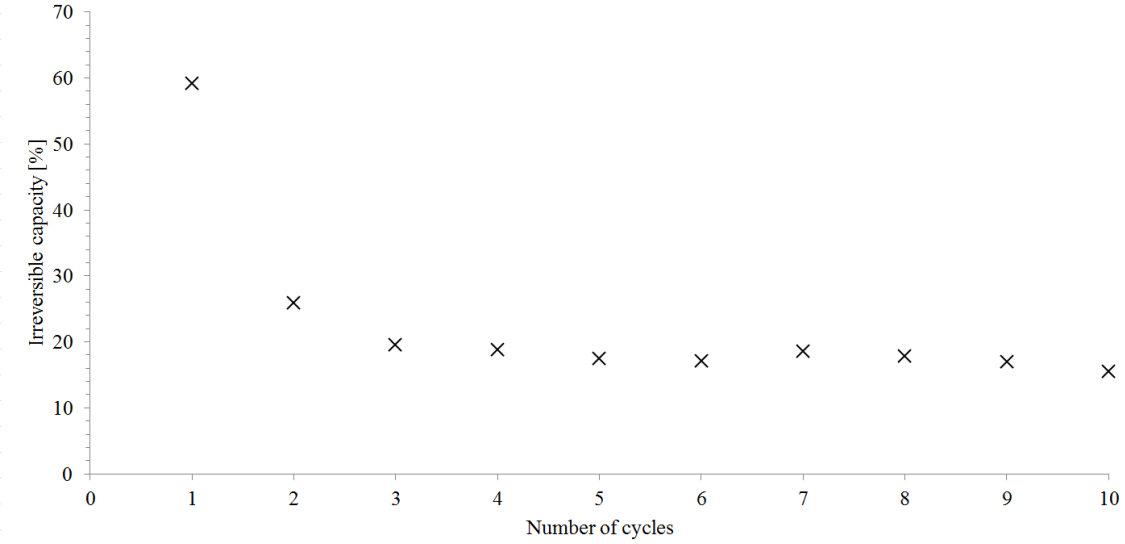

Figure 8.25 The irreversible capacity in percentage (6 wt.% of P84)

For the smallest, 3 wt.%, amount of P84 the mass of the electrode material was 5,7 mg and a ± 371 µA current was calculated. Measuring the ten cycles took a little less than 88 hours.

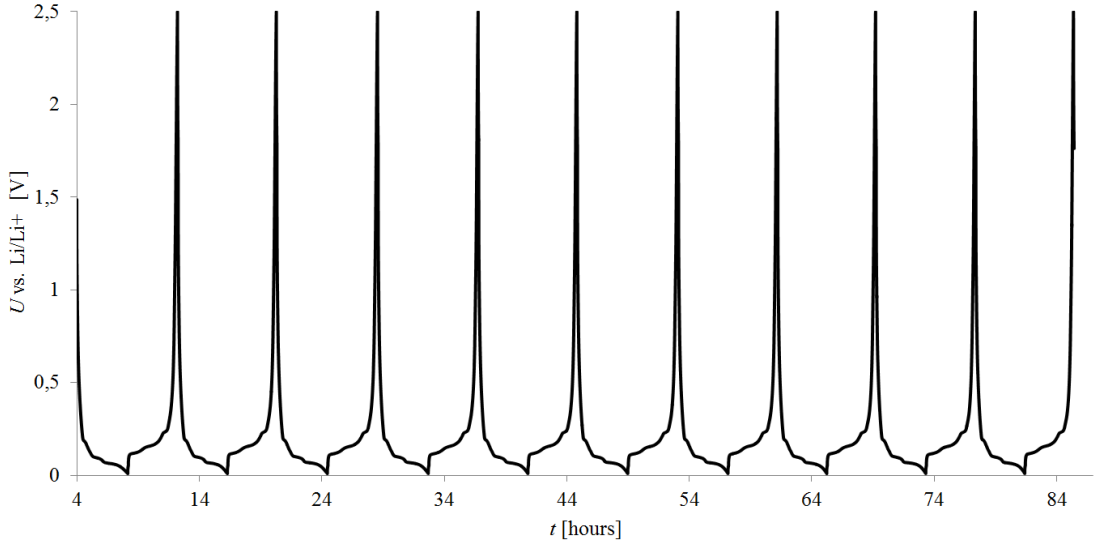

Figure 8.26 Voltage spikes in every cycle (3 wt.% of P84)

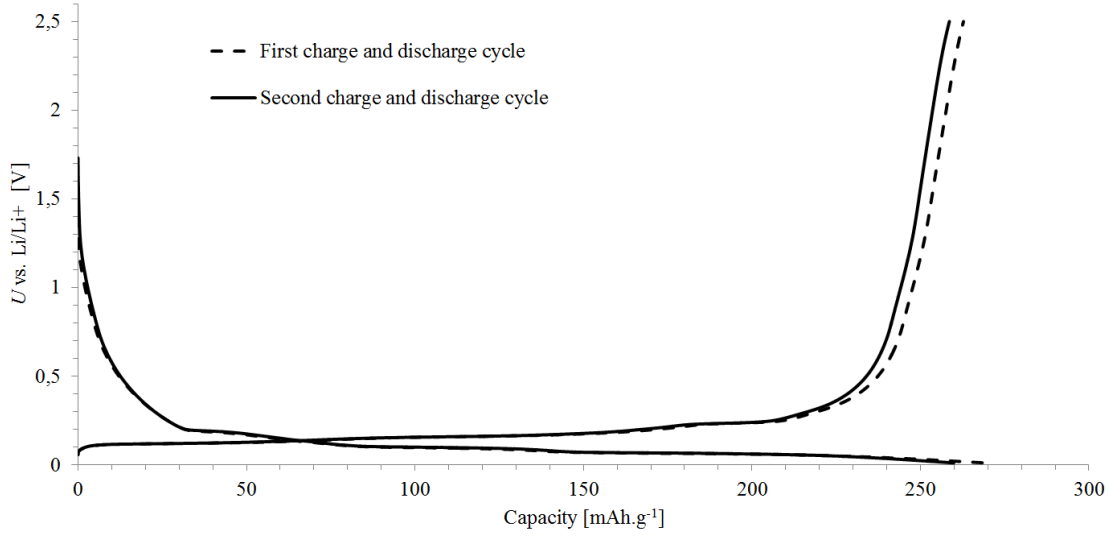

Figure 8.27 The first two charging and discharging cycles (3 wt.% of P84)

Like before the next three characteristics show the charge and discharge capacity spikes across the cycles, the Coulomb efficiency and the irreversible capacity. With this binder the 3 wt.% sample performed flawlessly. In all of the cycles the charging capacity was around 260 mAh/g, the lowest being 258 mAh/g. The Coulomb efficiency reached over a 100 % in cycles 6, 8 and 10, which means that all of the received charge was discharged.

Table 8.6 Charge and discharge values, Coulomb efficiency and irreversible capacity (3 wt.% of P84)

Cycle	Charge [mAh/g]	Discharge [mAh/g]	C. Efficiency [%]	Irr. Capacity [%]
1	269	263	97,8	2,2
2	260	259	99,6	0,4
3	266	265	99,6	0,04
4	265	264	99,6	0,4
5	260	259	99,6	0,4
6	265	265	100,0	0,0
7	261	260	99,6	0,4
8	258	258	100,0	0,0
9	262	261	99,6	0,4
10	258	258	100,0	0,0

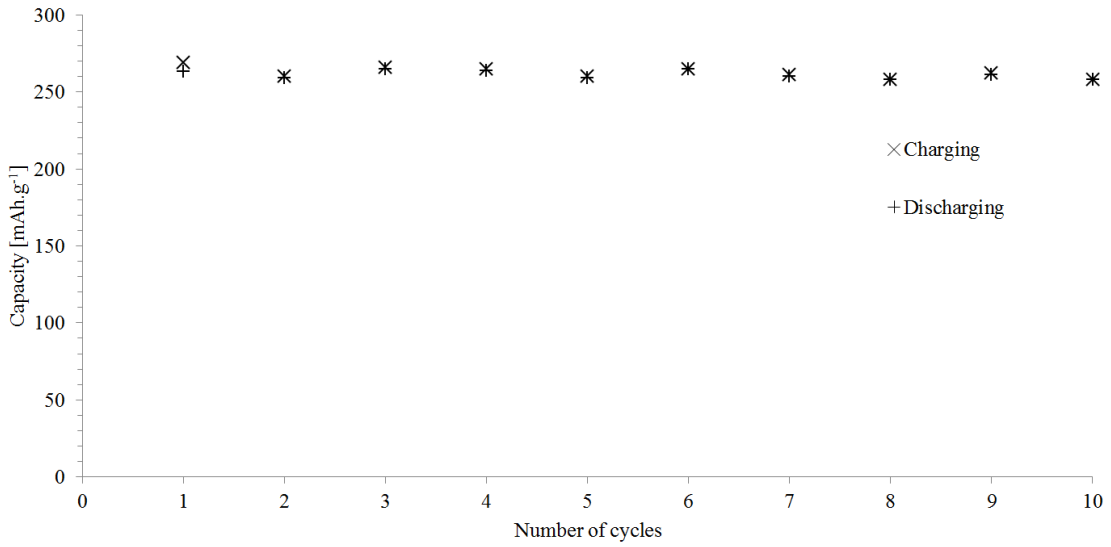

Figure 8.28 The charge and discharge capacity spikes across the cycles (3 wt.% of P84)

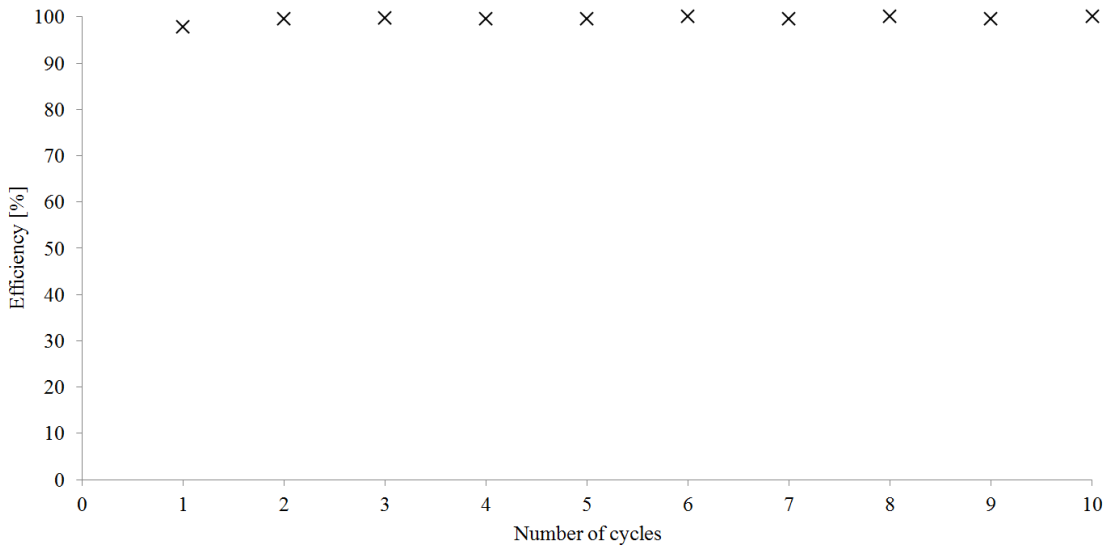

Figure 8.29 The Coulomb efficiency (3 wt.% of P84)

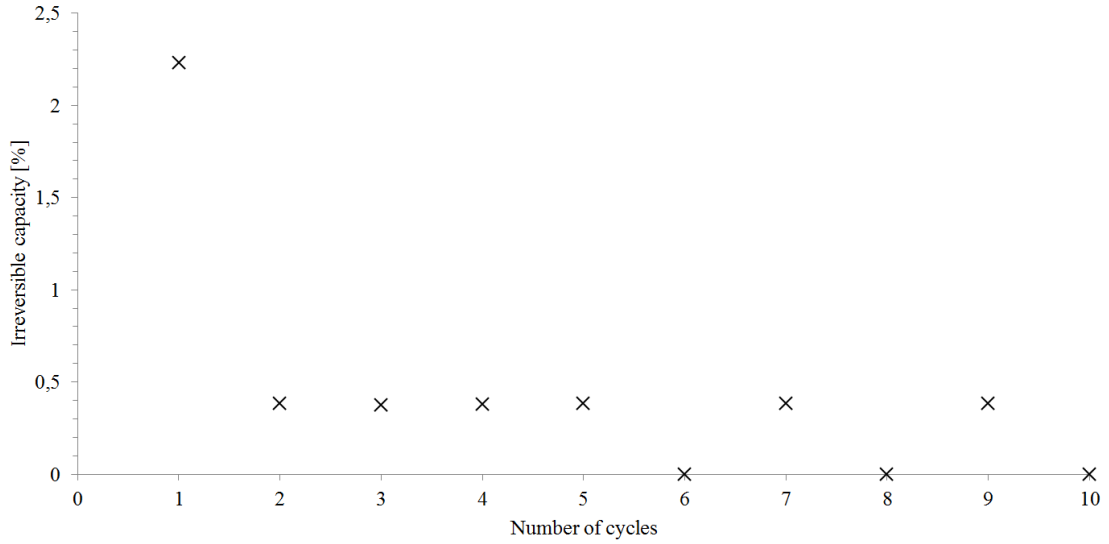

Figure 8.30 The irreversible capacity in percentage (3 wt.% of P84)

The results with this type of binder were mixed. The 10 wt.% performed poorly, while the results with the least amount of binder, 3 wt.%, were outstanding. Using 6 wt.% also proved to be not optimal, while it performed better than the first one, it still had rather low values of capacity. The drastic difference between the samples may be caused by the amount of binder, the right amount being somewhere between 3 and 6 wt.%.

8.3 Results with the SBR binder

The results with the last type of binder are on figures 8.31 to 8.35 (6 wt.% of SBR), 8.36 to 8.40 (4 wt.% of SBR) and 8.41 to 8.45 (2 wt.% of SBR). Capacity values are also included in Tables 8.7, 8.8 and 8.9.

For the 6 wt.% of SBR the mass of the electrode material was 5,6 mg and the calculated current was ± 215 µA. Measuring the ten cycles took around 68 hours.

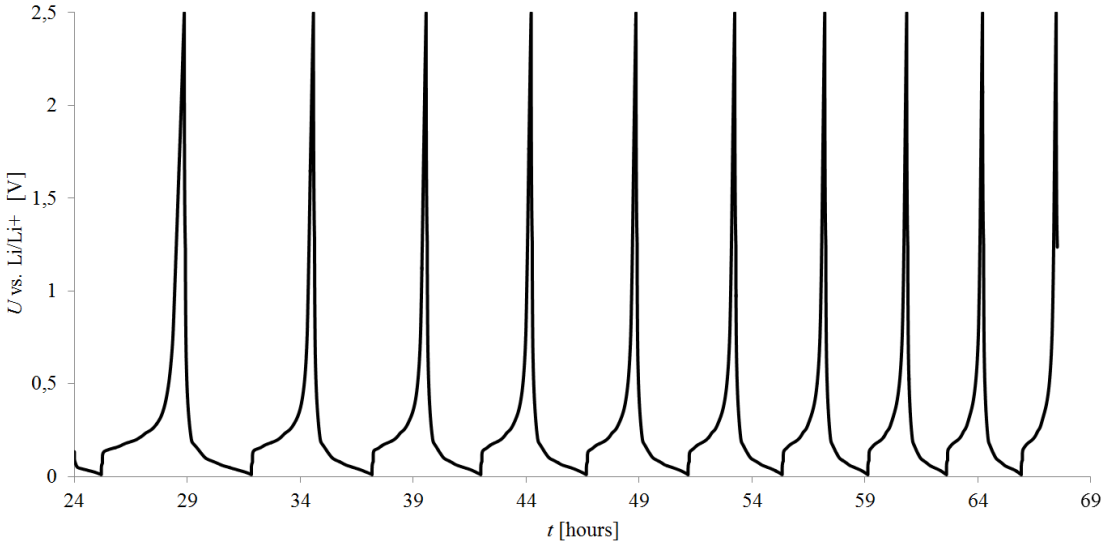

Figure 8.31 Voltage spikes in every cycle (6 wt.% of SBR)

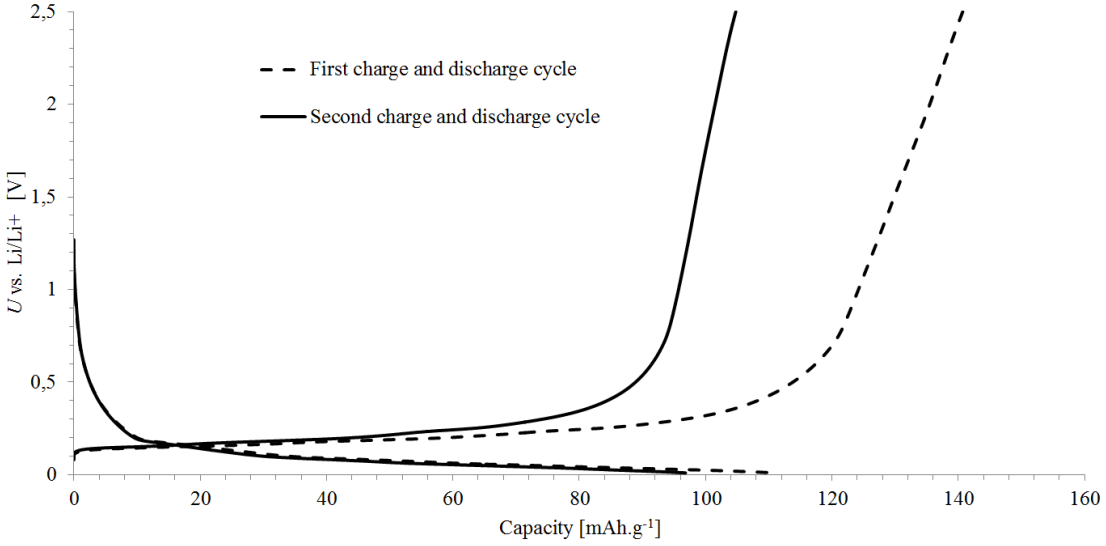

Figure 8.32 The first two charging and discharging cycles (6 wt.% of SBR)

The next characteristics, and table, show the charge and discharge capacity spikes, the Coulomb efficiency and the irreversible capacity. These results show a more or less optimal decline in the charge values, however the first charge and discharge capacities were not as high as the values with the PVDF binder.

Table 8.7 Charge and discharge values, Coulomb efficiency and irreversible capacity (6 wt.% of SBR)

Cycle	Charge [mAh/g]	Discharge [mAh/g]	C. Efficiency [%]	Irr. Capacity [%]
1	141	111	78,7	21,3
2	105	98	93,3	6, 7
3	91	90	98,9	1,1
4	85	91	107,1	-7,1
5	83	86	103,6	-3,6
6	78	78	100,0	0,0
7	71	70	98,6	1,4
8	65	45	69,2	30,8
9	60	20	33,3	66,7
10	58	63	108,6	-8,6

In cycles 4, 5 and 10 a negative irreversible capacity was measured. Like before this is probably caused by the trapped lithium atoms. In this case, as well, the numbers affect the Coulomb efficiency numbers and characteristics. In these cycles the efficiency is over a 100 %, the highest being 108,6 % in cycle 10.

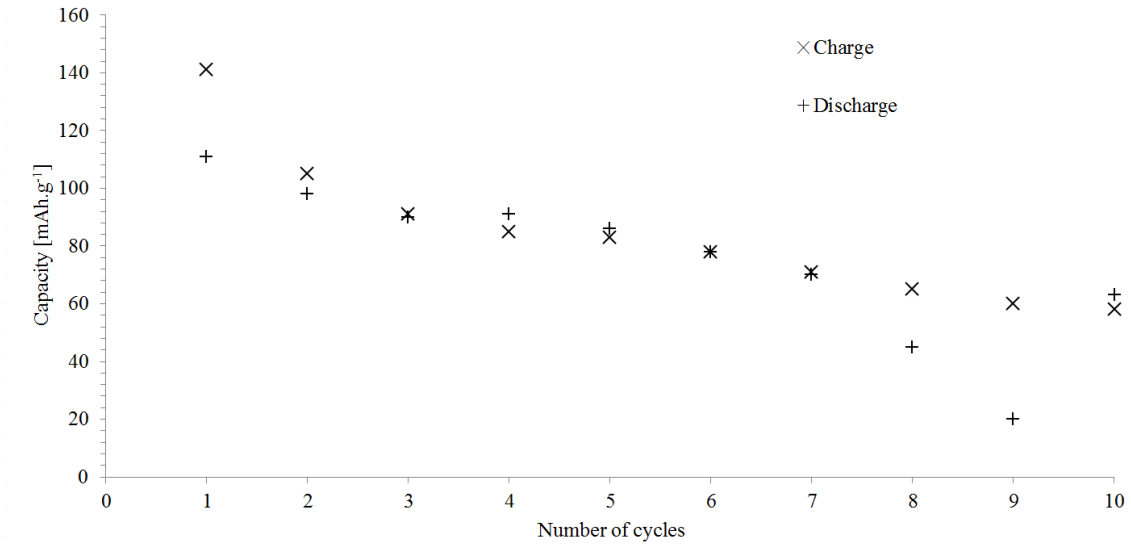

Figure 8.33 The charge and discharge capacity spikes across the cycles (6 wt.% of SBR)

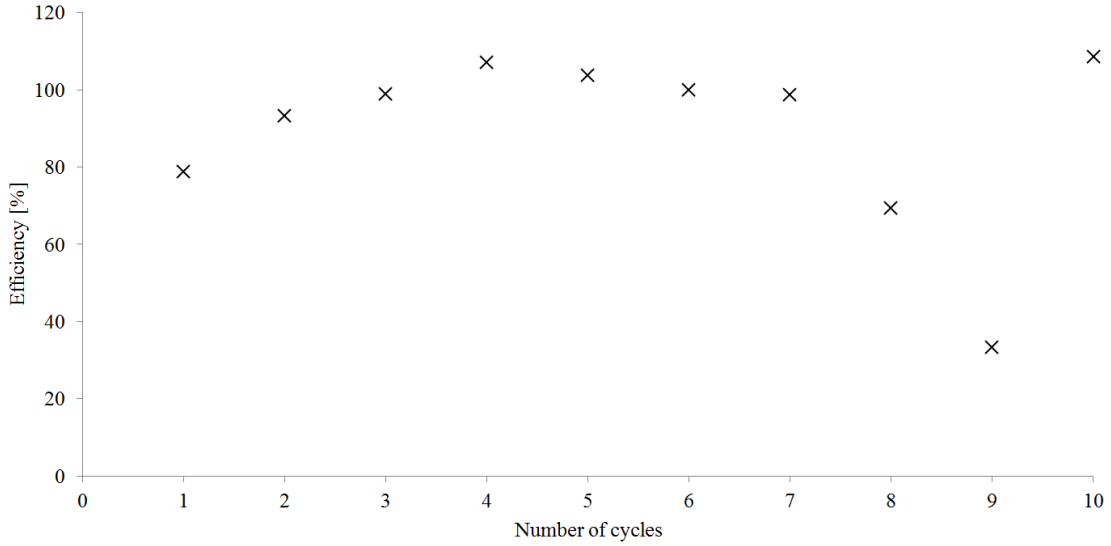

Figure 8.34 The Coulomb efficiency (6 wt.% of SBR)

The last characteristic shows the negative value of the irreversible capacity. A possible explanation for this lays in the growth of the surface film layer, and also in the irreversible intercalation of lithium-ions.

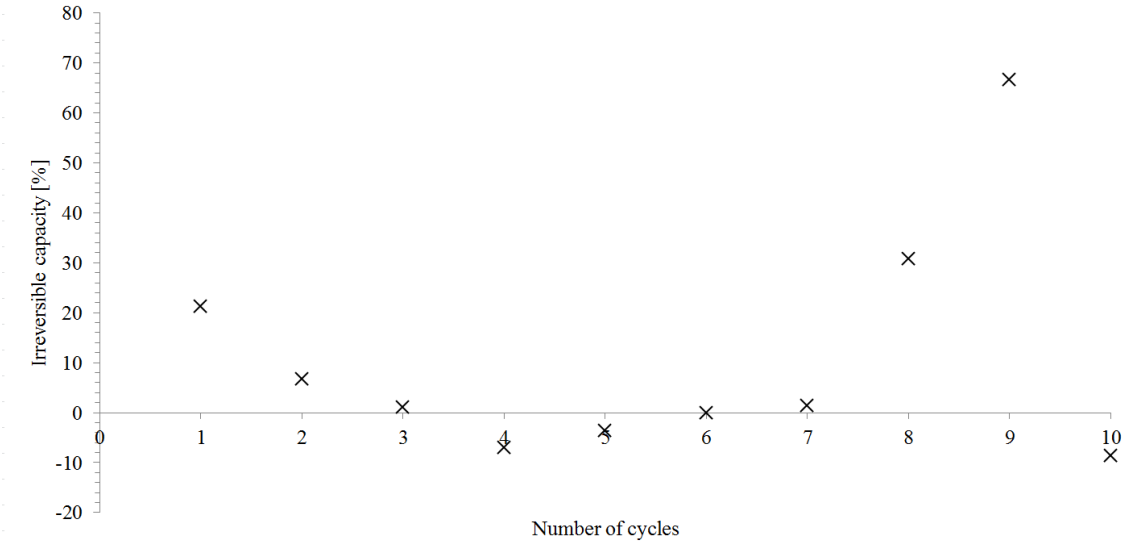

Figure 8.35 The irreversible capacity in percentage (6 wt.% of SBR)

With 4 wt.% of SBR the mass was 2,9 mg and the current was ± 135 µA. Measuring the ten cycles took around 35 hours.

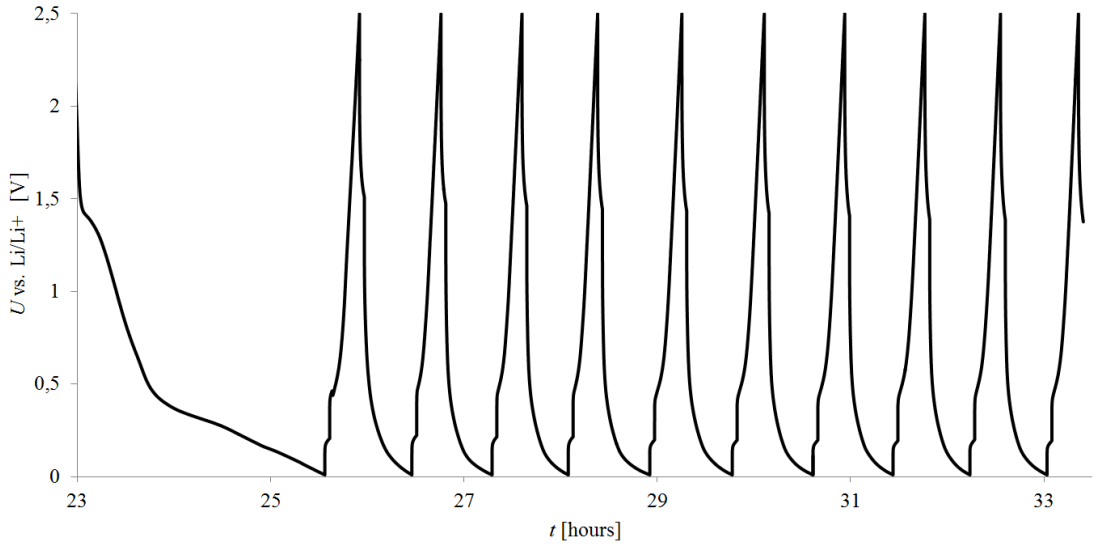

Figure 8.36 Voltage spikes in every cycle (4 wt.% of SBR)

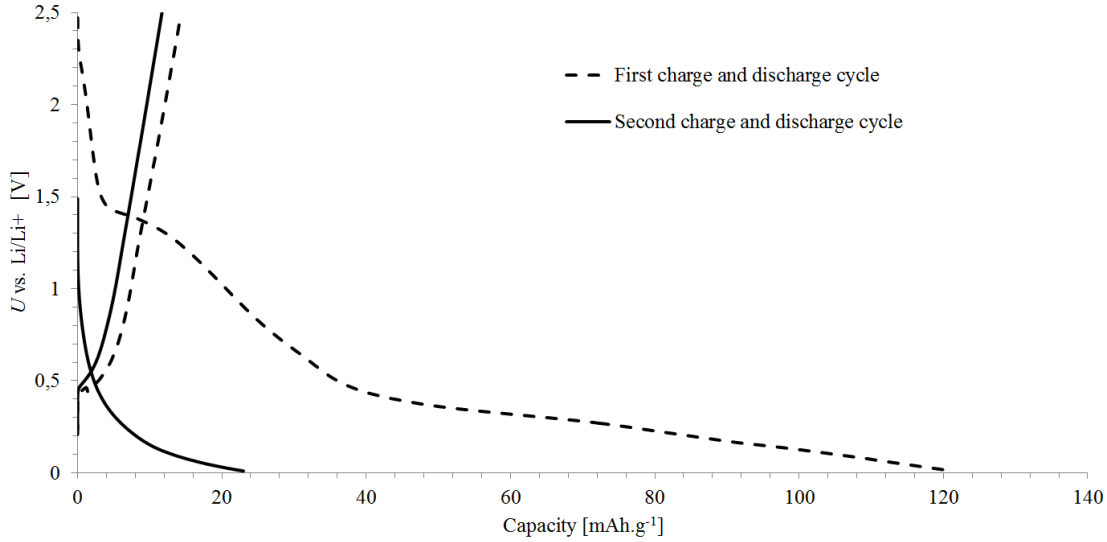

Figure 8.37 The first two charging and discharging cycles (4 wt.% of SBR)

The charge and discharge capacity spikes across the cycles show a decline from 122 to 20 mAh/g. These numbers are not showing the best results, they're not even close to the results with PVDF binder.

Table 8.8 Charge and discharge values, Coulomb efficiency and irreversible capacity (4 wt.% of SBR)

Cycle	Charge [mAh/g]	Discharge [mAh/g]	C. Efficiency [%]	Irr. Capacity [%]
1	122	14	11,5	88,5
2	23	12	52,2	47,8
3	22	12	54,5	45,5
4	20	12	60,0	40,0
5	23	13	56,5	43,5
6	22	13	59,1	40,9
7	21	13	61,9	38,1
8	21	13	61,9	38,1
9	19	12	63,2	36,8
10	20	13	65,0	35,0

The Coulomb efficiency and the irreversible capacity are shown on the next three characteristics. These results show a 50 to 65 % of efficiency in most of the cycles.

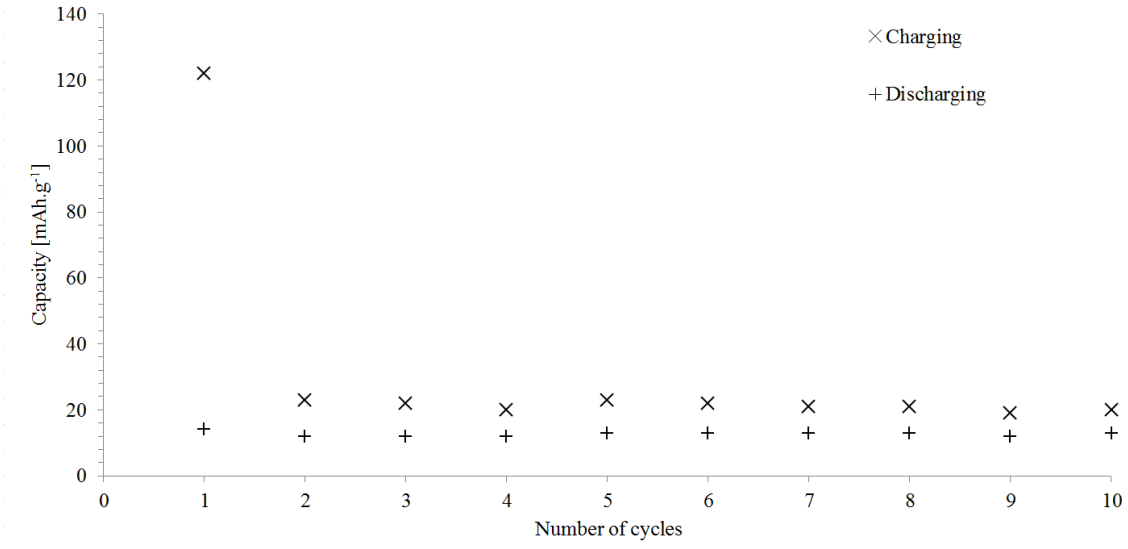

Figure 8.38 The charge and discharge capacity spikes across the cycles (4 wt.% of SBR)

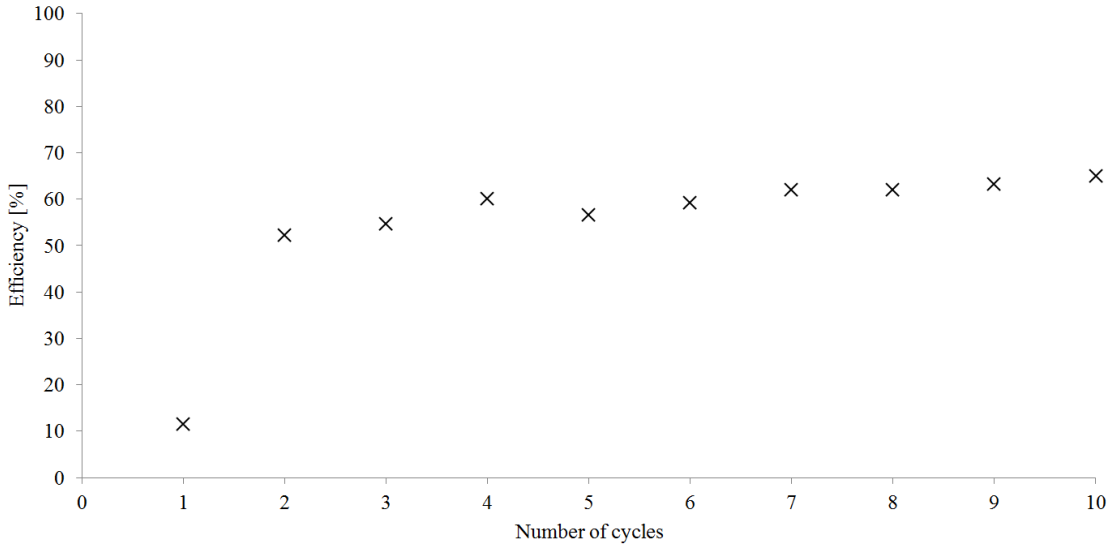

Figure 8.39 The Coulomb efficiency (4 wt.% of SBR)

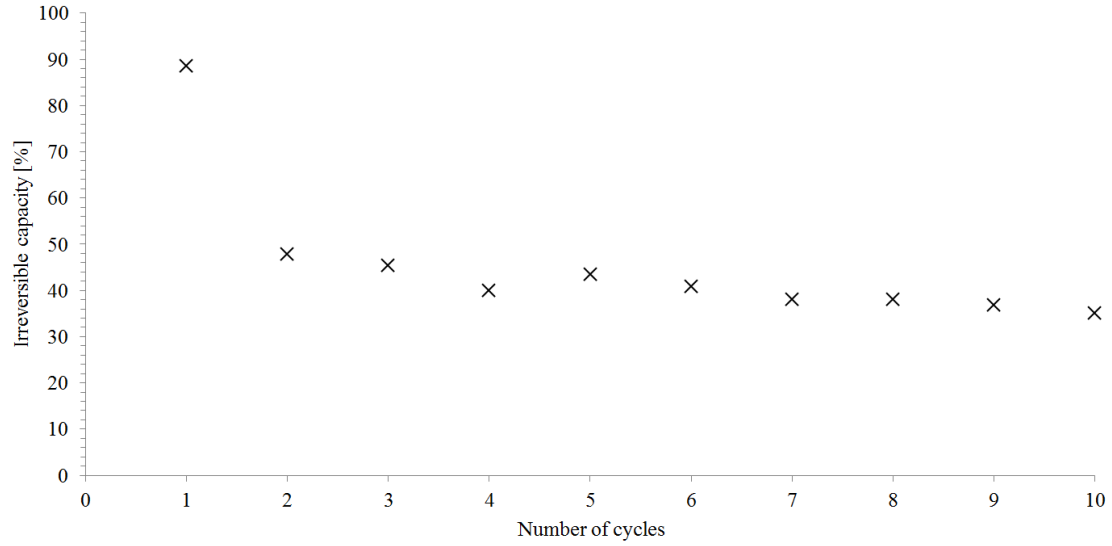

Figure 8.40 The irreversible capacity in percentage (4 wt.% of SBR)

The negative electrode mass with 2 wt.% of SBR was 4,2 mg. A current of ± 112 µA was calculated. Measuring the ten cycles took a little less than 65 hours.

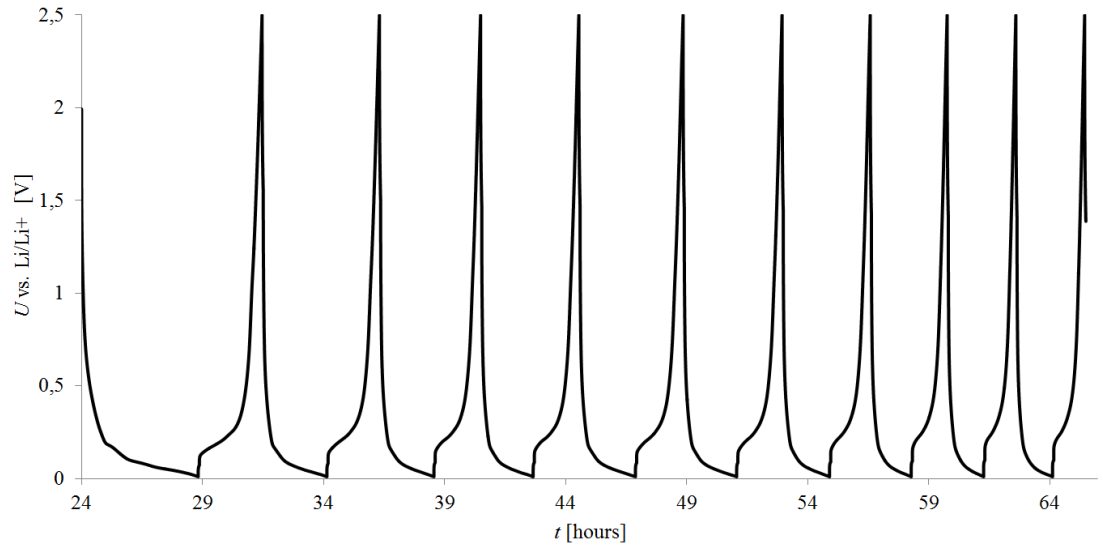

Figure 8.41 Voltage spikes in every cycle (2 wt.% of SBR)

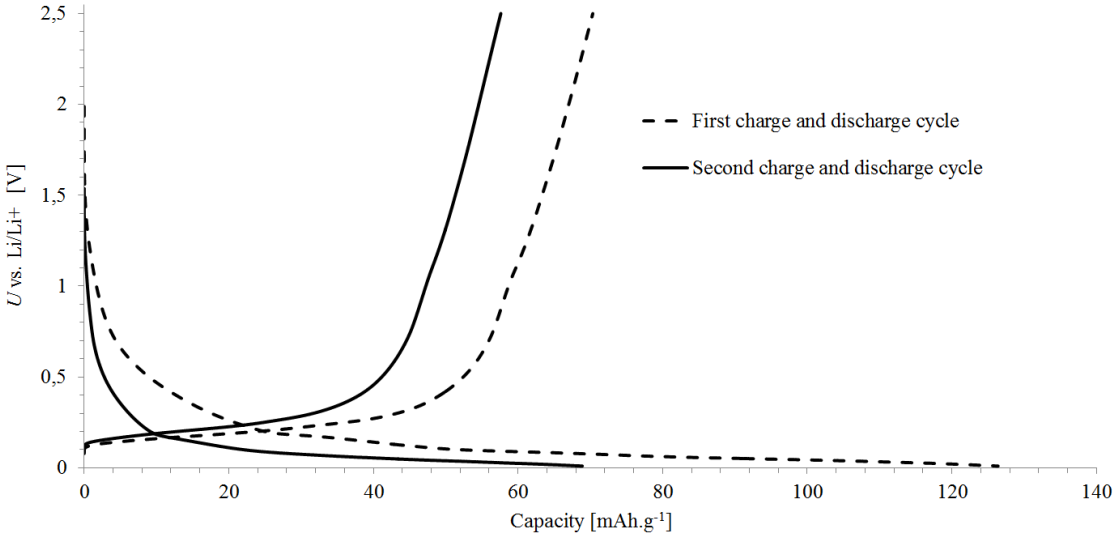

Figure 8.42 The first two charging and discharging cycles (2 wt.% of SBR)

In every cycle the irreversible capacity was negative, meaning that a larger amount of charge was received than delivered. With only 2 wt.% the volume change of the electrode was too fast. These numbers affect the Coulomb efficiency numbers, which were over a 100 % in every cycle, reaching eve 172 % in cycle nine.

Table 8.9 Charge and discharge values, Coulomb efficiency and irreversible capacity (2 wt.% of SBR)

Cycle	Charge [mAh/g]	Discharge [mAh/g]	C. Efficiency [%]	Irr. Capacity [%]
1	70	126	180,0	-80,0
2	58	69	118,9	-18,9
3	51	58	113,7	-13,7
4	50	56	112,0	-12,0
5	52	60	115,4	-15,4
6	50	57	114,0	-14,0
7	44	50	113,6	-13,6
8	39	43	110,3	-10,3
9	22	38	172,7	-72,7
10	35	38	108,6	-8,6

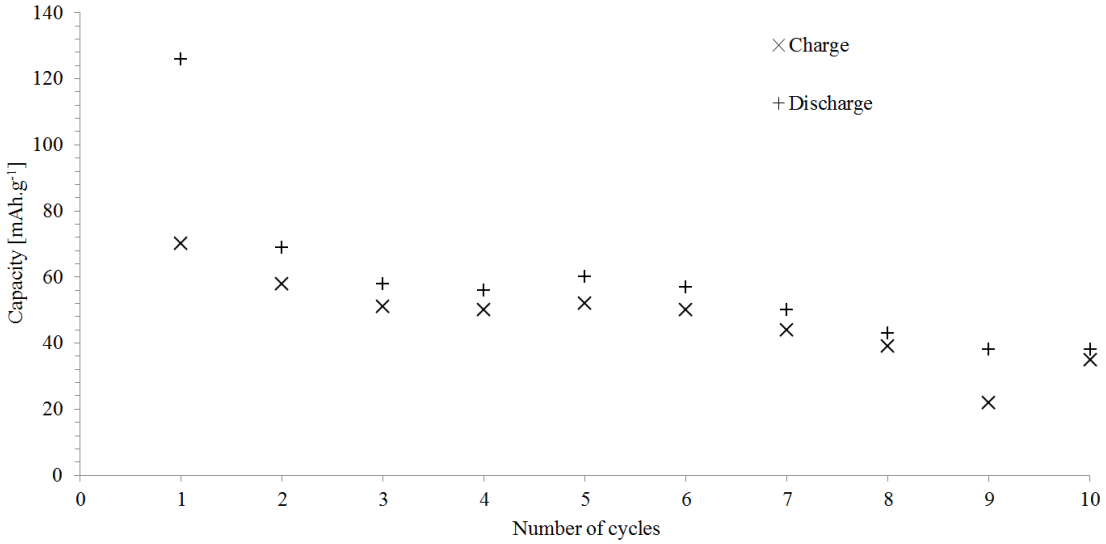

Figure 8.43 The charge and discharge capacity spikes across the cycles (2 wt.% of SBR)

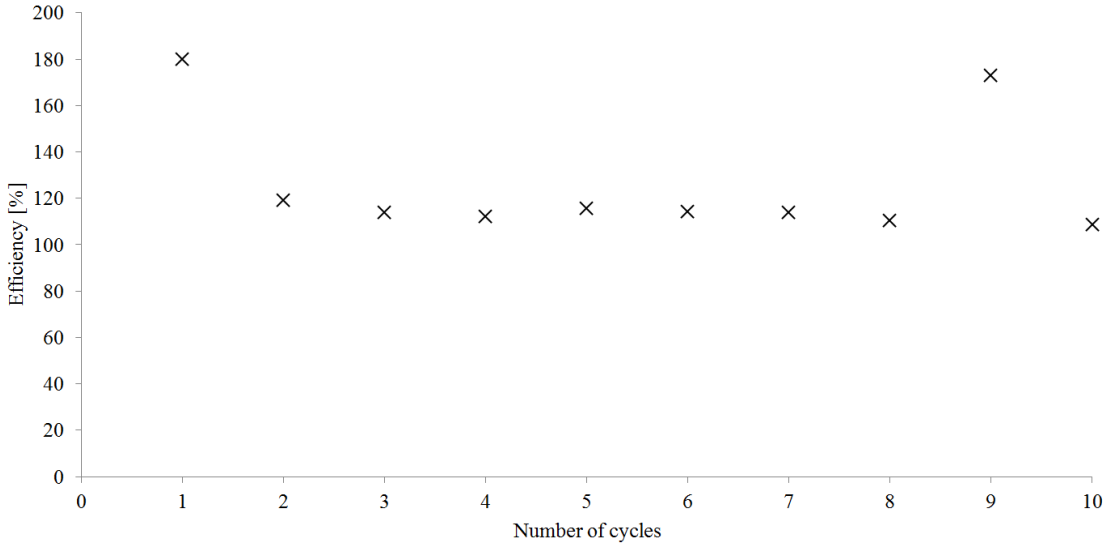

Figure 8.44 The Coulomb efficiency (2 wt.% of SBR)

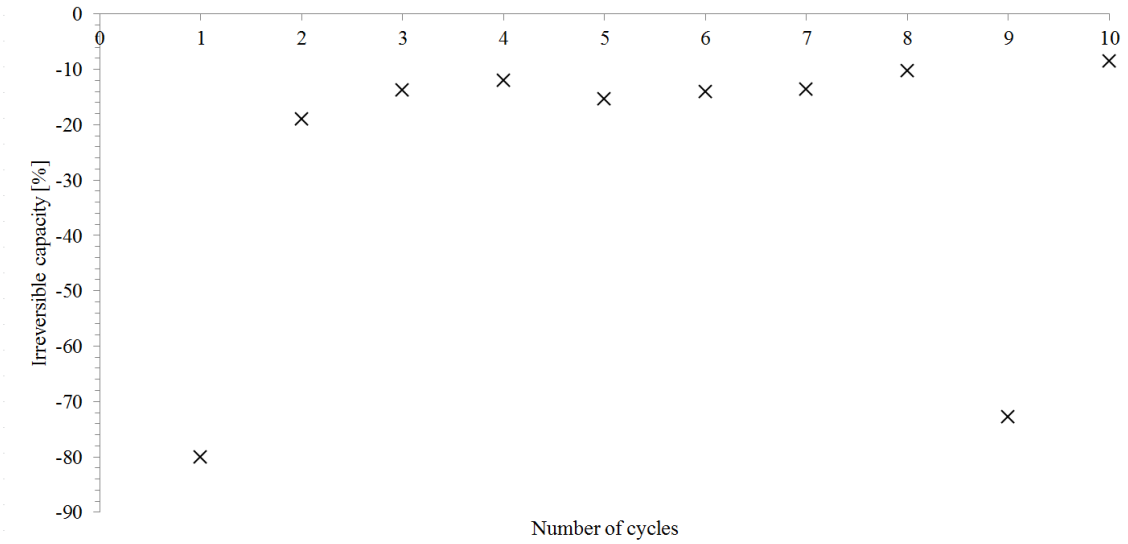

Figure 8.45 The irreversible capacity in percentage (2 wt.% of SBR)

These measurements conclude that the 6 and 4 wt.% of SBR binder might be usable in battery applications. However the use of only 2 wt.% is not recommended, due to its insufficient behavior. This binder after the assembly showed promise, every assembled cell produced more than 3 Volts.

8.4 Summary

To summarize the results a table containing the last value of the discharge, the irreversible capacity and the Coulomb efficiency was created. The best results were achieved with all three samples of the binder PVDF and with the sample containing 3 wt.% of the P84 binder. These results are shown in chapters 8.1 and 8.2, more precisely the characteristics 8.1 to 8.15, 8.26 to 8.30 and tables 8.1, 8.2, 8.3 and 8.6. This summarizing table contains information about the irreversible capacity and coulomb efficiency, which shows that the best samples have only a small amount of irreversible capacity and an efficiency over 88 %. Out of the applicable results the 3 wt.% of P84 performed the best, the efficiency was 97,8 %, the capacity values only decreased 4 % over the cycles.

Table 8.10 Summarization

Samples	Discharge in the last (10th) cycle [mAh/g]	Irr. Capacity in the first charge-discharge cycle [%]	C. Efficiency in the first cycle [%]
10 wt.% of PVDF	130	8,3	91,7
6 wt.% of PVDF	238	11,4	88,6
3 wt.% of PVDF	262	2,9	97,1
10 wt.% of P84	4	82,1	17,9
6 wt.% of P84	49	59,2	40,8
3 wt.% of P84	258	2,2	97,8
6 wt.% of SBR	63	21,3	78,7
4 wt.% of SBR	13	88,5	11,5
2 wt.% of SBR	38	-80,0	180,0

With the SBR binder the best results were reached with the 6 wt.% sample. These results are shown on 8.31 to 8.35 and in Table 8.7. However these results are not even close to the other results mentioned above. The sample with 4 wt.% performed very similarly, showing the results are characteristics 8.36 to 8.40 and the Table 8.8. This binder performed poorly with every sample. The use of these amounts of SBR was inspired by a publication from the Lawrence Berkeley National Laboratory, in Berkeley, California. [34] In this publication they tried out 4 wt.% of binder, however based on the results, a larger amount of binder and conductive additive might perform better.

The worst results were produced by the 10 wt.% sample with the P84 binder and the 2 wt.% sample with the SBR binder. With the SBR binder the capacity values were low and in every cycle a negative irreversible capacity was measured, figeres 8.40 to 8.45 and table 8.9 show these results. Unfotunately the result with the P84 binder were even worse, the capacities were extremely low, the irreversible capacity values were high, reaching even 82 %. Even the voltage spikes were distorted, showin these results are the characteristics 8.16 to 8.20 and the Table 8.4.

9 CONCLUSION

This bachelor's thesis focuses on the effects of the binder material on the overall performance of the negative electrode material in a lithium-ion battery. The process described in chapter seven was followed to create the electrodes. The preparation of the electrodes with the P84 binder took a few attempts, in the end the conclusion was that this binder required only 1200 µl compared to the 3000 µl needed for the PVDF binder. Assembling the measuring cells required the skill to work with lithium. Taking too much time and too many brushes with the scalpel results in the "melting" of the lithium, in that case it is nearly impossible to cut it out and place it in the cell. The assembled cells were producing at least 2,5 Volts, with the samples containing the SBR binder all cells produced above 3 Volts.

The PVDF binder was already an established material, all three samples (with 3,6 and 10 wt.%) were adequate. Out of these samples the 3 and 6 wt.% ones had a discharge capacity of 262 and 238 mAh/g at the end of the last measuring cycle. Another very promising result was achieved with the binder P84 in its 3 wt.% sample, which had a discharge capacity of 258 mAh/g at its last measuring cycle. This sample performed the best out of all the samples, showing the best numerical results and characteristics. The remaining samples were inadequate, the 10 wt.% of P84 performed very poorly, even though after the initial cycles it didn't show any defect. The capacity values with this were very low, only a 4 mAh/g was discharged in the last cycle. The 6 wt.% of both the P84 and SBR binder performed similarly, they had 49 and 63 mAh/g discharging capacity in the last cycle. The 4 wt.% SBR sample performed in a similar way, however it had even lower capacities, only 13 mAh/g in the last cycle. Another poor performance was received from the sample containing the least amount of SBR binder, 2 wt.%, which had negative irreversible capacity values throughout all the cycle.

The preparation of the electrode material with the SBR binder differs from the other two binders, as a solvent demineralized water was used. If during the drying process the water did not fully evaporate, than an unwanted reaction with the lithium might have happened, which would explain the poor results. The P84 binder on the other hand proved to be a suitable replacement for the PVDF binder, due to its greener production and outstanding results with the 3 wt.% sample. The usable range of wt.% is between 3 and 6. A possible way to improve the samples, would be the use of a process called lithiation. During this process the electrodes are doped with lithium before the assembly, which can result in a 18 to 45 % capacity rise.

The results received during these experiments showed that every binder works to a certain extent. A possible way to continue this thesis would be to determine the exact amount of P84 and SBR binders needed. A series of rate capability measurements would also indicate the effect of the binders. Also the use of the above mentioned lithiation process, or the use of treated natural graphite (smaller particle-grains, enhanced specific surface etc.) should provide better results, it is worth exploring.

LITERATURE

[1] History of the battery. In: *Wikipedia: the free encyclopedia* [online]. San Francisco (CA): Wikimedia Foundation, 2001- [cit. 2016-05-28]. Available from: https://en.wikipedia.org/wiki/History_of_the_battery#cite_note-36

[2] Cell Chemistries – How Batteries Work. [online]. [cit. 2016-05-28]. Available from: http://www.mpoweruk.com/chemistries.htm

[3] How do Lithium Batteries Work?. [online]. [cit. 2016-05-28]. Available from: http://batteryuniversity.com/learn/article/lithium_based_batteries

[4] Is Lithium-ion the Ideal Battery?. [online]. [cit. 2016-05-28]. Available from: http://batteryuniversity.com/learn/article/is_lithium_ion_the_ideal_battery

[5] Lithium-ion battery. In: *Wikipedia: the free encyclopedia* [online]. San Francisco (CA): Wikimedia Foundation, 2001- [cit. 2016-05-28]. Available from: https://en.wikipedia.org/wiki/Lithium-ion_battery

[6] PISTOIA, G. *Lithium-ion batteries: advances and applications*. Amsterdam: Elsevier, 2014. ISBN 0444595139.

[7] Designing Applications with Li-ion Batteries. [online]. [cit. 2016-05-28]. Available: http://www.richtek.com/battery-management/en/designing-liion.html

[8] RAHN, Christopher D. *Battery systems engineering*. Chichester, West Sussex, United Kingdom: John Wiley & Sons Ltd., Publication, 2013. ISBN 9781119979500.

[9] ŠIKUDA, M. *Záporné elektrodové materiály v lithium-iontovém akumulátoru.* Brno: Vysoké učení technické v Brně, Fakulta elektrotechniky a komunikačních technologií, 2015. 79 s. Vedoucí diplomové práce Ing. Jiří Libich

[10] DRAHOKOUPIL, P. Výzkum záporných elektrod pro lithno-iontové akumulátory. Brno: Vysoké učení technické v Brně, Fakulta elektrotechniky a komunikačních technologií, 2013. 51 s. Vedoucí diplomové práce doc. Ing. Marie Sedlaříková, CS

[11] NAKAHARA, Kiyoshi, Ryosuke NAKAJIMA, Tomoko MATSUSHIMA a Hiroshi MAJIMA. Preparation of particulate Li4Ti5O12 having excellent characteristics as an electrode active material for power storage cells. *Journal of Power Sources*. 2003, Vol. 117, 1-2, s. 131-136. ISSN 03787753. Available from: http://linkinghub.elsevier.com/retrieve/pii/S0378775303001691

[12] SANDHYA, C. P., Bibin JOHN a C. GOURI. Lithium titanate as anode material for lithium-ion cells: a review. *Ionics*. 2014, Vol. 20, issue 5, s. 601-620. ISSN 0947-7047. Available from: http://link.springer.com/10.1007/s11581-014-1113-4

[13] GUERFI, A., S. SÉVIGNY, M. LAGACÉ, P. HOVINGTON, K. KINOSHITA a K. ZAGHIB. Li4Ti5O12 spinel as electrode for electrochemical generators. *Journal of Power Sources*. 2003, 119-121, s. 88-94. ISSN 03787753.Available: http://linkinghub.elsevier.com/retrieve/pii/S0378775303001319

[14] VENUGOPAL, Ganesh, Andrew HUNT a Faisal ALAMGIR. Nanomaterials for Energy Storage in Lithium-ion Battrery Applications. *Material Matters* [online]. 2010č. 42 [cit. 2016-05-28]. Available from:

http://www.sigmaaldrich.com/catalog/product/aldrich/702277?

[15] LI, Junrong, Zilong TANG a Zhongtai ZHANG. Controllable formation and electrochemical properties of one-dimensional nanostructured spinel Li4Ti5O12. *Electrochemistry Communications* [online]. 2005, s. 894-899 [cit. 2016-05-28]. ISSN 13882481. Available from: http://linkinghub.elsevier.com/retrieve/pii/S1388248105001840

[16] NORDH, TIm. *Li4Ti5O12 as an anode material for Li ion batteries in situ XRD and XPS studies*. Uppsala, 2013. ISBN 1650-8297. Available from: http://urn.kb.se/resolve?urn=urn:nbn:se:uu:diva-196056. Student thesis. Uppsala University.

[17] TANAKA, Shingo, Mitsunori KITTA, Tomoyuki TAMURA, Tomoki AKITA, Yasushi MAEDA a Masanori KOHYAMA. First-principles calculations of O- K ELNES/XANES of lithium titanate. *Journal of Physics D: Applied Physics* [online]. 2012-12, Vol. 45, issue 49, s. 494004- [cit. 2016-05-28]. ISSN 0022-3727. Available from: http://stacks.iop.org/0022-3727/45/i=49/a=494004?key=crossref.81c853b143f84f93ef9ab90872f9c0e1

[18] LI, N., Z. CHEN, W. REN, F. LI a H.-M. CHENG. Flexible graphene-based lithium ion batteries with ultrafast charge and discharge rates. *Proceedings of the National Academy of Sciences* [online]. 2012-10, Vol. 109, issue 43, s. 17360-17365 [cit. 2016-05-28]. ISSN 0027-8424. Available from: http://www.pnas.org/cgi/doi/10.1073/pnas.1210072109

[19] KWIECIńSKA, B a H.I PETERSEN. Graphite, semi-graphite, natural coke, and natural char classification—ICCP system. *International Journal of Coal Geology* [online]. 2004, Vol. 57, issue 2, s. 99-116 [cit. 2016-05-28]. ISSN 01665162. Available from: http://linkinghub.elsevier.com/retrieve/pii/S0166516203001666

[20] WISSLER, Mathis. Graphite and carbon powders for electrochemical applications. *Journal of Power Sources* [online]. 2006, Vol. 156, issue 2, s. 142-150 [cit. 2016-05-28]. ISSN 03787753. Available from: http://linkinghub.elsevier.com/retrieve/pii/S0378775306003430

[21] Lithium Ion Anode Materials – Ordered and Disordered Carbon. [online]. [cit. 2016-05-28]. Available from: http://batteryblog.ca/2010/06/lithium-ion-anode-materials-ordered-and-disordered-carbon/

[22] Australia's MRL Corporation to commence graphite drilling in Sri Lanka. [online]. [cit. 2016-05-28]. Available from: http://www.lankadesha.com/australias-mrl-corporation-commence-graphite-drilling-sri-lanka/

[23] GRAFGUARD® Expandable Graphite Flake. [online]. [cit. 2016-05-28]. Available from: http://www.graftech.com/products/grafguard/

[24] DOH, Chil-Hoon, Byung-Chan HAN, Bong-Soo JIN a Hal-Bon GU. Structures and Formation Energies of LixC6 (x=1-3) and its Homologues for Lithium Rechargeable Batteries. *Bulletin of the Korean Chemical Society* [online]. 2011-06, Vol. 32, issue 6, s. 2045-2050 [cit. 2016-05-28]. ISSN 0253-2964. Available from: http://koreascience.or.kr/journal/view.jsp?kj=JCGMCS

[25] What is Graphite?. In: *Canada carbon* [online]. 2014 [cit. 2016-05-28]. Available

from: http://www.canadacarbon.com/what-is-graphite

[26] YAKOVLEV, A. V., A. I. FINAENOV, S. L. ZABUD'KOV a E. V. YAKOVLEVA. Thermally expanded graphite: Synthesis, properties, and prospects for use. *Russian Journal of Applied Chemistry* [online]. 2006, Vol. 79, issue 11, s. 1741-1751 [cit. 2016- 05-28]. ISSN 1070-4272. Available from: http://link.springer.com/10.1134/S1070427206110012

[27] TAMASHAUSKY, Albert. *An introduction to Synthetic Graphite* [online]. 2006 [cit. 2016-05-28]. Available from: http://asbury.com/pdf/SyntheticGraphitePartI.pdf

[28] EUROPEAN CARBON AND GRAPHITE ASSOCIATION. *Graphite production and further processing* [online]. 2014 [cit. 2016-05-28]. Available from: http://www.carbonandgraphite.org/

[29] The Influence of Polymer Binders on the Performance of Cathodes for Lithium-Ion Batteries . [online]. [cit. 2016-05-28]. Available from: https://ortus.rtu.lv/science/en/publications/8067/fulltext

[30] Polyvinylidene fluoride. In: *Wikipedia: the free encyclopedia* [online]. San Francisco (CA): Wikimedia Foundation, 2001- [cit. 2016-05-28]. Available from: https://en.wikipedia.org/wiki/Polyvinylidene_fluoride

[31] 70% PVDF - A Highly Weatherable and Sustainable Coating. In: Wikipedia: the free encyclopedia [online]. San Francisco (CA): Wikimedia Foundation, 2001- [cit. 2016-05-28]. Available from: http://www.linetec.com/Finishing_Facts/PVDF-promotes-sustainability.html

[32] Styrene-butadiene. In: *Wikipedia: the free encyclopedia* [online]. San Francisco (CA): Wikimedia Foundation, 2001- [cit. 2016-05-28]. Available from: https://en.wikipedia.org/wiki/Styrene-butadiene

[33] Styrene butadiene rubber. In: Wikipedia: the free encyclopedia [online]. San Francisco (CA): Wikimedia Foundation, 2001- [cit. 2016-05-28]. Available from: http://www.slideshare.net/kareemtharaa/styrene-butadiene-rubber-42687408

[34] Optimization of ratio and amount of CMC/SBR binder for a graphite anode . [online]. [cit. 2016-05-28]. Available from: http://ma.ecsdl.org/content/MA2010-02/4/200.full.pdf

[35] Polyimide P84. In: *Wikipedia: the free encyclopedia* [online]. San Francisco (CA): Wikimedia Foundation, 2001- [cit. 2016-05-28]. Available from: https://en.wikipedia.org/wiki/Polyimide_P84

[36] Potentiostat. In: *Wikipedia: the free encyclopedia* [online]. San Francisco (CA): Wikimedia Foundation, 2001- [cit. 2016-05-28]. Available from: https://en.wikipedia.org/wiki/Potentiostat

[37] Libich, J. Záporná elektroda pro lithno-iontové akumulátory, Vysoké učení technické v Brně, Fakulta elektrotechniky a komunikačních technologií, Ústav elektrotechnologie, 108 s., Brno, 2015. Vedoucí práce prof. Ing. Jiří Vondrák, DrSc.

Electrochemical Test Cell. [online]. [cit. 2016-05-28]. Available from: http://el-cell.com/wp-content/uploads/manuals/ECC-Ref_quick_ref.pdf